Carbon dioxide gas separation from syngas to increase conversion of Reverse Water Gas Shift reaction via polymeric and mixed matrix membranes

Lauren Rose

Thesis submitted to the Faculty of Graduate and Postdoctoral Studies in partial requirements for the M.A.Sc. degree in Chemical Engineering

Department of Chemical and Biological Engineering

University of Ottawa

Abstract

Membranes are a promising, effective and energy efficient separation strategy for effluent gases in the Reverse Water Gas Shift (RWGS) reaction to increase the overall conversion of CO_2 to CO. This process involves a separation and recycling process to reuse the unreacted CO_2 from the RWGS reactor. The carbon monoxide produced from this reaction, alongside hydrogen (composing syngas), can be used in the Fischer-Tropsch process to create synthetic fuel, turning stationary CO_2 emissions into a useable resource. A literature review was performed to select suitable polymers with high CO_2 permeability and selectivities of CO_2 over CO and H_2. PDMS (polydimethylsiloxane) was selected and commercial and in-house PDMS membranes were tested. The highest CO_2 permeability observed was 5,883 Barrers, including a CO_2/H_2 selectivity of 21 and a CO_2/CO selectivity of 9, with ternary gas feeds. HY zeolite, silica gel and activated carbon were selected from previous research for their CO_2 separation capabilities, to be investigated in PDMS mixed matrix membranes in 4 wt % loadings. Activated carbon in PDMS proved to be the best performing mixed matrix membrane with a CO_2 permeability of 2,447 Barrers and comparable selectivities for CO_2/H_2 and CO_2/CO of 14 and 9, respectively. It was believed that swelling, compaction and the homogeneity of the selective layer were responsible for trends in permeability with respect to driving force. The HY and silica gel mixed matrix PDMS membranes were believed to experience constraints in performance due to particle and polymer interfaces within the membrane matrix.

Sommaire

Les membranes constituent une stratégie de séparation prometteuse, efficace et économe en énergie pour traiter les effluents gazeux de la reaction inverse du gaz à l'eau du gaz à l'eau inverse (RWGS) pour favoriser la conversion du CO_2 en CO. Ce procédé implique une étape de séparation et de recyclage afin de réutiliser le CO_2 n'ayant pas réagi dans le réacteur RWGS. Le monoxyde de carbone produit par cette réaction ainsi que l'hydrogène (composant ensemble le gaz de synthèse) peuvent ensuite être utilisés dans un procédé Fischer-Tropsch pour produire un carburant de synthèse, menant à la production d'une ressource utile à partir d'émissions de CO_2. Une revue de littérature a été complétée afin de sélectionner des polymères appropriés comportant une perméabilité au CO_2 élevée ainsi qu'une haute sélectivité au CO_2 par comparaison au CO ou H_2. Le PDMS (polydiméthylsiloxane) a été choisi et des tests ont été menés sur des membranes au PDMS commerciales et synthétisée en laboratoire. La plus haute perméabilité au CO_2 observée était de 5,883 Barrers, avec une sélectivité CO_2/H_2 de 21 et une sélectivité CO_2/CO de 9, pour une alimentation de gaz ternaire. Une zéolithe HY, du gel de silice et du charbon actif ont aussi été sélectionnés pour leur capacité de séparation du CO_2 en accord avec les résultats de la revue de littérature. Les tests sur ces matériaux ont été effectués sur des membranes de PDMS à matrice mixte avec une charge massique de 4 %. Le charbon actif dans le PDMS a mené aux meilleurs résultats de membranes mixtes avec une perméabilité au CO_2 de 2,447 Barrers et des sélectivités au CO_2/H_2 et CO_2/CO de 14 et 9 respectivement. Il est probable que les phénomènes de plastification et de compactage et l'homogénéité de la couche sélective des membranes soient' responsables des tendances observées sur la perméabilité vis-à-vis de la force motrice. Il a été supposé que les membranes mixte de PDMS avec la zéolite HY ou le gel de silice ont montré de performances inférieures dû aux interfaces entre le polymère et les particules dans la matrice de la membrane.

Acknowledgements

Firstly, I would like to thank my supervisor Dr. F. Handan Tezel for reaching out to me to initiate this partnership and supporting me during my graduate degree. Thanks to her guidance and feedback I was able to successfully finish my thesis, while overcoming inevitable setbacks and developing many skills I will take with me after graduation. I would like to extend a huge thank you to the departmental technical staff, Louis Tremblay, Franco Ziroldo and Gérard Nina. They have given their time unforgivingly to put together the laboratory set-up, answering all my questions and helping to troubleshoot experimental problems all while ensuring safety. It would not have been possible without their help.

Many thanks to my colleagues: David Carter, Hoda Azimi, Dean Kennedy, Sean Wilson, Maja Mujcin and Mohammadali Baghbanzadeh. I have appreciated all your time answering my questions, providing suggestions when I needed direction and offering additional resources. Finally, I would like to thank my parents and sister for their encouragement and support during my graduate studies.

I would like to thank Natural Resources Canada and NSERC (Natural Sciences and Engineering Council of Canada) for providing funding through the Science and Technology Internship Program. I would also like to recognize Phoenix Canada Oil Company Ltd. and MITACS (Mathematics of Information Technology and Complex Systems) for making this project possible.

Statement of Contribution of Collaborators

I hereby declare that solely I have written the work presented in this thesis under the direct supervision of Dr. F. Handan Tezel. I performed the entirety of the experiments discussed in this work. The design of this set-up was primarily my work with feedback from Dr. F. Handan Tezel, Louis Tremblay, Franco Ziroldo and Gerard Nina. Data acquisition for the gas chromatograph was set up and configured by Gérard Nina. The experimental system was constructed with the help of Franco Ziroldo and Louis Tremblay. Hoda Azimi provided two membranes discussed in this work (referenced as PDMS-PAN II and AC-PDMS-PAN II), including polyacrylonitrile support material. Her membrane synthesis method was used for the membranes synthesized in the laboratory and used in this work. For future publications, she will be a co-author in the corresponding chapters: Chapter 3 and Chapter 4. Maja Mujcin performed a sieve analysis for an adsorbent material used in this work, and the particle size is reported in Chapter 4.

Table of Contents

List of Figures

List of Tables

Chapter 1: Introduction

1.1 CO_2 EMISSIONS

Carbon dioxide is no stranger to the topic of global warming. It is one of the most discussed and the most significant greenhouse gases to date, and for a good reason. CO_2 is considered one of the most significant greenhouse gases to date [1]. Emissions of CO_2 in Canada (in 2014) reached a total of 732 Mt (Megatonnes) and were mostly from large stationary point sources like the oil and gas industry [2]. There have been efforts from intergovernmental organizations like the UN (United Nations) to hold leaders accountable in capping emissions to regulate the global warming effect to a maximum of 2 ºC/year [1,3,4]. However, part of this responsibility lies in innovating ways to not only reduce and capture CO_2 emissions, but also finding routes to convert and consume this greenhouse gas into more useful products. Since a significant portion of CO_2 emissions are from stationary sources, where it is not released transiently in the atmosphere, there is a greater opportunity for its capture and future use.

There are several capture techniques dependent on where CO_2 is present in an industrial process. From here, CO_2 can be purified to be sold, sequestered to a specific location or used in other processes. Enhanced oil recovery (EOR) is an example of utilizing liquid CO_2 emissions through deep injection into the ground to allow for easier extraction of oil [1]. Although there are multiple avenues for handling CO_2 emissions once they are captured, a more promising route entails eliminating and converting CO_2 into a useful product for additional use. This presents an opportunity for large companies with significant CO_2 emissions to capitalize on products that can be made from CO_2 emissions, versus investing in CO_2 sequestering. By incorporating a simple separation process (like adsorption or absorption for flue gases), it becomes possible.

One viable option for using CO_2 as a raw material, is conversion into carbon monoxide, which is a valuable precursor for many chemicals (such as phosgene, ammonia and synthetic liquid fuel). The Fischer Tropsch (FT) process is of particular interest, as it reacts syngas (the combination of CO and H_2) to form a liquid synthetic fuel alternative to gasoline from fossil fuel. Therefore, CO_2 emissions can be converted into a liquid synthetic fuel to compete with fossil fuel derived gasoline. A route that makes sense from an energy standpoint, is capturing CO_2 from a stationary source, and using the Reverse Water Gas Shift (RWGS) reaction to form CO. Hydrogen is a reactant alongside CO_2 in this reaction, and it can be generated from a multitude of processes, including renewable sources [5,6]. While RWGS is still in research and development stages, companies like Sunfire

(Germany) and Sasol (South Africa) are examples of larger scaled versions of the FT process in use today [7,8].

1.2 REVERSE WATER GAS SHIFT REACTION

The RWGS equilibrium reaction consumes CO_2 and H_2 in an equal molar ratio to produce CO and H_2O. It is an endothermic reaction (enthalpy of reaction of 41 kJ/mol) and requires high temperature operation (upwards of 1,000 ºC) to push the reaction forward, as seen below [9,10].

$$CO_2 + H_2 \leftrightarrow CO + H_2O \qquad (1)$$

The reaction is usually performed over metal catalysts such as Ni, Co, Fe, Pd on metal oxide supports. Even at high operating temperatures, it is challenging to maximize CO_2 conversion with a single pass through the reactor [9,10]. Condensing water from the product stream helps to drive the reaction to increase CO production, however this would require lowering the product stream temperature to well below its operating condition. The remaining gases after condensation would include CO_2, CO and H_2. The recycling of CO_2 into the RWGS reaction is critical in providing a higher overall reaction conversion and most industrial uses for syngas require CO_2 to be separated for purification purposes. This leaves CO and H_2 to be prepared as reactants for the FT process, and the general reaction is seen below.

$$(n)\ CO + (2n + 1)\ H_2 \rightarrow C_nH_{(2n+2)} + (n)\ H_2O \qquad (2)$$

The value of n is usually 8 or greater to favour production of gasoline and diesel products [11]. For the RWGS progression to Fischer-Tropsch to make sense from an efficiency perspective, the overall conversion of the RWGS needs to be high to avoid emitting more CO_2 into the atmosphere. This can be achieved by implementing a separation method to recycle any unreacted CO_2. In addition to this, it is likely that hydrogen may have to be added as required by the FT process, to make-up any differences between the RWGS product stream and the FT feed requirements.

Conventionally, processes like adsorption, absorption and stripping and cryogenic temperatures have been used to separate CO_2 from other gases. While these methods are successful and practiced commercially, they are often time consuming upon start-up and have demanding energy requirements. Membranes offer a simple solution as a separation process that is efficient with low energy requirements [12,13].

1.3 GAS MEMBRANE SEPARATION

Gas separation membranes require a driving force – a positive pressure differential in the direction of gas flow to initiate separation via a concentration gradient. The pressure difference can be induced by a vacuum or with an applied feed pressure to the selective side of the membrane. Apart from the capital cost of the membrane material, the only major operating cost associated with membrane separation is typically spent to maintain a pressure gradient across the membrane. This semi-permeable material provides a means to pass select gaseous species more slowly than others, inducing separation. The basic parts of a membrane separation involve a multicomponent fluid feed stream contacting a selective semi-permeable barrier and splitting into a retentate and permeate stream. The retentate is the fluid retained by the membrane wall, where the permeate passes through the membrane and is considered separated fluid.

Penetrant gas flow is often expressed as permeability, which is a standardized and normalized permeate flux. High permeability is desired for membrane separations in order to maximize permeate flow rate and the overall rate of separation for scale-up prospects. Selectivity is another equally important membrane performance characteristic, which describes a membrane's ability to selectively permeate one component more, compared to another. This is expressed as the ratio of feed and permeate mole fractions for a multicomponent gas feed.

1.3.1 Polymeric Membranes

Polymeric membranes are widely used and studied for gas separations. Depending on the type of polymer, separation can occur based on size exclusion or solubility preferences. Polymers that are crystalline in nature will exhibit a more ordered polymer-chain stacking structure, where amorphous polymers exhibit the opposite trend, with an unordered and random polymer chain arrangement. These physical properties help dictate whether a polymer will have defined pore structures or random, and almost non-existent pores. The latter is described as dense or nonporous materials and the membrane selectivity is often governed by differences in penetrant solubility than particle size [14]. Molecularly, CO_2 has a large quadrupole moment which creates stronger interactions with the polymer from greater chemical affinity [15,16]. This gives CO_2 a solubility advantage over lighter gases like H_2 and more linear molecules like CO [14]. Permeability of gases through polymeric membranes can be described using the Solution-Diffusion model which

illustrates the dependence on gas solubility and diffusivity. Permeability (P_i) is expressed as a product of solubility (S_i) and diffusivity (D_i) properties of each gas [17].

$$P_i = S_i \cdot D_i \quad (3)$$

Two common operating concerns surrounding polymeric membranes are swelling and compaction. Molecules like CO_2 have low vapour pressures and large dipole moments, giving it characteristics to effectively increase the fractional free volume of a polymer and noticeably increase gas permeability of all penetrants [18]. Stabilizing additives can be incorporated into the membrane and operating conditions can be optimized to minimize the effects of swelling and maximize usable membrane life [19].

Compaction presents an opposing issue, where high feed pressures can effectively decrease the thickness of a membrane and increase the polymer density. This phenomenon noticeably increases the resistance for gas flow through the membrane and decreases penetrant gas permeability [20]. Fortunately, the addition of inorganic particles helps to stabilize polymeric membranes from the unavoidable operating pressure differential [21].

1.3.2 Mixed Matrix Membranes

Dispersing selective adsorbent particles uniformly in a polymer matrix is the basis of a mixed matrix membrane. Not only can a separation occur through polymer transport mechanisms, but selective adsorbent particles can enhance this and work in parallel to increase gas selectivity. Adsorbents can work similarly to polymers in the sense that gases with larger dipole moments – like CO_2 – can have preferential adsorption capabilities, in spite of molecular size [15]. Additionally, they facilitate faster permeate flow rates due to ordered pore structures with defined pore sizes [15]. Adsorbents also provide some mechanical strength from high operating pressures to oppose compaction [21]. Weight loadings of adsorbents in polymer matrices are usually low enough to maintain flexibility to avoid the inevitable brittleness of purely inorganic membranes. The Maxwell model is a commonly used and recognized way of modelling the permeability through these organic and inorganic phases [22–24].

1.4 THESIS OBJECTIVES

The primary goal of this work was to identify and test suitable polymeric membranes and mixed matrix membranes for the separation of CO_2 from CO and H_2, to increase the overall

conversion of the Reverse Water Gas Shift reaction. This thesis involves an extensive literature review, identifying various suitable polymeric, inorganic and mixed matrix membrane materials. The selected polymeric material was tested using an experimental system constructed and optimized to perform single, binary and ternary gas experiments including CO_2, CO and H_2. After validating appropriate membrane performance properties, adsorbents tested from previous research were incorporated into the selected polymer matrix and subject to the same gas experiments. The polymeric and mixed matrix membrane permeability and selectivity data were compared to confirm if the introduction of selective adsorbents enhanced the overall separation of the membrane.

1.5 THESIS OUTLINE

The thesis is presented in a total of five chapters. Chapter 1 introduces the need to combat CO_2 emissions with processes like the Reverse Water Gas Shift reaction to convert a greenhouse gas into components of syngas for alternate energy sources. Polymeric and mixed matrix membranes are presented to perform the separation of CO_2 from CO and H_2. This implements an increase in the overall conversion of the RWGS by recycling a reactant (CO_2) and permeating a syngas mixture (CO and H_2).

Chapter 2 examines a generous collection of published polymeric, inorganic and mixed matrix membranes studied for CO_2 separation from H_2 and/or CO. This chapter has been prepared as a manuscript for publication and focuses on the same separation but for the purposes of gasification (purely for patent purposes). This literature review focuses on CO_2 permeability and CO_2 selectivity over H_2 and CO to determine which materials are best suited for the desired separation. Selectivity vs. permeability plots are used to select published membranes suitable for further investigation in this research.

Chapter 3 presents results obtained from performing single, binary and ternary gas feed experiments of CO_2, H_2 and CO over polymeric PDMS membranes. Three membranes were tested and include a commercial PDMS membrane and two synthesized PDMS membranes fabricated in the laboratory. The experimental system, membrane synthesis and permeation measurements are described in detail. The results from single, binary and ternary gas experiments are presented graphically and permeability trends are discussed. Selectivity-permeability plots are used to plot the data from this work against a collection of published literature data for further analysis.

Chapter 4 examines the incorporation of three selective adsorbents into PDMS matrices to use as mixed matrix membranes. The experimental system and membrane synthesis techniques unique to the mixed matrix membranes, are described in detail. Single, binary and ternary gas feed experimental data is presented, and permeability trends are discussed. Selectivity-permeability plots are used to compare the data from this work to literature.

Chapter 5 concludes this work, the investigation of polymeric and mixed matrix membranes for the separation of CO_2 from syngas to increase the conversion of the RWGS reaction. It summarizes the results from the experimental results presented in Chapters 2 and 3 It also provides recommendations for future work.

1.6 REFERENCES

[1] S.A. Rackley, Carbon Capture and Storage, 1st ed., Butterworth-Heinemann, 2009.

[2] Environment and Climate Change Canada - National Inventory Report 1990-2014: GHG Sources and Sinks in Canada, 2016.

[3] S.I. Seneviratne, M.G. Donat, A.J. Pitman, R. Knutti, R.L. Wilby, Allowable CO_2 emissions based on regional and impact-related climate targets, Nature. 529 (2016) 477–483.

[4] K. Zickfeld, M. Eby, H.D. Matthews, A.J. Weaver, Setting cumulative emissions targets to reduce the risk of dangerous climate change., in: Proc. Natl. Acad. Sci. U. S. A., 2009: pp. 16129–16134.

[5] P. Nikolaidis, A. Poullikkas, A comparative overview of hydrogen production processes, Renew. Sustain. Energy Rev. 67 (2017) 597–611.

[6] A. López Ortiz, M.J. Meléndez Zaragoza, V. Collins-Martínez, Hydrogen production research in Mexico: A review, Int. J. Hydrogen Energy. 41 (2016) 23363–23379.

[7] O. Strohbach, Fuel of the future: Research facility in Dresden produces first batch of Audi e-diesel, (2015).

[8] National Energy Technology Laboratory: FISCHER-TROPSCH SYNTHESIS, U.S. Department of Energy, (2017).

[9] F. Abdollahi, F.H. Tezel, S. Aplin, Increasing Conversion of CO_2 To CO Via RWGS Reaction: Simulation and Process Design, Altern. Energy. 2 (2013) 1–6.

[10] U.R. Bajirao, Kinetics and Reaction Engineering Aspects of Syngas Production by the Heterogeneously Catalysed Reverse Water Gas Shift Reaction, Ph.D. Thesis, University of Bayreuth, 2012.

[11] J.G. Speight, Hydrocarbons from Synthesis Gas, in: Handb. Ind. Hydrocarb. Process., Gulf Professional Publishing, 2011: pp. 281–323.

[12] L.M. Robeson, The upper bound revisited, J. Memb. Sci. 320 (2008) 390–400.

[13] P. Bernardo, E. Drioli, G. Golemme, Membrane Gas Separation: A Review / State of the Art,

Ind. Eng. Chem. Eng. Res. 48 (2009) 4638–4663.

[14] T.C. Merkel, V.I. Bondar, K. Nagai, B.D. Freeman, I. Pinnau, Gas sorption, diffusion, and permeation in poly(dimethylsiloxane), J. Polym. Sci. Part B Polym. Phys. 38 (2000) 415–434.

[15] D. Bastani, N. Esmaeili, M. Asadollahi, Polymeric mixed matrix membranes containing zeolites as a filler for gas separation applications: A review, J. Ind. Eng. Chem. 19 (2013) 375–393.

[16] M.A. Morrison, P.J. Hay, Molecular properties of N_2 and CO_2 as functions of nuclear geometry: Polarizabilities, quadrupole moments, and dipole moments, J. Chem. Phys. 70 (1979) 4034–4043.

[17] K. Ghosal, B.D. Freeman, Gas Separation Using Polymer Membranes: An Overview, Polym. Adv. Technol. 5 (2003) 673–697.

[18] E.H. Immergut, H.F. Mark, Principles of Plasticization, Plast. Plasticizer Processes. 48 (1965) 1–26.

[19] E.M. Maya, M.L. Sanchez, A. Marcos, J.G. de la Campa, J. de Abajo, Preparation and Properties of Catalyzed Polyimide/ Dicyanate Semi-Interpenetrating Networks for Polymer Gas Membrane with Suppressed CO_2-Plasticization, J. Appl. Polym. Sci. 124 (2013) 713–722.

[20] K.W. Lawson, M.S. Hall, D.R. Lloyd, Compaction of microporous membranes used in membrane distillation. I. Effect on gas permeability, J. Memb. Sci. 101 (1995) 99–108.

[21] Y. Zhao, B.T. Jung, L. Ansaloni, W.S.W. Ho, Multiwalled carbon nanotube mixed matrix membranes containing amines for high pressure CO_2/H_2 separation, J. Memb. Sci. 459 (2014) 233–243.

[22] J. Maxwell, A Treatise on Electricity and Magnetism : Volume II, Dover Publications, 1873.

[23] V. Kramer, M. Kraume, Development of a Mechnistic Model for Sorption Selective Mixed-Matrix Membranes for Gas Separation, Tech. Trans. 109 (2012) 126–135.

[24] C.M. Zimmerman, A. Singh, W.J. Koros, Tailoring mixed matrix composite membranes for gas separations, J. Memb. Sci. 137 (1997) 145–154.

Chapter 2: A review of carbon dioxide and syngas separation via organic, inorganic and mixed matrix membranes

2.1 ABSTRACT

The two components of syngas (CO and H_2) are reactants in the Fischer-Tropsch process which generate synthetic liquid fuels; a greener alterative to the use of present day oil and gas which increases atmospheric concentrations of CO_2. Gasification is becoming a conventional way to generate syngas. However, this process requires separation of CO_2 from CO and H_2. Membranes of the organic, inorganic, and mixed matrix variety were reviewed specifically for the capture of CO_2 from syngas. This included collecting a multitude of published data for membranes that had been tested for CO_2, H_2 and CO in single, binary or ternary experiments. The literature values of selectivity were plotted against permeability for different membranes to identify which one of these membranes were best suited for maximizing both values. Among all those reviewed, PDMS (polydimethylsiloxane), PEO-PBT (polyethyleneoxide – polybutyleneterephthalate) based, PEGMEA-PEGDA (polyethyleneglycolmethyletheracrylate – polyethlyeneglycoldiacrylate) and two SLMs (supported liquid membranes) made with PTMEGDAc (polytetramethyleneetherglycoldiacetate) and PEGDME (polyethyleneglycoldimethylether) were the better performing polymeric materials with CO_2 permeabilities upwards of 3,800 Barrers. Silicalite and Na-Y showed the greatest potential from the inorganic membrane summary with high permeance ratios for CO_2/H_2 and CO_2/CO of 52 and 12, respectively. PEBAX (polyether block amide) with ZIF-8/ZIF-11 and MEE PPZ (methoxyethoxy ethanol substituted polyphosphazene) with SAPO/AlPO displayed the greatest CO_2/H_2 separations of the mixed matrix membranes examined with selectivities reaching 12.

2.2 INTRODUCTION

2.2.1 CO_2 Emissions and Capture

It is estimated that the fossil fuel resources on earth, developed over several hundred million years, are composed of 4,000 to 6,000 Gigatonnes of carbon [1]. This large predicted quantity is a result of the carbon dioxide concentration that used to be present in the atmosphere, 360 million years ago, constituting 1500 ppm [1]. Since the industrial revolution, coupled with an increase in population, carbon dioxide (CO_2) emissions from combustion processes (primarily fossil fuel combustion) have been on the rise; carbon dioxide being “the most significant anthropogenic greenhouse gas (GHG)” [1].

In 2009, fossil fuels accounted for around 85% of the global energy demand and approximately the same extent for the global generation of electricity [1]. More recently in 2014, oil and gas and transportation CO_2 equivalent emissions alone made up 49 % of the total CO_2 emissions of 732 Megatonnes in Canada (seen in Figure 2-1). It is evident that fossil fuel is the leading source in worldwide energy production, which is unlikely to change in the predicted future. This unavoidably raises the issue of increased CO_2 emissions. Even if the amount of CO_2 emissions were to decrease, the effects of it in the environment would persist long after. This constituted climate policies to introduce a global warming mean limit of 2 ºC/year [1–3]. To minimize the effects of this GHG on the environment and prevent its accumulation in the atmosphere, it is necessary to implement capture, storage and recycle techniques.

There are several available technologies to contain and transport carbon dioxide from industrial, stationary sources. The three main techniques used currently are dependent on where CO_2 is released in a process. These include: pre-combustion, post-combustion and oxy-fuel combustion capture. Pre-combustion carbon capture involves partially gasifying a fuel to produce the components of syngas (CO and H_2), which then is shifted with H_2O – also known as the water gas shift (WGS) reaction – to produce CO_2 and H_2. Pure CO_2 is captured and separated from H_2 which can be burned to create steam and generate electricity via turbine [4]. Post-combustion carbon capture involves capturing CO_2 from the flue gases, post combustion of fossil fuels (most often from power plant facilities or other large stationary point sources). Typically this is done using absorption via an absorber and stripper column (often with an amine solvent) [5]. Oxy-fuel combustion utilizes pure oxygen, instead of air, to combust fossil fuel. Oxygen is separated from N_2 and the product combustion gases are composed almost entirely of H_2O and CO_2. The steam can be used to generate electricity (or condensed out), while the CO_2 can easily be separated for further transport/storage [1].

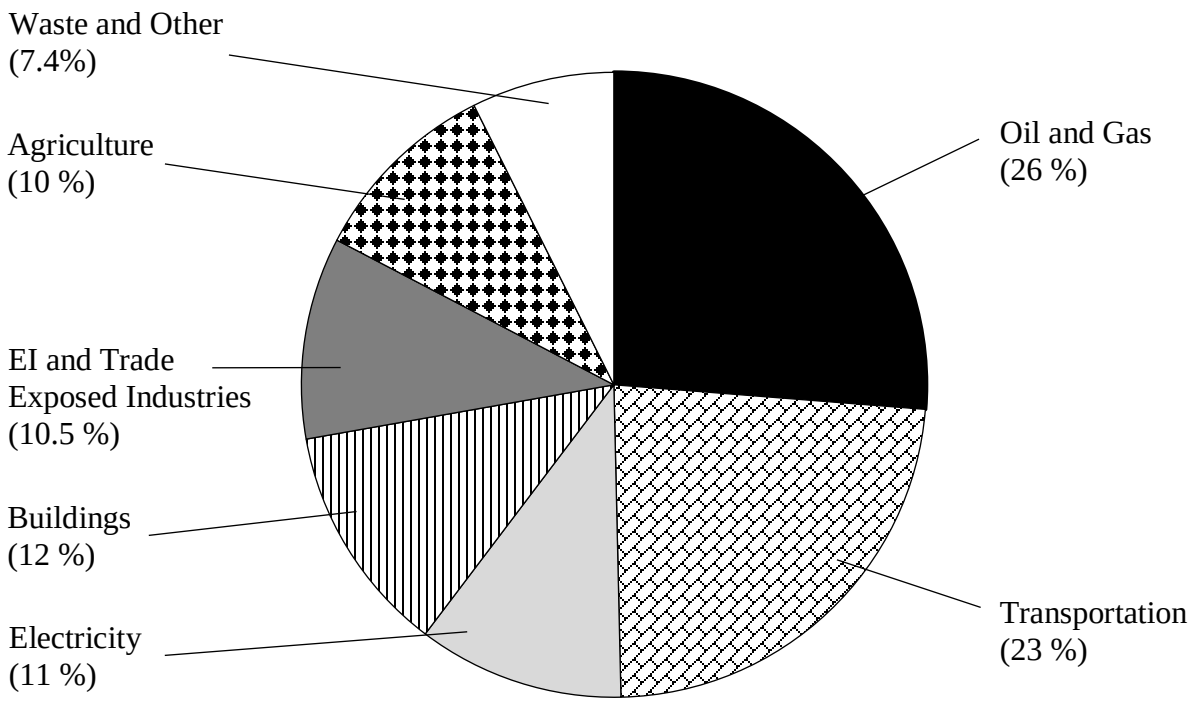

Figure 2-1: CO_2 emissions by source in Canada from 2014; EI (Emission-intensive) and Trade Exposed Industries include mining, smelting and refining, pulp and paper, iron and steel, cement, lime and gypsum, chemicals and fillers; Waste and Other include light manufacturing, construction, forest resources, waste, coal production [6]

2.2.2 CO_2 and Gasification

Gasification is becoming a mainstream process to produce syngas from either fossil or bio-fuel feedstocks. It is a continuously developing technology that partially oxidizes a fuel at high temperature and pressure to produce primarily CO and H_2, also known as syngas. In combination, these two gases have a multitude of uses including electricity generation, a gateway to methanol and ammonia production, as well as synthetic fuel generation in the Fischer-Tropsch process.

Analogous to pre-combustion carbon capture, should the syngas from a gasification product stream need to be cleaned and purified (but not shifted with the WGS reaction), the major impurity required for removal would be CO_2, not including any heavy hydrocarbons or tars and ashes that would be removed initially. CO_2 removal can be performed in many ways (absorption and stripping, cryogenic temperatures), however, membranes are becoming a more prevalent means to efficiently and easily separate CO_2 from other gases.

2.2.3 CO_2 Storage and End Uses

Although much of the focus on syngas purification is the separation, it is important to consider storage and post-separation use for the CO_2 gas. Directly after separation from exhaust and flue gases, it can be purified and is then ready to either be sold (at a specified purity) or sequestered in a set location. Carbon dioxide (with a normal boiling point of approximately -78 °C [7]) can be transported to a set location in gas or liquid phase, depending on its end use. Moving CO_2 via pipeline in its liquefied state is considered the most economically favourable and reliable for CCS (carbon capture and storage) purposes. There are always risks and technical challenges associated with transporting pressurized liquid chemicals, however, the petroleum industry in North America is well equipped to handle liquid CO_2 transportation. Natural gas, liquid hydrocarbon and CO_2 transport for EOR (enhanced oil recovery) are among the transport mechanisms that are applicable in almost every sense to CO_2 transport for CCS [8].

The injection of captured CO_2 into underground geological reserves is considered one of "the most promising and developed method[s]" [8]. There are different avenues for geological sequestration such as deep saline aquifers, depleted oil/gas reservoirs, EOR or unmineable coal beds [8,9]. Of these options, deep saline aquifers are considered the most promising with a large volume for potential injection, however the uncertainty associated with their useable capacities and geological/geochemical properties pose the need for further research before widespread implementation [8]. Although it is also possible to inject CO_2 deep into the ocean, it poses a large risk to marine ecosystems and the acidity of seawater, as CO_2 reacts with water to form carbonic acid. Other risks associated with this technique have not been researched in sufficient depth [8]. For these reasons, it is not discussed further in this review.

One of the most advantageous end uses for carbon dioxide is enhanced oil recovery method. In its supercritical state (under high pressure), CO_2 can be injected deep into the ground (typically greater than 2,000 feet) near oil reserves to mix with the oil – where it is miscible – and allows the oil to swell and reduce in viscosity. This allows the reserves to be more easily extracted. In the U.S.A, gas injection (including CO_2) accounts for approximately 60% of EOR methods, with over 2 billion ft^3 of CO_2 injected every year [10].

2.2.4 Importance of CO_2 Separation and Membranes

The separation of CO_2 from syngas is an important process step for purification purposes. Not only does it prepare syngas for downstream uses, like conversion into synthetic fuels, it is a method of segregating CO_2 from being released in other processes. There are many avenues for pursuing CO_2 separation that have been used in industry, but many have high energy requirements that are not as appealing from a monetary perspective. They are often favoured over other separation processes such as settling, adsorption, extraction, absorption and distillation. This is due to several factors, such as a reduced footprint, higher separation and energy efficiency and simpler operation [4,11,12]. They also offer low power usage and portability in terms of compactness [13].

Membranes can be defined as a selective, interphase barrier used to separate a fluid mixture into two phases by restricting the transport of particular components [14]. After passing through the membrane, the membrane feed is split into a retentate (or reject) and a permeate stream. When the retentate stream houses the desired product, it is common to include a sweep stream that exits with the permeate and to increase the driving force for permeation. Separation through the membrane can be governed by several mechanisms depending on the membrane structure, facilitating the transport of the permeating components.

For gas separation, membranes have been a competitive separation technology since their serial production began in 1980 [11]. "It is estimated that membrane gas separation will play an increasingly important role in reducing the environmental impact and costs of industrial processes" [11]. Separation in the gas phase over a membrane is driven by the partial pressure of the feed components and utilizes differences in molecular, thermodynamic and transport properties as mechanisms for separation [14].

In this work, several membranes are examined for the separation of CO_2 from CO and H_2. The classes of the examined membranes are categorized by material type, focusing on organic, inorganic and mixed matrix materials. Gas permeabilities and selectivities of CO_2 over CO and H_2 are discussed as the defining properties that dictate the most promising and best performing membrane materials to select for further testing.

2.3 CO_2 SELECTIVE MEMBRANES

For the syngas application, it was desired to choose a membrane, which would selectively separate CO_2 from CO and H_2. For this reason, it was not desired to examine membranes that

selectively separated H_2 from CO_2 or CO. Since CO and CO_2 share similar properties, as outlined in Table 2-1, it is likely they will most often compete for transportation through a given material, whereas H_2 is more easily separated from CO_2 based on the greater difference in their gas properties. This is also very dependent on the mass transfer mechanism governing the transport through the membrane itself. The performance of each component is subject to change with respect to many factors (such as interacting components, temperature, pressure).

Table 2-1: Characteristics of important chemical compounds discussed in this work [15]

Chemical	Kinetic Diameter [Å]	Critical Temperature [K]
H_2	2.89	33
CO_2	3.30	304
H_2S	3.60	373
N_2	3.64	126
CO	3.76	134
CH_4	3.80	191

With the exclusion of one PDMS membrane (reporting data with a feed including gasification impurities [16]), and for the purposes of this paper, it is desired to neglect the possibility of impurities in the feed gas when comparing the performance of each membrane material. However, a realistic separation would include trace amounts of other gas components, such as hydrogen sulfide (H_2S), methane (CH_4), nitrogen (N_2), water (H_2O), heavy hydrocarbons, tar, and ash.

2.3.1 Membrane Overview

Basic characterization of a membrane used for gas separation is dependent on few performance factors; these include permeability and selectivity. Figure 2-2 depicts the general schematic for a membrane separation of components A and B.

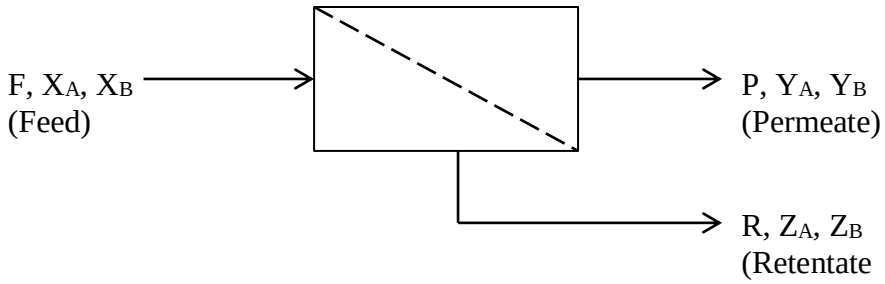

Figure 2-2: General membrane schematic for separation of components A and B

F, P and R are the feed, permeate and retentate flow rates, respectively; X, Y and Z are the mole fractions of component A and B in the feed, permeate and retentate, respectively, in Figure 2-2. In order for separation to occur between the two components, an assumption is made that a driving force (a difference in chemical potential across the membrane) must be present [14]. For gas separations, this is often the applied feed pressure that induces a total and partial pressure difference for the gas penetrants from the feed side to the permeate side of the membrane. Permeability is a standard unit for analyzing normalized gas permeate flux. It is defined as a pressure and thickness normalized flux for a single gas component across the membrane. It can be defined more generally as written in equation 1.

$$P_i = \frac{n_i \cdot L}{A \cdot (driving\ force)} \qquad (1)$$

where P_i is the permeability of component i $\left(\text{in SI units: } \frac{\text{cm}^3\ \text{(STP)}\ \text{cm}}{\text{s}\cdot\text{cm}^2\cdot\text{cmHg}}\right)$, n_i is the volumetric flow rate of component i in the permeate (cm^3 (STP)/s), L is the membrane thickness (cm), A is the membrane area (cm^2) and the driving force is the partial pressure difference across the membrane for component i (cmHg). The Barrer is a standard format for expressing component permeability in a gas separation $\left(1\ \text{Barrer}=10^{-10}\ \frac{\text{cm}^3\ \text{(STP)}\ \text{cm}}{\text{s}\cdot\text{cm}^2\cdot\text{cmHg}}\right)$.

The flux of a permeating gas component can also be described in the unit of permeance, which is normalized to all the same membrane properties (except for selective membrane thickness). It is often expressed in the GPU (gas permeation unit), which is standardized using the same units as the Barrer. Permeance is calculated as given in equation 2.

$$\overline{P}_i = \frac{n_i}{A \cdot (driving\ force)} \qquad (2)$$

where $\overline{P}_i$ is the permeance of component i $\left(\text{in SI units: } \frac{\text{cm}^3\text{ (STP)}}{\text{s}\cdot\text{cm}^2\cdot\text{cmHg}}\right)$, n_i is the volumetric flow rate of component i in the permeate (cm^3 (STP)/s), A is the membrane area (cm^2) and the driving force is the partial pressure difference across the membrane for component i (cmHg). Much like the Barrer, permeance is expressed in the recognized GPU unit, the gas permeation unit $\left(1\text{ GPU}=10^{-6}\frac{\text{cm}^3\text{ (STP)}}{\text{s}\cdot\text{cm}^2\cdot\text{cmHg}}\right)$.

The ideal selectivity ($\alpha^*_{A/B}$), or permselectivity, of a membrane can be defined as the permeability ratio of the desired component (A) to the undesired component (B) for separation. This is described in equation 3.

$$\alpha^*_{A/B} = \frac{P_A}{P_B} \tag{3}$$

The actual selectivity ($\alpha_{A/B}$), or separation factor, of a membrane can be defined by equation 4 for multicomponent gas feeds [14], where X is the mole fraction of component A or B in the feed, and Y is the mole fraction of component A or B in the permeate. The performance of the membranes examined in this report will focus on permeability/permeance and selectivity of the desired components.

$$\alpha_{A/B} = \frac{Y_A/Y_B}{X_A/X_B} \tag{4}$$

2.4 MEMBRANE CLASSIFICATION FOR CO_2 SEPARATION

There are several ways to classify membranes based on physical properties. This work will focus on two major classifications of membranes based on pore structure and material type. The two classes based on pore structure are porous and nonporous (or dense). These titles describe the pore size and configuration (or morphology) of the membranes. The classes based on material are organic (polymeric), inorganic and mixed matrix (a combination of inorganic particles dispersed in a polymeric matrix).

Nonporous membranes are usually made up of a very thin, selective layer that resides on porous support material, to optimize the flux through the membrane. Their pore sizes are usually no greater than a few Å in diameter. If this thin, dense layer is made from different material than the support, it is considered a 'thin film composite membrane' [14]. More porous materials are used to support these thin selective layers or films when large pressure differentials are required for operation, in order to facilitate high flux across the more resistant selective layer [14].

Porous membranes can be further categorized into macroporous, mesoporous and microporous. Macroporous membranes have pore diameters greater than 50 nm where microporous membranes have pore diameters less than 2 nm and mesoporous membranes fall in between this range [14]. Table 2-2 outlines some defining characteristics of these membrane classifications.

Table 2-2: Membrane classification by pore size with example applications [14]

Membrane Type	Pore Diameter	Example Separations
Dense / Nonporous	< a few Å	Gas Separation
Microporous	< 2 nm	Reverse Osmosis
Mesoporous	2 – 50 nm	Ultrafiltration
Macroporous	> 50 nm	Conventional Filtration

However, a more common way of describing and classifying membranes is by material type. Polymeric (organic) and adsorbent (inorganic) materials make up the majority of the most commonly used and studied membranes. Polymeric membranes are commercially used to perform gas and liquid separations. Inorganic membranes are also used commercially, primarily for gas separations (e.g., hydrogen).

2.4.1 Membrane Classification by Material for CO_2 Separation

2.4.1.1 Organic Membranes

Organic membranes are typically made from carbon-based polymer chains, commonly referred to as polymeric or polymer membranes. Polymers can either be classified as amorphous or crystalline, depending on the regularity, arrangement and compactness of the polymer chains. Purely crystalline polymers, with a highly ordered crystalline structure, have melting points at which the polymer becomes a 'melt' or disordered liquid. Conversely, amorphous polymers, with a more random and unordered structure, experience what is known as a glass transition temperature, where the polymer transitions from a glassy to rubbery state, without any release of latent heat. Many polymers are combinations of both crystalline and amorphous structures (from 5 – 90 % crystallinity), allowing some polymers to have both a melting and glass transition temperature and to incorporate the benefits of each structure [14].

Table 2-3 outlines some examples of common polymeric membrane materials and their typical structure. Glassy polymeric membranes (amorphous polymers below their glass transition temperature) exhibit low permeability and high selectivity, while rubbery polymeric membranes

(amorphous polymers above their glass transition temperature) exhibit the opposite with higher permeabilities and lower selectivities [17]. Crystalline polymers exhibit ordered, porous structures and amorphous polymers can be porous but are often nonporous or dense [18].

The polymer chain mobility in an amorphous material differs based on whether the material is above or below the glass transition temperature. Glassy polymers experience little chain segment movement in comparison to rubbery state polymers, making them a better candidate to form microporous materials [19]. Therefore, with more chain mobility, rubbery polymers are more likely to form dense layers where their chain segments can arrange themselves with greater ease to create extremely small or even transient, pores. This is of interest for CO_2 separation from CO and H_2 as membrane separations with dense, rubbery polymers are largely influenced by a penetrant's gas condensability. Gas separation using polymers with larger more structured pores act more as a sieve for smaller gas penetrant molecules (e.g. H_2 over CO_2) and rubbery polymer penetrant transport prioritizes gas solubility over diffusivity [13,14,20].

Supported liquid membranes (SLM) are mentioned in this summary and are a particular, non-dispersive class of liquid polymeric membranes whose selective polymer phase is immobilized in the pores of a support [21].

Table 2-3: Common polymeric membrane material physical states [14,16]

Material	Monomer Structure	Standard State
Polyamide (aromatic)	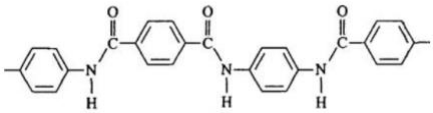	Crystalline
Polyimide	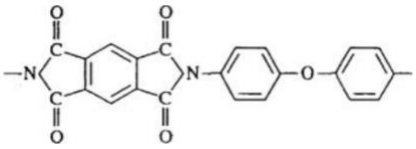	Amorphous (glassy)
Polydimethylsiloxane	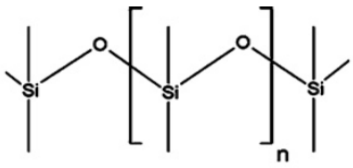	Amorphous (rubbery)

There are a variety of polymeric membranes that have been tested for the separation of CO_2 from H_2 and/or CO. In general, polymeric membranes performed well in terms of CO_2 selectivity

over H_2 and CO. Table 2-4 outlines the polymeric membrane materials of discussion in this section, including their commonly abbreviated and full polymer names. When collecting published data from literature, the most common separation studied and related to this work was CO_2 from H_2. There was published data available for polymeric membranes for separation including CO_2, H_2 and CO. However, this data was not as widespread as CO_2 separation from H_2, which is prevalent in the extent of this review. The materials discussed in the polymeric section below was selected based on CO_2 permeability and CO_2 separation over H_2 and CO.

Table 2-4: Polymers used in the polymeric membranes from literature

Polymer Name	Full Chemical Name
MEE PPZ	Methoxy ethoxy ethanol substituted polyphosphazene
PEBAX	Poly ether block amide
PEG	Poly ethylene glycol
PEGA	Crosslinked poly ethylene glycol acrylate
PEGDA	Poly ethlyene glycol diacrylate
PEGDME	Poly ethylene glycol dimethyl ether
PEGMEA-PEGDA	Poly ethylene glycol methylether acrylate - PEGDA
PEO-PBT	Poly ethylene oxide – poly butylene terephthalate
PEO-PBT + PEG	PEO-PBT + poly ethylene glycol
PEO-PBT + PEG-BE	PEO-PBT + poly ethylene glycol + butyl ether spacers
PEO-PBT + PEG-DBE	PEO-PBT + poly ethylene glycol + dibutyl ether spacers
PDMS	Poly dimethyl siloxane
PI	Polyimide
PPGDME	Poly propylene glycol di-acetate
PTMEGDA	Polytetramethylene ether glycol diacrylate
PTMEGDAc	Polytetramethylene ether glycol diacetate
PTMSP	Poly(1-trimethylsilyl-1-propyne)

The Solution-Diffusion model governs the selective transport through dense, nonporous, polymeric membranes and permeability is expressed as a product of gas diffusivity and solubility as both properties play a role in separation ($P_i = S_i \cdot D_i$) [22,23]. This model can be divided into three mass transfer steps: sorption, diffusion and desorption [14,24]. Since permeability can be expressed as a product of solubility and diffusivity properties, ideal selectivity can be re-written as shown in equation 5 [24].

$$\alpha^*_{A/B} = \left(\frac{S_A}{S_B}\right)\left(\frac{D_A}{D_B}\right) \qquad (5)$$

where S_A is the solubility of component A, S_B is the solubility of component B, D_A is the diffusivity of component A and D_B is the diffusivity of component B. In general, solubility increases with condensability of a gas, while diffusivity increases with smaller gas particle size and greater fractional free volume in a polymer [25].

The solubility of a penetrant gas in a polymer is determined in part by the penetrant-polymer interactions and the penetrant's condensability [26]. The stronger the interactions, the more soluble the gas will be in the polymer. More condensable gases are typically more soluble in these materials, as solubility is a thermodynamic property. "Therefore, CO_2, which has a quadrupolar moment, is highly soluble in polar polymers" [17]. These characteristics are important as H_2 can diffuse much quicker through a pore, however dense, rubbery polymers typically have a weak ability to separate gas molecules primarily by size (strictly diffusing). Therefore, overall selectivity for these membranes is dominated by differences in solubility [26]. This allows larger and more soluble molecules like CO_2 and CO to be selectively permeated over smaller and less soluble molecules like H_2.

While these membranes have useful separation capabilities, they also have operating limits and have been known to experience a decrease in performance under certain conditions. Polymeric membranes can experience compaction, when the material increases in density due to a loss of rigidity in the polymer chains at high pressures. Unfortunately this causes the membrane to lose permeability and separation capabilities over time [27]. These materials also have an upper temperature operating limit below which they maintain basic structural integrity. On top of these difficulties, swelling from CO_2 offers an additional challenge for long term operation [28]. CO_2 can increase chain mobility and fractional free volume within a polymer. The physical conditions for which swelling can occur, are different for every polymer and in some cases, operating below certain temperatures and pressures can reduce or eliminate this irreversible phenomenon [29].

Table 2-5 outlines a collection of published data for several CO_2 selective polymeric membranes, experimentally tested in literature for CO_2, H_2 and/or CO separation, arranged in descending order of CO_2 permeability. Unless otherwise stated, the selectivities presented in this table are expressed as permeability ratios of CO_2 over H_2 or CO. Although the permeability ratios are not always indicative of selectivity for gas mixtures, it is used as a suitable estimate and provides a reasonable comparison to single gas results [16].

Table 2-5: Permeabilities from literature for CO_2 selective polymeric membranes in descending order of CO_2 permeability

Membrane	CO_2 Permeability		H_2 Permeability		CO Permeability		CO_2/H_2	CO_2/CO	Temp. [°C]	Feed P [atm]	Ref.
	Single [Barrers]	**Mixed** [Barrers]	**Single** [Barrers]	**Mixed** [Barrers]	**Single** [Barrers]	**Mixed** [Barrers]					
PTMSP		18,200 in $CO_2/H_2/CO/H_2S$		11,800 in $CO_2/H_2/CO/H_2S$		5,400 in $CO_2/H_2/CO/H_2S$	1.5	3.4	23	2.4	[26]
PDMS	3,800		890				4.3 [I]		35	2 - 17	[20]
PDMS	3,760		940				4.0 [I]		3 – 112	3 – 29	[16,30]
PDMS		3,200 in $CO_2/H_2/CO/H_2S$		950 in $CO_2/H_2/CO/H_2S$		500 in $CO_2/H_2/CO/H_2S$	3.4	6.4	23	2.4	[26]
PDMS	3,100		715				4.3 [I]		35	15	[31]
PDMS		2,848 in $CO_2/H_2/Ar$		813 in $CO_2/H_2/Ar$			3.5 [AS]		37	1.1	[32,33]
*PDMS [1]		2,194 in $CO_2/H_2/Ar$		617 in $CO_2/H_2/Ar$			3.6		37	1.1	[32,33]
PDMS		1,993 in pilot plant syngas		291 in pilot plant syngas		185 in pilot plant syngas	6.8	10.8	35	8.1	[16]
*PDMS [2]		1,517 in $CO_2/H_2/Ar$		414 in $CO_2/H_2/Ar$			3.7		37	1.1	[32,33]
PDMS	1,300		375				3.5 [I]		30	2.0	[34]
*PTMEGDAc		956 in $CO_2/H_2/Ar$		109 in $CO_2/H_2/Ar$			8.9		37	1.1	[32,33]
*PEGDME		814 in $CO_2/H_2/Ar$		74 in $CO_2/H_2/Ar$			11.1		37	1.1	[32,33]
PEO-PBT + PEG-DBE	750		61				12.4 [I]		30	0.3	[35,36]
*PPGDME		518 in $CO_2/H_2/Ar$		88 in $CO_2/H_2/Ar$			5.9		37	1.1	[32,33]

PEGMEA:PEGDA (91:9)	515 in $CO_2/H_2/H_2O$	48 in $CO_2/H_2/H_2O$		12		22	8	[25,37]
PEGMEA:PEGDA (70:30)	440 in CO_2/H_2	47 in CO_2/H_2		9.4		35	17	[37]
PEO-PBT + PEG-BE	400	34		11.8 [I]		30	0.3	[35,36]
PTMEGDA	329 in CO_2/H_2/Ar	59 in CO_2/H_2/Ar		5.6		37	1.1	[32,33]
PEO-PBT + PEG	208	18		11.6 [I]		30	0.3	[35,36]
PEG	170 in pilot plant syngas	50 in pilot plant syngas		2.9		50	8.1	[16]
PEO-PBT	150	15		10.3 [I]		30	0.3	[35,36]
PEBAX	135 in pilot plant syngas	85 in pilot plant syngas	70 in pilot plant syngas	1.6	1.9	35	8.1	[16]
PEBAX	121	25.9		4.7 [I]		3 – 112	3 – 29	[16,30]
PPZ	71	8.4		8.5 [I]		22	3.5	[38]
PEG	66	17		3.9 [I]		3 – 112	3 – 29	[16,30]
PEGDA	52 in CO_2/H_2/Ar	11 in CO_2/H_2/Ar		4.7		37	1.1	[32,33]
PI	6.4	24	0.44	0.27 [I]	14.5 [I]	30	2.0	[13]
PI	5.2	23	0.43	0.23 [I]	12.1 [I]	30	5.9	[13]

** Indicates SLM (supported liquid membranes)*
[I] Indicates ideal selectivity
[1] M_W = 770 g/mol, [2] M_W = 1000 g/mol
[AS] Indicates actual selectivity based on feed and permeate concentrations, unless otherwise noted assume permeability ratios

2.4.1.1.1 PTMSP

PTMSP is a structurally unique polymer used for membrane separations. Although it is glassy in physical nature, it has an exceptionally high free volume, permitting large gas permeabilities [24,26,39]. This is also due to the fact that it has high solubility values for the desired gas in this separation (CO_2) [26,39]. Merkel et al. studied PTMSP for CO_2 separation with syngas components including CO_2, CO and H_2 [26]. As expected, it reported the highest permeabilities of all three gases of the polymeric membranes examined in this work. However, PTMSP had a low selectivity for CO_2 over H_2 of 1.5 at 23 °C and 2.4 atm of feed pressure [26]. It exhibited higher separation over CO under the same conditions, with a CO_2/CO selectivity of 3.4.

2.4.1.1.2 PDMS

Merkel et al. examined the solubility, diffusivity and permeability of CO_2 and H_2 in PDMS membranes [20]. PDMS composite membranes were crosslinked on a highly microporous support. Permeation experiments were carried out at 35 °C and up to 17 atm feed pressure. They reported the highest single gas CO_2 permeability in this polymeric membrane summary (3,800 Barrers in Table 2-5). The ideal selectivity for CO_2/H_2 in this work was reported to be 4.3. They investigated and confirmed that CO_2 solubility in PDMS was two orders of magnitude greater than H_2, with respect to transmembrane pressure differential [20]. Additionally, it was determined that CO_2 was one order of magnitude less diffusive than H_2. However, diffusivity did not change as significantly as solubility with respect to pressure for CO_2 and H_2, specifically in a rubbery polymer like PDMS. Therefore, a gas penetrant's permeability was mostly governed by its solubility in rubbery PDMS and CO_2 could be separated from H_2 using this membrane.

In terms of penetrant trends, Merkel et al. determined that solubility of more condensable gas components (CO_2) increased with pressure [20]. The solubility of less condensable gases (such as H_2) was more-or-less independent of pressure and diffusivity decreased slightly with increasing pressure, due to membrane compaction from high gas feed pressure. This caused permeability to decrease slightly for gases like H_2, when the transmembrane pressure differential was increased.

Scholes et al. reported that commercially available PDMS (polydimethylsiloxane) performed well with respect to pure gas permeabilities of CO_2 and H_2 at 35 °C and 8.1 atm [16]. At these conditions, the pure component permeabilities of CO_2 and H_2 were determined to be 3,760 and 940 Barrers, respectively, with a CO_2/H_2 selectivity of 4.0. When tested with 'pilot plant' syngas

(that includes several common impurities), this membrane also showed promising results. This is a more realistic approach to the desired separation, since it is unlikely for a pure upstream mixture of CO_2, CO and H_2 to be available in an industrial scale process. The composition of this 'pilot plant' gas mixture is displayed in Table 2-6, and is representative of air-blown gasification of Victorian brown coal [16].

Table 2-6: Pilot plant syngas composition [16]

Component	**Molar** [%]
CO_2	14.0
H_2	11.7
CO	11.5
N_2	60.0
CH_4	2.5
Heavy hydrocarbons	0.21
H_2O	0.11

Using this feed gas mixture at 35 °C, the permeability of CO_2 and H_2 are reduced from the pure gas permeabilities to 1,993 (47% reduction) and 291 (69% reduction) Barrers, respectively. This decrease is expected for CO_2, as N_2 occupies a "considerable volume" within the membrane, which limits the amount of CO_2 that can permeate [40]. H_2 experienced an even greater reduction, most likely due to competitive sorption, as PDMS has an affinity for CO_2. The component permeabilities of CO_2, H_2 and CO, as a function of temperature for pilot plant syngas feed, can be viewed in Figure 2-3. It is evident that there is an increasing trend with temperature for all components, however at 35 °C, the permeability of CO_2 is still much higher overall, than H_2 and CO. The permeability ratios (selectivities) of CO_2 to CO and H_2 can be seen in Figure 2-4, as a function of temperature. At 35 °C, these ratios of CO_2/CO and CO_2/H_2 are approximately 10.8 and 6.8, respectively. Therefore, with a pilot plant syngas feedstock, PDMS can reasonably and selectively separate CO_2 from the other major components.

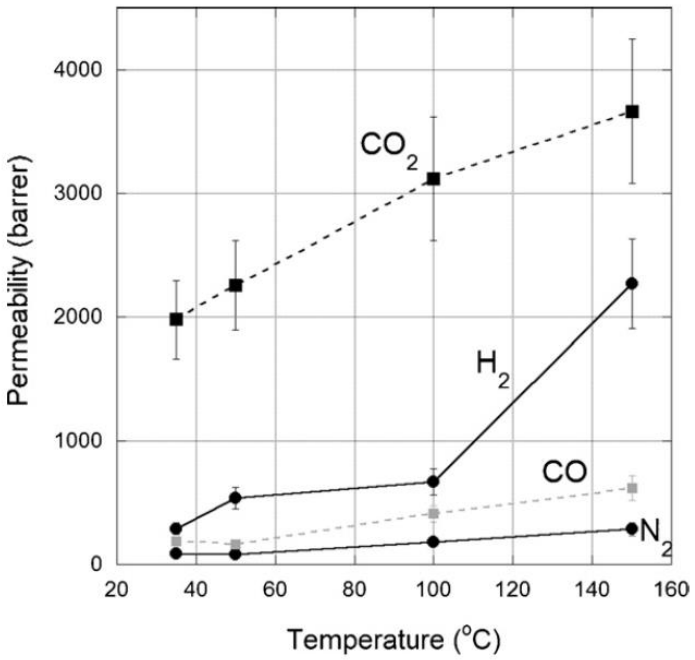

Figure 2-3: CO_2, H_2, CO gas permeabilities with pilot plant syngas feed over PDMS with 8.1 atm feed pressure [16]

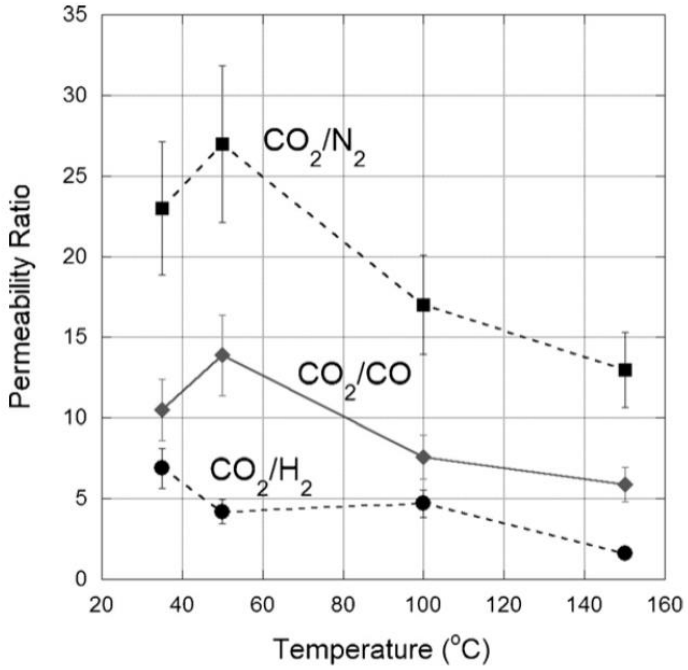

Figure 2-4: Permeability ratios of CO_2 to N_2, CO and H_2 with pilot plant syngas feed over PDMS with 8.1 atm feed pressure [16]

Merkel et al. tested a PDMS membrane under the same conditions as the PTMSP membrane reported earlier (23 °C and 2.4 atm feed pressure), with a simulated syngas mixture (CO_2, CO, H_2 and H_2S) [26]. They reported a CO_2 permeability of 3,200 Barrers and a CO_2/H_2 and CO_2/CO selectivity of 3.4 and 6.4, respectively [26]. This was the highest mixed gas CO_2 permeability reported in this paper, with a notable selectivity for CO_2 over CO. Bondar et al. reported a similar value for single gas permeability data for CO_2 and H_2 over PDMS [31]. Their reported CO_2 permeability was 3,100 Barrers, with a CO_2/H_2 selectivity of 4.3 at 35 °C.

Orme et al. [34] examined several membranes to select H_2 over CO_2, however they reported PDMS to have a single gas CO_2 permeability of 1,300 Barrers, and a CO_2/H_2 selectivity of approximately 3.5, at 30 °C.

2.4.1.1.3 SLMs (PDMS, PEGDME, PTMEGDAc and PPGDME)

Supported liquid membranes (SLM) are synthesized by filling the pores of a porous support with an organic liquid, such as a selective polymer [21]. This liquid is kept in the pores of the support by capillary forces, however under feed pressures that exceed these capillary forces, the membrane liquid can be lost from the support [41,42].

Barillas et al. [32] observed similar results for crosslinked PDMS and SLM PDMS membranes, with mixed feeds of CO_2 and H_2. The crosslinked membrane was commercially available and the SLM membranes were fabricated using a drop-coating technique to allow the polymer to diffuse into the porous support for approximately 3 hours. The SLMs were made with two polymers of different molecular weights (MW): 770 and 1,000 g/mol, respectively. A feed composition of CO_2, H_2 and argon (excluding CO) was used to test these materials at 37 °C and 1.1 atm of feed pressure [32]. Without CO in the feed, CO_2 and H_2 permeabilities were higher than those reported by Scholes et al. with a pilot plant syngas gas feed [16]. The increased permeabilities of crosslinked and two SLM PDMS membranes (from 1,517 to 2,848 Barrers) are likely due to a reduction in competitive sorption from CO.

Barillas et al. examined several SLMs, which exhibited particularly high selectivity of CO_2 over H_2 under mixed gas feeds at 37 °C and 1.1 atm of feed pressure. These polymers included PEGDME, PTMEGDAc and PPGDME [32]. Each polymer (like the PDMS SLMs discussed above) was drop-coated onto a porous support and patted dry to remove excess polymer. PEGDME demonstrated the highest selectivity of 11.1 from all the polymeric membranes tested by Barillas et

al. from this publication, with a CO_2 permeability of 814 Barrers. This approached the same order of magnitude of permeability observed with PDMS. PEGDME, PTMEGDAc and PPGDME SLMs were all at least twice as selective as PDMS, also reported by Barillas et al. at 37 °C with mixed gas feeds [32].

2.4.1.1.4 PEO-PBT

PEO-PBT nanostructured polymeric membranes were fabricated by Yave et al. [35] where they observed the effects of two specific polyethylene glycol ether spacers. The PEO-PBT multiblock copolymer incorporated PEG or functionalized PEGs acting as fillers or spacers, on a PAN (polyacrylonitrile) microporous support [35]. Yave et al. also determined the solubility and diffusivity coefficients of CO_2 and H_2 in these membranes. By introducing specific PEG spacers into the already CO_2 soluble PEO-PBT membrane, the diffusivity and solubility of CO_2 increases significantly and its permeability is increased five-fold from 150 (PEO-PBT) to 750 Barrers (PEO-PBT + PEG-DBE) for single gas experiments at 30 °C and 0.3 atm of feed pressure [35]. CO_2/H_2 selectivity also increased with permeability in this case from 10.8 (PEO-PBT) to 12.4 (PEO-PBT + polyethylene glycol-dibutyl ether spacers), which was the highest reported for CO_2/H_2 of the polymeric membranes examined in this work [35].

2.4.1.1.5 PEGMEA-PEGDA

Lin et al. [37] examined the effects of PEGDA in PEGMEA (the effect of fractional free volume with increases in PEGMEA content) on CO_2 separation from H_2 with binary feeds. The purpose of this was to determine the effect of ethylene oxide molecules on the selective solubility of CO_2 in the copolymer blend. For a PEGMEA:PEGDA polymer membrane in a 70:30 weight ratio, the permeability of CO_2 was approximately 440 Barrers at 35 °C and a feed pressure of 17 atm (an order of magnitude less than PDMS). However, it exhibited a relatively high CO_2/H_2 selectivity of 9.4. When this ratio was increased to 91:9 for PEGMEA:PEGDA and water was introduced to the CO_2:H_2 feed, CO_2 permeability increased to 515 Barrers at 22 °C and a feed pressure of 8 atm. CO_2/H_2 separation increased to 12 under these conditions. These values did not alter significantly when feed pressure was reduced to atmospheric, suggesting an applicable broad range of operating pressures [37].

2.4.1.1.6 PEG

Scholes et al. considered cross-linked PEG (polyethylene glycol) as a membrane for CO_2 separation from 'pilot plant' syngas [16]. These membranes were synthesized and crosslinked from polyethylene glycol methyl ether acrylate (Sigma-Aldrich) and cast as flat sheet membranes. Single and mixed gas permeabilities of CO_2 were reported to be 66 and 170 Barrers, respectively [16]. The mixed gas CO_2/H_2 selectivity was 2.9, which was lower than the selectivity reported for PDMS (4.0) with the same mixed gas feed. This specific membrane was tested at a minimum of 50 °C and 8.1 atm of feed pressure for mixed gas feeds. While PEG remained a CO_2 selective membrane for pilot plant syngas, it fell short in direct comparison to PDMS with respect to separation capabilities and permeabilities of CO_2 [16].

2.4.1.1.7 PEBAX

Scholes et al. tested a third polymeric, PEBAX membrane that was cast as flat sheet membrane [16]. This polymer experienced swelling during testing which reduced the membrane's ability to selectively separate CO_2 because of competitive sorption with a larger 'fractional free volume' for diffusion, increasing the permeability of all the components. However, even with polymer swelling, it only reached 135 Barrers for CO_2 permeability, in comparison to 1,993 Barrers for CO_2 permeability through PDMS in the same study with the feed mixture studied (at 35 °C and 8.1 atm). CO_2/H_2 and CO_2/CO selectivities were determined to be 1.6 and 1.9, respectively [16].

2.4.1.1.8 Polyimide

As part of graduate research, David [13] investigated a flat-sheet polyimide (PI) membrane. This polymer exhibits a high glass transition temperature of approximately 229 ºC, meaning it was used and tested in its glassy state at 30 ºC. Single gas experiments showed separation of H_2 over CO_2 and separation of CO_2 from CO only (with feed pressures of both 2.0 and 5.9 atm). Gas mixtures of H_2/CO_2, H_2/CO and $H_2/CO_2/CO/N_2$ were also tested over the membrane and these separation trends did not change. The polymer chains in this glassy state are rigid and if the free volume is not high, then the separation is dominated by molecular sieving where gas diffusivity properties direct the gas separation. The order of permeability for this polymer is correlated to the respective gas kinetic diameters (H_2 permeating over CO_2, CO) [13,39]. For this reason, it would not be desired to investigate polyimide further as a polymeric material for selective CO_2 separation.

2.4.1.1.9 Others

Barillas et al. [32] examined two other crosslinked PTMEGDA and PEGDA membranes for separation of CO_2 over H_2. These polymeric membranes were synthesized on a porous, nylon support. Both membranes were selective for CO_2 over H_2, and had selectivities greater than the PDMS in SLM form and crosslinked membrane reported by Barillas et al. [32]. However, they were not nearly as permeable for CO_2 during ternary gas feed experiments (CO_2, H_2 and Ar mixture) at 37 °C and feed pressure of 1.1 atm [32]. CO_2 permeabilities for PTMEGDA and PEGDA were reported to be 329 and 52 Barrers, respectively. CO_2/H_2 selectivities were measured to be 5.6 and 4.7 for PTMEGDA and PEGDA membranes, respectively [32].

Jha & Way [38] reported data for a MEE (methoxy-ethoxy-ethanol) substituted PPZ (polyphosphazene) membrane for separation of CO_2 and H_2. At 22 °C and 3.5 atm of feed pressure for single gas experiments, they reported a CO_2 permeability of approximately 71 Barrers, with a CO_2/H_2 ideal selectivity of 8.5. This paper also reported higher selectivities for MEE PPZ mixed matrix membranes which are discussed later. While this selectivity shows good potential, the CO_2 permeability reported is much lower than many of the other reported membranes in Table 2-5 and would not be expected to increase for binary or ternary gas feeds.

2.4.1.1.10 Polymeric Materials Overview

A selectivity-permeability plot is an efficient visual way to analyze basic membrane performance characteristics, based on previously tested and published membrane data. It can help determine where the selectivity and permeability trade off lies, and which membranes surpass the general trend. Figure 2-5 displays all of the polymeric membranes examined in this paper against a selectivity-permeability plot published by Lin et al. [37]. As mentioned in their paper, separations based strongly on size sieving membranes create a tradeoff between permeability and selectivity with a negative slope on the well-known Robeson plot. However, weakly size sieving membranes may achieve high permeability and selectivity (in the case of CO_2 separation from H_2) simultaneously [37]. This graph only considers separation of CO_2 from H_2 for the membranes outlined in Table 2-5, as this separation is studied in more detail compared to CO_2 separation from CO. The x-axis of the plot in Figure 2-5 was extended to fit additional data that would not have otherwise been visible. Solid circular data points indicate PDMS results and square/triangle points indicate other polymer results. By examining the characteristics of these organic materials, it is

evident that some polymers exhibit sufficient CO_2 permeability and selectivity to be considered for further testing for this separation. The better preforming membranes on this graph should fall in the upper right quadrant, where both permeability and selectivity are at a maximum.

PTMSP was the only point which fell outside the range of the preset graph, falling between 10^4 and 10^5 Barrers for CO_2 permeability. While it was extremely permeable for CO_2, it was not nearly as selective for CO_2 over H_2, as seen clearly in Figure 2-5 [26]. Almost all the PDMS data (circular data points) fell into the same area of this plot. Aside from PTSMP, it was the only polymer to achieve high CO_2 permeabilities observed in this collection of data. The highest CO_2/H_2 selectivity out of all the PDMS membranes reported here was for a mixed gas feed of 6.8 (from Scholes et al. [16]), which was promising, as other single gas experiments reported less selectivity for PDMS.

The data reported by Yave et al. (PEO-PBT polymer blends), definitely surpassed the general trend in Figure 2-5, with higher CO_2/H_2 single gas selectivities between 10 and 12, while less permeable than PDMS [35,36]. These PEO-PBT based membranes displayed great potential for further testing with binary and ternary gas feeds. The SLMs (PTMEGDAc, PEGDME, PPGDME) reported by Barillas et al. [32] also showed good potential when exposed to CO_2 and H_2 feeds with higher CO_2 permeabilities and CO_2/H_2 selectivities. SLMs may be more difficult to manufacture at a commercial level, so crosslinking these materials should be investigated.

Anything to the left of the aforementioned membranes observe a significant decrease in permeability because of the logarithmic scale. When selecting polymeric materials best suited for further testing, it is desired to select a membrane which has permeabilities that would bode well with a large-scale membrane system (as commercializing this technology is a goal, maximizing permeate flow rate is essential). These membranes, while still selective, do not possess CO_2 permeabilities great enough to justify pursuing further research for commercial use. These include PEBAX, PEG, PEGA, PEGMEA-PEGDA and PI.

Therefore, from the collected membrane information, PDMS would be an acceptable candidate to move forward with, as it showed higher CO_2 permeability and CO_2/H_2 selectivity under mixed gas conditions. It also showed great potential for CO_2/CO separation under mixed gas conditions with the highest CO_2/CO selectivity noted in Table 2-5 that was also selective for CO_2 over H_2 (unlike polyimide with higher CO_2/CO selectivities). It can also be purchased commercially, and is a widely-used material for other applications such as microfluidic devices, biosensors and

pervaporation [43–45]. Additionally, it is in its rubbery state at standard conditions, allowing its polymer chains to more easily come into contact with adsorbent particles, should it be used in a mixed matrix membrane [46]. The other promising candidates would either require further testing with binary and ternary feeds or crosslinking techniques as the current form would not scale up to a pilot or industrial scale with ease.

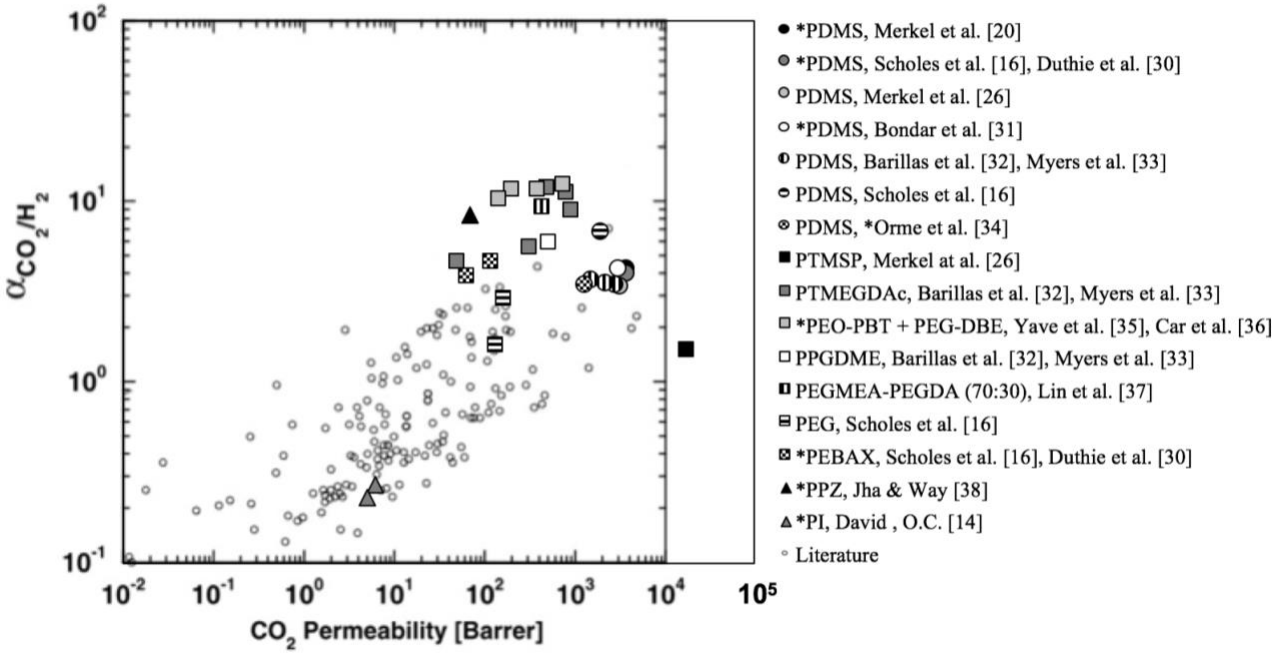

Figure 2-5: Selectivity-permeability CO_2/H_2 plot for published organic membranes listed in descending order of CO_2 permeability from Table 2-5; solid circular points indicate PDMS, solid square/triangle points indicate other polymers; * indicates single gas data [37]

2.4.1.2 Inorganic Membranes

Inorganic membranes are made from materials such as ceramics, zeolites, silica, and a variety of other metals. These materials are commonly microporous (pore sizes in the realm of Angstroms [Ä]) and used for gas separations when polymeric materials may not be able to withstand harsher operating environments, such as high temperatures and certain chemical interactions [14,47]. They are often used in a thin film configuration along a porous support where the support can be saturated with a selective material [48]. In contrast to polymers, inorganic membranes have pores sizes that are more structured and can be tailored very specifically. They also report high permeate flux which is often greater than polymeric membranes by many orders of magnitude.

While inorganic membranes can separate materials based purely on molecular size (referred to as molecular sieving), they are also capable of preferentially adsorbing select molecules, not exclusive of size due to preferential adsorption [49,50]. Molecules that experience larger dipole moments are subject to high heats of adsorption, which give them preferential adsorption capabilities. In general, CO_2 will often have preferential adsorption over lighter gases because of its larger quadrupole moment [17]. This mechanism becomes useful for the desired separation of this project, considering that CO_2 is a much larger molecule than H_2, but not quite as large as CO. This could allow CO_2 to be preferentially adsorbed over its syngas counterparts, and make up the majority of the composition in the permeate stream for an inorganic membrane process [51–53]. The transport through the membrane starts with adsorption on the pore surface, continues with diffusion through the pore and finishes with desorption into the permeate stream. During diffusion through the pore, sorption of the more condensable penetrant is expected to prevent the transport of the less condensable component [14].

The main challenges associated with inorganic membranes are cost and fabrication. These materials are much more expensive than their polymeric counterparts and the time-consuming process of making these membranes make them less attractive from a commercial stand point. However, inorganic, adsorbent membranes offer advantages over polymeric membranes that cannot be overlooked. These advantages include chemical and thermal stability and resistance to high temperatures and pressures. Polymeric membranes can physically degrade and lose structural integrity much more easily than inorganic materials [54].

Table 2-7 outlines the abbreviated names of the selective, inorganic membranes presented in the summary for reference. Table 2-8 outlines several inorganic membranes experimentally tested and published for CO_2, H_2 and/or CO separation, arranged in descending order of CO_2 permeance. It should be noted from the inorganic membranes presented in this summary, that under single gas experiments, some materials selectively permeate H_2 more than CO_2, while others permeate CO_2 more than H_2. However, when exposed to binary or ternary gas feeds, these materials prove to all selectively separate CO_2 from both CO and H_2. This shift in separation performance is unlike those presented in the polymeric section of this paper, as binary and ternary feeds typically introduce competitive sorption between penetrant gases which inhibits the separation capabilities of polymeric membranes. However, MFI adsorbents like silicalite and ZSM-5 can preferentially adsorb CO_2 over H_2 and CO when presented in binary or ternary feeds, where in single gas experiments smaller

molecules like H_2 may have higher permeate flux than larger molecules like CO_2. Seeing as the actual application of these materials involves the presence of a mixed gas feed, the focus of the data presented lies on the binary and ternary published work.

Permeate data is presented in the units of permeance, as this is the most common unit used to describe inorganic membranes in literature. Permeance is displayed in the unit of mol m^{-2} s^{-1} Pa^{-1} for homogeneity, as most of the collected permeate data was reported in this unit. To keep all units consistent for display in Table 2-8, some unit conversions were required. When assumptions were needed in these cases, room temperature was assumed to be 21 ºC (294 K), and when permeate pressures were not clearly stated, atmospheric pressure (1 atm, 101,325 Pa) was used.

Table 2-7: Inorganic materials used in the inorganic membranes from literature

Inorganic Name	Full Chemical Name
B-ZSM-5	Boron ion-exchanged ZSM-5
Ba-ZSM-5	Barium ion-exchanged ZSM-5
Li-ZSM-5	Lithium ion-exchanged ZSM-5
Na-A	Sodium ion-exchanged zeolite A
Na-Y	Sodium ion-exchanged zeolite Y
Na-ZSM-5	Sodium ion-exchanged ZSM-5
SAPO-34	Silico-alumino-phosphate
Silica	SiO_2
Silicalite	Silica polymorph
ZSM-5	Zeolite socony mobil-5

Table 2-8: Permeances and selectivities from literature for CO_2 selective inorganic membranes in descending order of CO_2 permeance

Inorganic	**CO_2 Permeance** [mol m^{-2} s^{-1} Pa^{-1}]	**H_2 Permeance** [mol m^{-2} s^{-1} Pa^{-1}]	**CO Permeance** [mol m^{-2} s^{-1} Pa^{-1}]	**CO_2/H_2**	**CO_2/CO**	**Temp.** [°C]	**Feed P.** [atm]	**Ref.**
Silicalite	9.30×10^{-6} in CO_2/H_2	4.00×10^{-7} in CO_2/H_2		23		23	10	[55]
Silicalite	7.00×10^{-6} in CO_2/H_2	1.30×10^{-7} in CO_2/H_2		52		2	10	[55]
Silicalite	5.50×10^{-6} in $CO_2/CO/H_2$	3.30×10^{-7} in $CO_2/CO/H_2$	8.00×10^{-7} in $CO_2/CO/H_2$	17	7	23	22	[55]
Silicalite	4.60×10^{-6} *	8.63×10^{-6} *	3.86×10^{-6} *	0.5 [I]	1.2 [I]	25	1.4	[56]
Silicalite	4.50×10^{-6} in $CO_2/CO/H_2$	1.30×10^{-7} in $CO_2/CO/H_2$	3.50×10^{-7} in $CO_2/CO/H_2$	35	12	2	15	[55]
Silicalite	3.50×10^{-6} *	1.60×10^{-5} *		0.2 [I]		22	35	[55]
Silicalite	2.13×10^{-6} in CO_2/H_2	1.78×10^{-7} in CO_2/H_2		12		0	5.0	[57]
Silicalite	2.05×10^{-6} in CO_2/H_2	1.50×10^{-7} in CO_2/H_2		14		23	25	[58]
Li-ZSM-5	1.80×10^{-6} in $CO_2/H_2/H_2O$	3.80×10^{-7} in $CO_2/H_2/H_2O$		4.9 [^]		22	1.0	[47]
Silicalite	1.15×10^{-6} in CO_2/H_2	5.00×10^{-8} in CO_2/H_2		23		3	25	[58]
Ba-ZSM-5	1.08×10^{-6} in CO_2/H_2	9.91×10^{-7} in CO_2/H_2		1.1		22	1.0	[47]
Silicalite	1.05×10^{-6} in $CO_2/H_2/H_2O$	5.00×10^{-7} in $CO_2/H_2/H_2O$		2.9 [^]		22	1.0	[47]
Na-ZSM-5	1.04×10^{-6} in $CO_2/H_2/H_2O$	2.20×10^{-7} in $CO_2/H_2/H_2O$		4.1 [^]		22	1.0	[47]
Silicalite	1.03×10^{-6} in CO_2/H_2	5.15×10^{-7} in CO_2/H_2		2.0		0	1.0	[57]

Ba-ZSM-5	1.01 x 10^{-6} in $CO_2/H_2/H_2O$	2.05 x 10^{-7} in $CO_2/H_2/H_2O$		6.2 ^		22	1.0	[47]
Na-Y	7.60 x 10^{-7} in CO_2/H_2	2.70 x 10^{-8} in CO_2/H_2		28		35	1.0	[59,60]
ZSM-5 (high silica)	5.90 x 10^{-7} *	2.00 x 10^{-7} *	1.40 x 10^{-7} *	3.0 I	4.1 I	21	$\leq$ 1.1	[61]
ZSM-5	5.50 x 10^{-7} in CO_2/N_2					25	1.0	[62]
Na-ZSM-5	3.89 x 10^{-7} in CO_2/N_2					25	$\leq$ 30	[63]
Na-A/carbon composite	3.39 x 10^{-7} *					21	1.0	[64]
B-ZSM-5	3.21 x 10^{-7} in CO_2/N_2					25	$\leq$ 30	[63]
Silica composite	2.54 x 10^{-7} *	4.70 x 10^{-7} *		0.5 I		25	1.0 – 2.0	[65]
SAPO-34	1.05 x 10^{-7} *	4.50 x 10^{-8} *		2.3 I		2	2.2	[66]
Silicalite	9.20 x 10^{-8} in $CO_2/CO/H_2$	1.50 x 10^{-8} in $CO_2/CO/H_2$	1.00 x 10^{-8} in $CO_2/CO/H_2$	6.1 ^	9.2 ^	25	3.0	[51]
Silicalite	8.50 x 10^{-8} *	2.40 x 10^{-7} *	6.50 x 10^{-8} *	0.4 I	1.3 I	25	3.0	[51]
Silicalite	5.00 x 10^{-8} *	1.0 x 10^{-7} *		0.5 I		25	1.0	[67]

** Indicates single gas permeance*
I Indicates ideal selectivity (single gas permeance ratio)
^ Indicates averaged permeance ratios using additional data from reference
Selectivities are expressed as permeance ratios in the table above

2.4.1.2.1 Silicalite

Several articles have been published focused on using silicalite as a selective inorganic material to separate CO_2 from gas mixtures, proving it to be a popular and well-studied material for this separation. These MFI type zeolites are of particular interest due to their pore size and ease of synthesis from a variety of sources [68].

Yildirim and Hughes [65] published single gas permeance data for a silicalite membrane prepared using a dip-coat method on an alumina tubular support. The focus of this study was for H_2 separation from CO_2 and other coal gasification products (CO, N_2, CH_4). CO_2/H_2 ideal selectivity was reported to be 0.5 for single gas experiments with a CO_2 permeance of 2.54 x 10^{-7} mol s^{-1} m^{-2} Pa^{-1}. Algieri et al. [56] and Burggraaf et al. [67] reported the same CO_2/H_2 selectivity of 0.5 for single gas experiments using silicalite membranes synthesized on alumina tubular and disc supports, respectively. Algieri et al. [56] reported a much higher CO_2 permeance of 4.60 x 10^{-6} mol s^{-1} m^{-2} Pa^{-1} while Burggraaf et al. [67] reported a lower CO_2 permeance of 5.00 x 10^{-8} mol s^{-1} m^{-2} Pa^{-1}. Algieri et al. [56] also tested CO in experiments, and reported a CO_2/CO selectivity of 1.2 for single gas experiments. Kanezashi and Lin [51] published data from both single and ternary gas feed experiments performed with a silicalite, alumina supported, disc membrane. With single gas experiments, ideal selectivities favoured H_2 over CO_2, and CO_2 over CO (CO_2/H_2 of 0.4 and CO_2/CO of 1.3). However, during ternary gas experiments (CO_2/CO/H_2 in equal molar ratios), H_2 and CO permeances dropped while CO_2 permeance increased. This led to increased selectivities of 6.1 and 9.2 for CO_2/H_2 and CO_2/CO, respectively [51]. CO_2 therefore has preferential adsorption over CO and H_2 at 25 ºC, as seen in Figure 2-6.

Akhtar et al. [57] examined CO_2:H_2 (1:1) binary separations at 0 ºC over a silicalite, alumina supported membrane, performing experiments from 1 to 5 bar. CO_2 permeance and CO_2/H_2 selectivity was higher at 5 bar, reported to be 2.13 x 10^{-6} mol s^{-1} m^{-2} Pa^{-1} and 12, respectively. Grahn and Hedlund [58] reported binary CO_2:H_2 (1:1) permeance data for two temperatures, with a silicalite membrane prepared on an alumina disc support. CO_2 permeance dropped from 2.05 x 10^{-6} to 1.15 x 10^{-6} mol s^{-1} m^{-2} Pa^{-1} with a 20 ºC decrease in temperature (23 to 3 ºC). CO_2/H_2 selectivity increased from 23 to 14, with the same 20 ºC decrease in temperature. Therefore, higher operating temperature yielded better CO_2 permeance and lower temperatures yielded better selectivity over H_2. Lindmark and Hedlund [47] explored binary (CO_2:H_2, 1:1) and ternary (CO_2:H_2:H_2O, 49:49:2) experiments over silicalite, alumina disc membranes. At 22 ºC for binary experiments, silicalite had

a selectivity just over 1 for CO_2/H_2. However, with ternary experiments including H_2O, this membrane reported a selectivity of 2.9 and a CO_2 permeance of 1.05×10^{-6} mol s^{-1} m^{-2} Pa^{-1}.

Lastly, Sandström et al. [55] reported high permeance data for pure, binary and ternary experiments over a silicalite, alumina disc membrane. While this membrane did not display selectivity over H_2 with single gas experiments, it did exhibit a higher CO_2 permeance of 3.50×10^{-6} mol s^{-1} m^{-2} Pa^{-1} at 22 ºC and a feed pressure of 35 atm. Binary experiments at 23 ºC, feed pressures of 10 atm and with an equimolar CO_2/H_2 feed, presented the highest CO_2 permeance and second highest CO_2/H_2 selectivity noted in this collection of published data. Lower temperatures (2 ºC) proved to make this silicalite membrane less permeable and more than twice as selective as single gas experiments. Ternary experiments displayed the same trends in terms of temperature effects on permeance and selectivities. CO_2/H_2 selectivities were the highest for ternary gas feeds observed from the data in Table 2-8. CO_2/CO selectivities were also among the highest for ternary gas feeds with a silicalite membrane (12 at 2 ºC and 15 atm). Kanezashi and Lin [51] reported a comparable selectivity of 9.2 (25 ºC and 3 atm) but with significantly lower gas permeance, also with a silicalite membrane. Sandström et al. [55] used a membrane film thickness of 0.5 µm while Kanezashi and Lin [51] reported their membrane film thickness to be 7 µm. A thinner membrane film would help to explain why Sandström et al. [55] reported much higher gas permeances than Kanezashi and Lin [51] by decreasing resistance for gas transport. A thicker film could also dictate higher selectivity, which was observed in the work reported by Kanezashi and Lin [51].

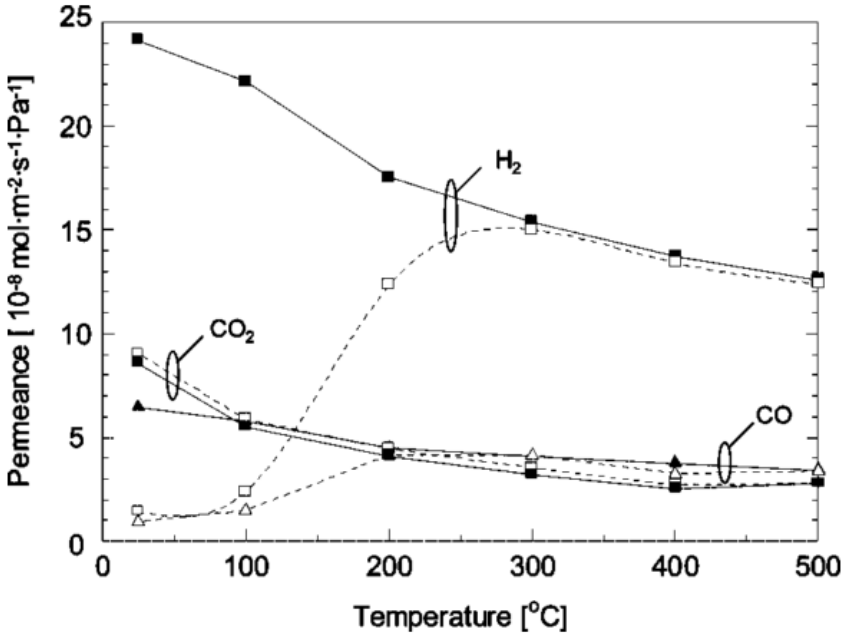

Figure 2-6: Mixed gas molar permeances through a silicalite membrane from 25 to 500 °C; closed symbols on solid lines are pure gas permeances, open symbols on dashed lines are ternary gas component permeances [51]

2.4.1.2.2 ZSM-5

ZSM-5 type membranes are commonly tested materials used for CO_2 separation. Shin et al. [62] synthesized tubular ZSM-5 membranes and reported a CO_2 permeance of 5.50 x 10^{-7} mol s^{-1} m^{-2} Pa^{-1} from a binary CO_2/N_2 equimolar feed (at 25 ºC and 1.0 atm of feed pressure). Sebastián et al. [63] reported similar CO_2 permeances for a binary CO_2/N_2 feed with sodium and boron ion-exchanged ZSM-5 membranes at 25 ºC. Bonhomme et al. [61] reported a similar CO_2 single gas permeance for a high silica ZSM-5 membrane (at 21 ºC) with ideal selectivities of 3.0 and 4.1 for CO_2/H_2 and CO_2/CO, respectively. Lindmark and Hedlund [47] tested three ion-exchanged ZSM-5 membranes (Li, Na, Ba) with ternary gas feeds of $CO_2/H_2/H_2O$ (49:49:2). Li-ZSM-5 had the highest reported CO_2 permeance of these membranes with 1.80 x 10^{-6} mol s^{-1} m^{-2} Pa^{-1}, while Ba-ZSM-5 had the highest CO_2/H_2 selectivity of 6.2 (at 22 ºC and 1.0 atm of feed pressure).

2.4.1.2.3 SAPO-34

Li et al. [66] fabricated and tested a SAPO-34 zeolite membrane on an alumina support for CO_2 and H_2 single gas permeances. This membrane was tested at 2 ºC with a feed pressure of 2.2 atm. CO_2 and H_2 permeance was approximately 1.05 x 10^{-7} and 4.50 x 10^{-8} mol s^{-1} m^{-2} Pa^{-1},

respectively, with an ideal CO_2/H_2 selectivity of 2.3. Therefore, it could not achieve the same high separation many of the silicalite materials presented in this summary (seen in Table 2-8).

2.4.1.2.4 A and Y-Type Zeolites

Zhou et al. [64] synthesized a novel Na-A/carbon nanocomposite membrane on an alumina support. They reported a single gas CO_2 permeance of 3.39 x 10^{-7} mol s^{-1} m^{-2} Pa^{-1} at room temperature (assumed to be 21 ºC). This material would have to be exposed to H_2 and CO to determine binary and ternary permeances and selectivities. However, only single gas data was available from this work and the reported CO_2 permeance was two orders of magnitude lower than others reported for silicalite.

Guan et al. [59] examined a Na-Y membrane made on an alumina tubular support. CO_2/H_2 equimolar binary mixtures were performed at 35 ºC with an atmospheric feed pressure. The CO_2 permeance and CO_2/H_2 selectivity were reported to be 7.60 x 10^{-7} mol s^{-1} m^{-2} Pa^{-1} and 28, respectively. This was an especially high separation, comparable to the better performing silicalite membranes, with a lower CO_2 permeance.

2.4.1.2.5 Inorganic Materials Overview

From the summary shown in Table 2-8, it is evident that silicalite is not only one of the most tested and published membranes, but also one of the better performing. While some of these materials did not show selectivity for CO_2 over H_2 or CO with single gas experiments, when exposed to binary and even ternary feeds, the opposite was true. Preferential adsorption of CO_2 over H_2 and/or CO in the pores of the material would dictate this type of change in separation. Lower temperatures proved to facilitate higher selectivities than those closer to room temperature. This is likely due to increased CO_2 adsorption at lower temperatures, in turn increasing the selectivity of the membrane [55]. The highest CO_2 permeance from this summary was 9.30 x 10^{-6} mol s^{-1} m^{-2} Pa^{-1} over a silicalite membrane with a CO_2/H_2 binary feed [55]. Translating to the unit of permeability, this would be approximately 14,068 Barrers (assuming a selective membrane thickness of 0.5 µm reported by Sandström et al. [55]). This is an exceptionally high permeability, when compared to many of the polymeric materials examined earlier. The highest CO_2/H_2 and CO_2/CO selectivities reported for the inorganic membranes examined in this summary were 52 and 12, respectively [55]. This was a much higher separation of CO_2 from H_2 than those by the polymeric materials discussed

previously. CO_2 separation from CO, however, was comparable to PDMS selectivities [16]. Additionally, Na-Y shows good potential under binary (CO_2/H_2) conditions with a selectivity of 28, favouring CO_2 separation from H_2, while significantly less permeable than the silicalite membranes examined in this summary.

2.4.1.3 Mixed Matrix Membranes

Mixed matrix membranes (MMMs) combine the properties of inorganic and organic membrane materials. These membranes typically use polymeric material as a medium to house dispersed, inorganic, and selective adsorbent particles. Adsorbents offer higher chemical, thermal and mechanical strength and uniform pore size distribution, where polymeric materials offer gas solubility separation preferences and structural flexibility as part of the matrix [69,70]. Mixed matrix membranes make up a unique area in the membrane field, as they are a combination of two different materials. Inorganic, adsorbent particles are dispersed in a polymer matrix to create a uniform, novel and ultimately more successful membrane. The abbreviated polymeric and inorganic materials discussed in this section are defined in Table 2-9. One of the biggest challenges associated with MMMs are the void spaces created at the interface between the particles and polymer due to poor mixing or incompatibility between the adsorbent and polymer interface. There are several ways to overcome this, such as surface modification of the particles (adding molecular groups to the adsorbent structures that adhere to the polymer chains) [71]. Even though it can be difficult to manufacture these membranes on a larger scale, the effective cost and increase in membrane performance is attractive [69].

Table 2-9: Polymeric and inorganic materials used in the mixed matrix membranes from literature

Polymer Name	**Full Chemical Name**
MEE PPZ	Methoxy ethoxy ethanol substituted polyphosphazene
PEBAX	Poly ether block amides
PDMS	Poly dimethyl siloxane
PIS	Poly(imide siloxane)
PTMSP	Poly(1-trimethyl-1-propyne)
Inorganic Name	**Full Chemical Name**
AlPO	Alumino-phosphate
CNTs	Carbon nanotubes
MgO	Magnesium oxide
SAPO-34	Silico-alumino-phosphate
ZIF-8/11	Zeolite imidazolate framework
ZSM-5	Zeolite socony mobil-5

Mixed matrix membranes (MMMs) combine the advantages of both organic and inorganic materials; the simplicity of polymers and the robustness of inorganics. Thus, they combine transport mechanisms of both materials. The Maxwell model has been deemed an effective and widely used tool for predicting MMM performance [46]. It is more simply an adaptation of "thermal or electrical conductivity models in composite materials" [70,72]. It assumes steady state for a dilute suspension of (inorganic) spheres in a (polymer) matrix [46,72,73]. It models effective permeability as a function of the volume fractions and individual permeabilities of both the continuous phase (polymer) and the dispersed phase (spherical, adsorbent particle). The effective permeability is optimal (maximized) when both phases operate in parallel with the direction of gas flow through the membrane (feed to permeate). Table 2-10 outlines several polymeric and inorganic membrane combinations that favour CO_2 separation over H_2 and CO, arranged in descending order of CO_2 permeability. The subsequent sections reference the performance parameters outlined in this table.

Table 2-10: Permeabilities and selectivities from literature for CO_2 selective mixed matrix membranes in descending order of CO_2 permeability

Polymer	Inorganic	CO_2 Permeability	H_2 Permeability	CO_2/H_2	Temp.	Feed P.	Ref.
		[Barrers]	[Barrers]		[°C]	[atm]	
PTMSP	MgO (20 vol %)	100,000 [I]	70,000 [I]	1.40 [I]	35	5.0	[74]
PDMS	ZSM-5 (66 wt %)	11,648 [I]					[46]
PEBAX	ZIF-11 (10 wt %)	213 [I]	25 [I]	8.52 [I]	20	2.0	[75]
PIS	CNTs (2 wt %)	191 [I]	79.6 [I]	2.40 [I]	35	4.0	[76]
	CNTs (10 wt %)	191 [I]	79.2 [I]	2.42 [I]	35	4.0	[76]
PEBAX	ZIF-8 (20 wt %)	140 [I]	13 [I]	10.5 [I]	25	1.0	[77]
MEE PPZ	SAPO-34 (22 wt %)	48 [I]	6.58 [I]	7.30 [I]	22	3.5	[38]
	SAPO-34 (22 wt %)	45 in CO_2/CH_4 or N_2			22	3.5	[38]
MEE PPZ	AlPO (22 wt %)	43 [I]	3.60 [I]	12.0 [I]	22	3.5	[38]
	AlPO (22 wt %)	39 in CO_2/H_2	4.70	8.30	22	4.2	[38]

[I] Indicates single gas data
** Calculated H_2 permeability, assuming ideal selectivity permeance ratio*

2.4.1.3.1 PTMSP and MgO

Matteucci et al. [74] investigated MgO nanoparticles in PTMSP with a 20 vol % loading. This nanocomposite membrane exhibited exceptionally high gas permeabilities (at least one to four orders of magnitudes greater than most of the permeabilities discussed in Table 2-10). This work explored the existence of membrane defects with increasing particle loading in PTMSP. They noted no change in gas permeability with pressure (implying no large defects), however upon examining ideal selectivity with respect to nanoparticle loading, it was evident there was change in the transport flow model (suggesting some defects were present). Single gas permeabilities of CO_2 and H_2 were reported as approximately 100,000 and 70,000 Barrers at 35 °C and 5 atm, respectively [74]. At a 20 vol % loading of MgO in PTSMP, the CO_2/H_2 ideal selectivity was reported to be 1.40 [74].

2.4.1.3.2 PDMS and ZSM-5

Hussain and König [46] examined ZSM-5 dispersed in PDMS, for the separation of CO_2 from N_2. From examining Table 2-5 and Table 2-8, both PDMS and ZSM-5 have been successfully investigated individually for separation of CO_2 from H_2 and CO. This paper examined weight loadings of ZSM-5 in PDMS from 0 to 66 wt %, where any amount greater would lead to structural instability and a dramatic decrease in separation [46]. This composite membrane (at 66 wt % loading of ZSM-5 in PDMS) exhibited high single gas permeabilities, specifically for CO_2 with 11,648 Barrers. These authors reported a selectivity of 11.1 for CO_2 over N_2 [46]. It is expected that ZSM-5 would selectively allow CO_2 to permeate over CO and H_2 when exposed to this ternary mixture.

2.4.1.3.3 PEBAX and ZIF-11, ZIF-8

Ehsani & Pakizeh [75] published single gas data with a PEBAX and ZIF-11 mixed matrix membrane. They reported data for CO_2 and H_2 permeability and CO_2/H_2 selectivity for 0 to 70 wt % loading of ZIF-11 in PEBAX. The 10 wt % loading of ZIF-11 in PEBAX had the highest reported ideal selectivity of approximately 8.52. The CO_2 permeability reported for this loading was approximately 213 Barrers (at 20 ºC), which was significantly less than the CO_2 permeabilities reported for PTMSP and PDMS mixed matrix membranes [46,74,75].

Li et al. [77] investigated PEBAX and ZIF-8 composite membranes from 0 to 20 wt % loading in the polymer matrix. They modified the ZIF-8 particles with an ionic liquid to further enhance the membranes performance, by improving the compatibility between the zeolite and polymer to eliminate defects and void spaces. They reported a single gas CO_2 permeability of 140 Barrers, with a CO_2/H_2 selectivity of 10.5, with a 20 wt % loading at 25 ºC [77].

2.4.1.3.4 PIS with CNTs

Carbon nanotubes (CNTs) were used in a poly(imide siloxane) copolymer to construct a mixed matrix membrane analyzed for CO_2 and H_2 separation [76]. The CNTs were incorporated into the copolymer with 2 and 10 wt % loadings, with no evidence of voids in the membrane matrix. There was little difference in gas permeability and selectivity data reported for between weight loadings of CNT in PIS at 35 ºC. Ideal selectivities were 2.40 and 2.42 for 2 and 10 wt % of CNTs, respectively. Single gas CO_2 permeabilities were virtually identical at 191 Barrers, rounded up for each MMM tested. However, these permeabilities and selectivities were too low for this material to be considered further due to the performance characteristics of the other materials presented.

2.4.1.3.5 MEE PPZ with SAPO-34, AlPO

Jha & Way [38] examined a methoxy ethoxy ethanol substituted (MEE) polyphosphazene (PPZ) polymer with AlPO and SAPO-34 inorganic particles. Each MMM (SAPO-34 and AlPO) reported similar CO_2 permeabilities with a 22 wt % loading, ranging from 39 to 48 Barrers, tested at 22 ºC [38]. However, CO_2/H_2 selectivities were the highest at 12.0 for single gas experiments and 8.30 for CO_2:H_2 equimolar binary gas data for the AlPO membrane. Out of the materials investigated in this work, these membranes reported the lowest gas permeabilities, five orders of magnitude less than the highest reported CO_2 permeability in Table 2-10.

2.4.1.3.6 Mixed Matrix Membrane Overview

The selectivity-permeability plot [37] was used again to examine the mixed matrix membranes outlined in this chapter against other published and studied membrane data for CO_2/H_2 separation. It was extended appropriately along the x-axis to accommodate greater CO_2 permeabilities. It is obvious that the PTMSP-MgO membrane had exceptionally high CO_2

permeability in comparison to the other MMMs examined including the published data for polymeric membranes on this graph. All the mixed matrix membranes (except for PIS-CNT and PTMSP-MgO) surpassed the general trend of this plot, reaching higher selectivities and suggesting minimal defects during synthesis. The membranes that did show potential in Figure 2-7 were not as permeable as many of the polymeric and inorganic membranes discussed in this summary. However, they serve as a good starting point to observe the potential of mixed matrix membranes for CO_2 separation from H_2 and CO for future optimization.

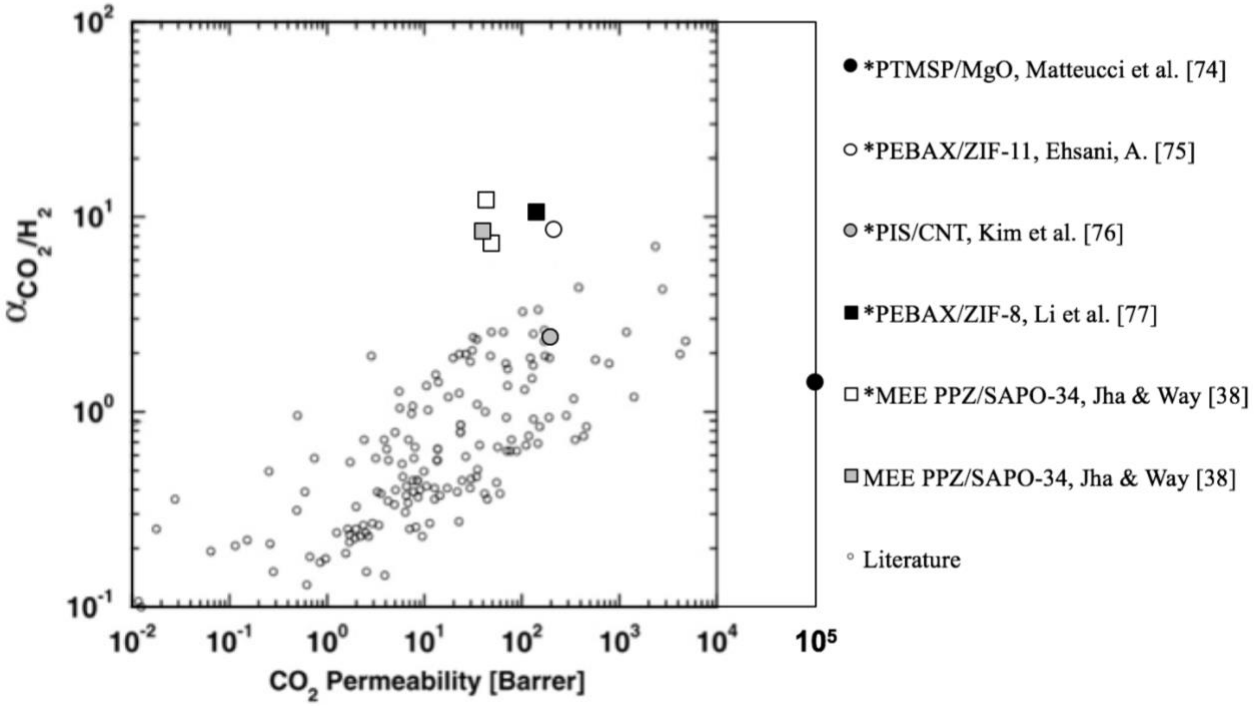

Figure 2-7: Selectivity-permeability CO_2/H_2 plot for mixed matrix membranes listed in descending order of CO_2 permeability from Table 2-10; * indicates single gas data [37]

2.5 CONCLUSIONS AND FUTURE WORK

A review was performed, where several organic, inorganic and mixed matrix membranes were examined for their ability to successfully separate CO_2 from syngas. Several polymeric membranes showed good potential, including PDMS, PEO-PBT based polymers, PEGMEA-PEGDA hybrids and SLMs in the form of PTMEGDAc and PEGDME. The inorganic membrane overview focused on MFI structured zeolites, where silicalite showed the greatest potential; Na-Y also displayed great separation capabilities. Of the mixed matrix membranes reviewed, PEBAX

with ZIF-8/ZIF-11 and MEE PPZ with SAPO/AlPO did show potential in terms of CO_2 separation over H_2. However, these composite materials were not nearly as permeable as most of the polymeric and inorganic membranes also examined and would need to be tested with CO. Of the materials reviewed in this paper, only a few were available commercially (mostly in the polymeric realm), making synthesis and scale-up visions more challenging. However, these obstacles can be overcome through further research and development.

2.6 ACKNOWLEDGEMENTS

The authors would like to acknowledge the financial support received from the University of Ottawa, NSERC (Natural Sciences and Engineering Research Council of Canada), NRCan (National Resources Canada), MITACS (Mathematics of Information Technology and Complex Systems) and Phoenix Canada Oil Company Ltd.

2.7 NOMENCLATURE

Symbol	Description	Unit
A	Membrane area	cm^2
D_i	Diffusivity of component i	cm^2/s
F	Flow rate of feed stream to membrane	g/s, kg/h
L	Membrane thickness	cm
MW	Molecular weight	g/mol
n_i	Volumetric flow of component i in permeate	cm^3 (STP)/s
P	Flow rate of permeate stream	g/s, kg/h
P_i	Permeability of component i	Barrer
$\overline{P}_i$	Permeance of component i	GPU, mol m^{-2} s^{-1} Pa^{-1}
R	Flow rate of retentate stream	g/s, kg/h
S_i	Solubility of component i	$\frac{cm^3\ (STP)}{cm^3 \cdot atm}$
X_i	Mole fraction of component i in feed stream	Dimensionless
Y_i	Mole fraction of component i in permeate stream	Dimensionless
Z_i	Mole fraction of component i in retentate stream	Dimensionless
$\alpha_{A/B}$	Actual selectivity of components A and B	Dimensionless
$\alpha^*_{A/B}$	Ideal selectivity of components A and B	Dimensionless

2.8 ABBREVIATIONS AND SYMBOLS

Symbol	Description
A	Component A
AlPO	Alumino-phosphate
B	Component B; Boron
Ba	Barium
BE	Butyl ether
B-ZSM-5	Boron ion-exchanged ZSM-5
Ba-ZSM-5	Barium ion-exchanged ZSM-5
CCS	Carbon capture and storage
CNTs	Carbon nanotubes
DBE	Dibutyl ether
EOR	Enhanced oil recovery
EI	Emission-intensive
FAU	Faujasite zeolite
FT	Fischer-Tropsch
GHG	Greenhouse gas
GPU	Gas permeation unit
Li	Lithium
Li-ZSM-5	Lithium ion-exchanged ZSM-5
MEE	Methoxy ethoxy ethanol
MEE PPZ	Methoxy ethoxy ethanol substituted poly phosphazene
MFI	Mordenite framework inverted
MgO	Magnesium oxide
MMM	Mixed matrix membrane
Na	Sodium
Na-A	Sodium ion-exchanged A-type zeolite
Na-Y	Sodium ion-exchanged Y-type zeolite
Na-ZSM-5	Sodium ion-exchanged ZSM-5
PAN	Poly acrylonitrile
PBT	Poly butylene terephthalate
PDMS	Poly dimethyl siloxane
PEBAX	Poly ether block amide
PEG	Poly ethylene glycol
PEGA	Poly ethylene glycol acrylate
PEGDA	Poly ethlyene glycol diacrylate
PEGDME	Poly ethylene glycol dimethyl ether
PEG-BE	Poly ethylene glycol + Butyl ether spacers
PEG-DBE	Poly ethylene glycol + Dibutyl ether spacers
PEGMEA-PEGDA	Poly ethylene glycol methylether acrylate – Poly ethlyene glycol diacrylate
PEO	Poly ethylene oxide

PEO-PBT	Poly ethylene oxide – poly butylene terephthalate
PEO-PBT + PEG	Poly ethylene oxide – poly butylene terephthalate + Poly ethylene glycol
PEO-PBT + PEG-BE	Poly ethylene oxide – poly butylene terephthalate + Poly ethylene glycol + Butyl ether spacers
PEO-PBT + PEG-DBE	Poly ethylene oxide – poly butylene terephthalate + Poly ethylene glycol + Dibutyl ether spacers
PI	Polyimide
PIS	Poly(imide siloxane)
PPGDME	Poly propylene glycol di-acetate
PPZ	Poly phosphazene
PTMEGDA	Polytetramethylene ether glycol diacrylate
PTMEGDAc	Polytetramethylene ether glycol diacetate
PTMSP	Poly(1-trimethylsilyl 1-propyne)
SAPO-34	Silico-alumino-phosphate
SI	International System of Units (metric)
SLM	Supported liquid membrane
WGS	Water Gas Shift
ZIF-8/11	Zeolite imidazolate framework
ZSM-5	Zeolite socony mobil-5

2.9 REFERENCES

[1] S.A. Rackley, Carbon Capture and Storage, 1st ed., Butterworth-Heinemann, 2009.

[2] S.I. Seneviratne, M.G. Donat, A.J. Pitman, R. Knutti, R.L. Wilby, Allowable CO_2 emissions based on regional and impact-related climate targets, Nature. 529 (2016) 477–483.

[3] K. Zickfeld, M. Eby, H.D. Matthews, A.J. Weaver, Setting cumulative emissions targets to reduce the risk of dangerous climate change., in: Proc. Natl. Acad. Sci. U. S. A., 2009: pp. 16129–16134.

[4] S. Shelley, Capturing CO_2: Membrane Systems Move Forward, Chem. Eng. Prog. 105 (2009) 42–47.

[5] J. Gibbins, H. Chalmers, Carbon capture and storage, Energy Policy. 36 (2008) 4317–4322.

[6] Environment and Climate Change Canada - National Inventory Report 1990-2014: GHG Sources and Sinks in Canada, 2016.

[7] R.E. Dickerson, H.B. Gray, G.P. Haight, Chemical Principles, in: 3rd ed., The Benjamin/Cummings Publishing Company, Inc., Menlo Park, CA, 1979: pp. 662–692.

[8] S. Bouzalakos, M. Maroto-Valer, Overview of Carbon Dioxide (CO_2) Capture and Storage Technology, in: M.M. Maroto-Valer (Ed.), Woodhead Publishing, 2010: p. 560.

[9] T.D.T. Ngoc, E. Konstantinovskaya, R. Lefebvre, M. Malo, Geotechnical characterization of deep saline aquifers for CO_2 geological storage in the Bécancour region, Québec, Canada,

Geotech. Sustain. Dev. (2011) 623–632.

[10] US Department of Energy: Office of Fossil Energy (ENERGY.GOV | Enhanced Oil Recovery), (n.d.). http://energy.gov/fe/science-innovation/oil-gas-research/enhanced-oil-recovery (accessed April 1, 2015).

[11] P. Bernardo, E. Drioli, G. Golemme, Membrane Gas Separation: A Review / State of the Art, Ind. Eng. Chem. Eng. Res. 48 (2009) 4638–4663.

[12] W.J. Koros, Evolving Beyond the Thermal Age of Separation Processes: Membranes Can Lead the Way, AIChE J. 50 (2004) 2326–2334.

[13] O.C. David, Membrane technologies for hydrogen and carbon monoxide recovery from residual gas streams, Ph.D. Thesis, Universidad de Cantabria, 2012.

[14] J.D. Seader, E.J. Henley, K.D. Roper, Separation Process Principles: Chemical and Biochemical Operations, in: 3rd ed., Wiley, 2010: p. 848.

[15] S. Matteucci, Y. Yampolskii, B.D. Freeman, I. Pinnau, Transport of Gases and Vapors in Glassy and Rubbery Polymers, in: Y. Yampolskii, I. Pinnau, B.D. Freeman (Eds.), Mater. Sci. Membr. Gas Vap. Sep., John Wiley & Sons Ltd, 2006: p. 466.

[16] C.A. Scholes, J. Bacus, G.Q. Chen, W.X. Tao, G. Li, A. Qader, et al., Pilot plant performance of rubbery polymeric membranes for carbon dioxide separation from syngas, J. Memb. Sci. 389 (2012) 470–477.

[17] D. Bastani, N. Esmaeili, M. Asadollahi, Polymeric mixed matrix membranes containing zeolites as a filler for gas separation applications: A review, J. Ind. Eng. Chem. 19 (2013) 375–393.

[18] S. Qiu, T. Ben, Design Principle of Porous Polymers, in: P. Gale, J. Steed (Eds.), Porous Polym. Des. Synth. Appl., Royal Society of Chemistry, n.d.

[19] D.F. Graves, Rubber, in: J.A. Kent (Ed.), Kent Riegel's Handb. Ind. Chem. Biotechnol. Vol. 1, 11th Ed., Springer, 2012: pp. 689–719.

[20] T.C. Merkel, V.I. Bondar, K. Nagai, B.D. Freeman, I. Pinnau, Gas sorption, diffusion, and permeation in poly(dimethylsiloxane), J. Polym. Sci. Part B Polym. Phys. 38 (2000) 415–434.

[21] P.K. Parhi, Supported liquid membrane principle and its practices: A short review, J. Chem. 2013 (2013) 1–11.

[22] C.A. Scholes, K.H. Smith, S.E. Kentish, G.W. Stevens, CO_2 capture from pre-combustion processes - Strategies for membrane gas separation, Int. J. Greenh. Gas Control. 4 (2010) 739–755.

[23] J.H. Petropoulos, Mechanisms and Theories for Sorption and Diffusion of Gases in Polymers, in: D.R. Paul, Y. Yampolskii (Eds.), Polym. Gas Sep. Membr., Series CRC Press Inc., Boca Raton, 1994: pp. 17–78.

[24] K. Ghosal, B.D. Freeman, Gas Separation Using Polymer Membranes: An Overview, Polym. Adv. Technol. 5 (2003) 673–697.

[25] H. Lin, B.D. Freeman, Materials selection guidelines for membranes that remove CO_2 from gas mixtures, J. Mol. Struct. 739 (2005) 57–74.

[26] T.C. Merkel, R.P. Gupta, B.S. Turk, B.D. Freeman, Mixed-gas permeation of syngas components in poly(dimethylsiloxane) and poly(1-trimethylsilyl-1-propyne) at elevated temperatures, J. Memb. Sci. 191 (2001) 85–94.

[27] L. Ansaloni, Y. Zhao, B.T. Jung, K. Ramasubramanian, M.G. Baschetti, W.S.W. Ho, Facilitated transport membranes containing amino-functionalized multi-walled carbon nanotubes for high-pressure CO_2 separations, J. Memb. Sci. 490 (2015) 18–28.

[28] E.H. Immergut, H.F. Mark, Principles of Plasticization, Plast. Plasticizer Processes. 48 (1965) 1–26.

[29] A. Bos, I.G.M. Pünt, M. Wessling, H. Strathmann, CO_2-induced plasticization phenomena in glassy polymers, J. Memb. Sci. 155 (1999) 67–78.

[30] X. Duthie, S. Kentish, C. Powell, K. Nagai, G. Qiao, G.W. Stevens, Operating temperature effects on the plasticization of polyimide gas separation membranes, J. Memb. Sci. 294 (2007) 40–49.

[31] V.I. Bondar, B.D. Freeman, I. Pinnau, Gas transport properties of poly (ether-b-amide) segmented block copolymers, J. Polym. Sci. Part B Polym. Phys. 38 (2000) 2051–2062.

[32] M.K. Barillas, R.M. Enick, M. O'Brien, R. Perry, D.R. Luebke, B.D. Morreale, The CO_2 permeability and mixed gas CO_2/H_2 selectivity of membranes composed of CO_2-philic polymers, J. Memb. Sci. 372 (2011) 29–39.

[33] C. Myers, H. Pennline, D.R. Luebke, J. Ilconich, J.K. Dixon, E.J. Maginn, et al., High temperature separation of carbon dioxide/hydrogen mixtures using facilitated supported ionic liquid membranes, J. Memb. Sci. 322 (2008) 28–31.

[34] C.J. Orme, M.L. Stone, M.T. Benson, E.S. Peterson, Testing Of Polymer Membranes For The Selective Permeability Of Hydrogen, Sep. Sci. Technol. 38 (2003) 3225–3238.

[35] W. Yave, A. Car, S.S. Funari, S.P. Nunes, K.V. Peinemann, CO_2-Philic Polymer Membrane with Extremely High Separation Performance, Macromolecules. 43 (2010) 326–333.

[36] A. Car, C. Stropnik, W. Yave, K.V. Peinemann, Tailor-made polymeric membranes based on segmented block copolymers for CO_2 separation, Adv. Funct. Mater. 18 (2008) 2815–2823.

[37] H. Lin, E. Van Wagner, B.D. Freeman, L.G. Toy, R.P. Gupta, Plasticization-Enhanced Hydrogen Purification Using Polymeric Membranes, Science. 311 (2006) 639–642.

[38] P. Jha, J.D. Way, Carbon dioxide selective mixed-matrix membranes formulation and characterization using rubbery substituted polyphosphazene, J. Memb. Sci. 324 (2008) 151–161.

[39] A. Morisato, H.C. Shen, S.S. Sankar, B.D. Freeman, I. Pinnau, C.G. Casillas, Polymer characterization and gas permeability of poly(1-trimethylsilyl-1-propyne) [PTMSP], poly(1-phenyl-1-propyne) [PPP], and PTMSP/PPP blends, J. Polym. Sci. Part B Polym. Phys. 34 (1996) 2209–2222.

[40] C.A. Scholes, G.W. Stevens, S.E. Kentish, The effect of hydrogen sulfide, carbon monoxide and water on the performance of a PDMS membrane in carbon dioxide/nitrogen separation, J. Memb. Sci. 350 (2010) 189–199.

[41] N.M. Kocherginsky, Q. Yang, L. Seelam, Recent advances in supported liquid membrane technology, Sep. Purif. Technol. 53 (2007) 171–177.

[42] D.R. Luebke, L. Hong, C.R. Myers, United States Patent: 9186854 (Method of fabrication of supported liquid membranes), 9186854, 2015.

[43] A. Lamberti, S.L. Marasso, M. Cocuzza, PDMS membranes with tunable gas permeability for microfluidic applications, R. Soc. Chem. 4 (2014) 61415–61419.

[44] A. Lamberti, A. Virga, P. Rivolo, A. Angelini, F. Giorgis, Easy Tuning of Surface and Optical Properties of PDMS Decorated by Ag Nanoparticles, J. Phys. Chem. 119 (2015) 8194–8200.

[45] D. Sun, M.Q. Liu, J.H. Guo, J.Y. Zhang, B.B. Li, D.Y. Li, Preparation and characterization of PDMS-PVDF hydrophobic microporous membrane for membrane distillation, Desalination. 370 (2015) 63–71.

[46] M. Hussain, A. König, Mixed-Matrix Membrane for Gas Separation: Polydimethylsiloxane Filled with Zeolite, Chem. Eng. Technol. 35 (2012) 561–569.

[47] J. Lindmark, J. Hedlund, Carbon dioxide removal from synthesis gas using MFI membranes, J. Memb. Sci. 360 (2010) 284–291.

[48] D. Carter, D. Kennedy, F.H. Tezel, B. Kruczek, Characterization of Inorganic Silicalite - 1 Membrane to be used for the Separation of Greenhouse Gases, in: International Conference on New Trends in Transport Phenomena, 2014: pp. 1–6.

[49] C.J. Anderson, S.J. Pas, G. Arora, S.E. Kentish, A.J. Hill, S.I. Sandler, et al., Effect of pyrolysis temperature and operating temperature on the performance of nanoporous carbon membranes, J. Memb. Sci. 322 (2008) 19–27.

[50] Y. Ban, Z. Li, Y. Li, Y. Peng, H. Jin, W. Jiao, et al., Confinement of Ionic Liquids in Nanocages: Tailoring the Molecular Sieving Properties of ZIF-8 for Membrane-Based CO_2 Capture, Angew. Chemie - Int. Ed. 54 (2015) 15483–15487.

[51] M. Kanezashi, Y.S. Lin, Gas Permeation and Diffusion Characteristics of MFI-Type Zeolite Membranes at High Temperatures, J. Phys. Chem. C. 113 (2009) 3767–3774.

[52] J.H. Dong, Y.S. Lin, W. Liu, Multicomponent hydrogen/hydrocarbon separation by MFI-type zeolite membranes, AIChE J. 46 (2000) 1957–1966.

[53] M. Tawalbeh, Silicalite-1 Membranes Synthesis , Characterization , CO_2 / N_2 Separation and Modeling, University of Ottawa, 2014.

[54] B.D. Freeman, Y.P. Yampol'skii, I. Pinnau, Materials Science of Membranes for Gas and Vapor Separation, John Wiley & Sons Ltd., 2006.

[55] L. Sandström, E. Sjöberg, J. Hedlund, Very high flux MFI membrane for CO_2 separation, J. Memb. Sci. 380 (2011) 232–240.

[56] C. Algieri, P. Bernardo, G. Golemme, G. Barbieri, E. Drioli, Permeation properties of a thin silicalite-1 (MFI) membrane, J. Memb. Sci. 222 (2003) 181–190.

[57] F. Akhtar, E. Sjöberg, D. Korelskiy, M. Rayson, J. Hedlund, L. Bergström, Preparation of graded silicalite-1 substrates for all-zeolite membranes with excellent CO_2/H_2 separation performance, J. Memb. Sci. 493 (2015) 206–211.

[58] M. Grahn, J. Hedlund, Maxwell–Stefan modeling of high flux tubular silicalite-1 membranes for CO_2 removal from CO_2/H_2 gas mixtures, J. Membr. Sci. 471 (2014) 328–37.

[59] G. Guan, K. Kusakabe, S. Morooka, Gas Permeation Properties of Ion-Exchanged Faujasite-Type Zeolite Membranes, Sep. Sci. Technol. 36 (2001) 2233–2245.

[60] K. Kusakabe, T. Kuroda, S. Morooka, Separation of carbon dioxide from nitrogen using ion-exchanged faujasite-type zeolite membranes formed on porous support tubes, J. Memb. Sci. 148 (1998) 13–23.

[61] F. Bonhomme, M.E. Welk, T.M. Nenoff, CO_2 selectivity and lifetimes of high silica ZSM-5 membranes, Microporous Mesoporous Mater. 66 (2003) 181–188.

[62] D.W. Shin, S.H. Hyun, C.H. Cho, M.H. Han, Synthesis and CO_2/N_2 gas permeation characteristics of ZSM-5 zeolite membranes, Microporous Mesoporous Mater. 85 (2005) 313–323.

[63] V. Sebastián, I. Kumakiri, R. Bredesen, M. Menéndez, Zeolite membrane for CO_2 removal: Operating at high pressure, J. Memb. Sci. 292 (2007) 92–97.

[64] Z. Zhou, J. Yang, Y. Zhang, L. Chang, W. Sun, J. Wang, NaA zeolite/carbon nanocomposite thin films with high permeance for CO_2/N_2 separation, Sep. Purif. Technol. 55 (2007) 392–395.

[65] Y. Yildirim, R. Hughes, An Experimental Study of CO_2 Separation Using a Silica Based Composite Membrane, Process Saf. Environ. Prot. 81 (2003) 257–261.

[66] S. Li, J.L. Falconer, R.D. Noble, SAPO-34 membranes for CO_2/CH_4 separation, J. Memb. Sci. 241 (2004) 121–135.

[67] A.J. Burggraaf, Z. a E.P. Vroon, K. Keizer, H. Verweij, Permeation of single gases in thin zeolite MFI membranes, J. Memb. Sci. 144 (1998) 77–86.

[68] M. Tawalbeh, F.H. Tezel, B. Kruczek, S. Letaief, C. Detellier, Synthesis and characterization of silicalite-1 membrane prepared on a novel support by the pore plugging method, J. Porous Mater. 20 (2013) 1407–1421.

[69] O. Bakhtiari, S. Mosleh, T. Khosravi, T. Mohammadi, Preparation, Characterization and Gas Permeation of Polyimide Mixed Matrix Membranes, Membr. Sci. Technol. 1 (2011) 1–6.

[70] V. Kramer, M. Kraume, Development of a Mechnistic Model for Sorption Selective Mixed-Matrix Membranes for Gas Separation, Tech. Trans. 109 (2012) 126–135.

[71] M. Wang, Z. Wang, N. Li, J. Liao, S. Zhao, J. Wang, et al., Relationship between polymer-filler interfaces in separation layers and gas transport properties of mixed matrix composite membranes, J. Memb. Sci. 495 (2015) 252–268.

[72] J. Maxwell, A Treatise on Electricity and Magnetism : Volume II, Dover Publications, 1873.

[73] C.M. Zimmerman, A. Singh, W.J. Koros, Tailoring mixed matrix composite membranes for gas separations, J. Memb. Sci. 137 (1997) 145–154.

[74] S. Matteucci, V.A. Kusuma, S.D. Kelman, B.D. Freeman, Gas transport properties of MgO filled poly(1-trimethylsilyl-1-propyne) nanocomposites, Polymer. 49 (2008) 1659–1675.

[75] A. Ehsani, M. Pakizeh, Synthesis, characterization and gas permeation study of ZIF-11/Pebax

2533 mixed matrix membranes, J. Taiwan Inst. Chem. Eng. 66 (2016) 414–423.

[76] S. Kim, T.W. Pechar, E. Marand, Poly(imide siloxane) and carbon nanotube mixed matrix membranes for gas separation, Desalination. 192 (2006) 330–339.

[77] H. Li, L. Tuo, K. Yang, H.K. Jeong, Y. Dai, G. He, et al., Simultaneous enhancement of mechanical properties and CO_2 selectivity of ZIF-8 mixed matrix membranes: Interfacial toughening effect of ionic liquid, J. Memb. Sci. 511 (2016) 130–142.

Chapter 3: Separation of CO_2 from syngas to increase the conversion of the RWGS reaction using PDMS membranes

3.1 ABSTRACT

The Reverse Water Gas Shift (RWGS) reaction is a means to convert CO_2 emissions (from large stationary sources) and H_2 into CO, a component of syngas. However, overall conversion of the reaction can be considerably increased by implementing a recycle of unreacted CO_2. The remaining CO and H_2 (syngas) are precursors to products like methanol, ammonia and even liquid synthetic fuels. Polydimethylsiloxane (PDMS) membranes have been proven to separate CO_2 from both CO and H_2, with a higher solubility affinity for CO_2. A commercial PDMS membrane and two synthesized PDMS membranes (PDMS-PAN I, PDMS-PAN II) were investigated and characterized in this study for the separation of CO_2 from syngas with single, binary and ternary gas feeds at room temperature (23 – 25 ºC) and total feed pressures up to 11 atm. The commercial PDMS membrane was the most permeable among the membranes looked at in this study with the highest reported CO_2 permeability in this work of 5,883 Barrers for ternary feeds (1:1:1, CO_2:CO:H_2), surpassing the literature data specific to this type of membrane. The PDMS-PAN I membrane was the least permeable for all experiments, with the highest selectivity reported in this work of 21 for CO_2 separation from H_2 from ternary gas feeds. The PDMS-PAN II membrane proved to strike a balance between permeability and separation, with the highest CO_2/CO selectivity of 9 for ternary gas feeds. Membrane compaction proved to be a notable issue for the commercial PDMS membrane, while swelling by CO_2 affected the thickest PDMS membrane (PDMS-PAN I) the most.

3.2 INTRODUCTION

3.2.1 CO_2 Emissions and RWGS

Release of carbon dioxide into the atmosphere is not a new environmental issue the 21st century is facing, thanks to a cultivation of several industrial factors. CO_2 has been named the most significant human generated greenhouse gas, ever since the industrial revolution. While the public relies on many of these industries to survive, even if the release of CO_2 were to stop completely, its effects on the environment would persist [1]. There are many efforts being made to combat these global issues, such as the United Nations Climate Change Conference held in Paris in 2015, where international leaders agreed on setting an environmental temperature limit to an increase of no more than 2 °C per year, to better control and regulate these emissions [2]. Currently CO_2 emissions can be, for example, purified and sold or sequestered into the ground or the ocean [1].

However, even with an optimal decrease or plateau in CO_2 emissions, there is a way for CO_2 to be consumed in a reaction to produce alterative gases for more useful processes. The Reverse Water Gas Shift (RWGS) equilibrium reaction converts CO_2 and H_2 to form CO and H_2O at high temperature (700 – 1100 °C) and at atmospheric pressure, over a catalyst as seen in equation 1.

$$CO_2 + H_2 \leftrightarrow CO + H_2O \qquad (1)$$

The enthalpy of this endothermic reaction is approximately 41 kJ/mol [3]. Additionally, parallel or side reactions including the Sabatier, Bosch, Boudouard, methanation (of CO) and WGS (Water Gas Shift) reactions are all possible [4].

CO_2 conversion for this reaction can vary, depending on the operating temperature of the reaction, the ratio of H_2 to CO_2 in the feed, and the potential for side reactions. The effect of the feed ratio (R) of H_2/CO_2 on the conversion of CO_2 was studied by Bajirao [4]. Increasing the ratio of H_2 to CO_2, while increasing the temperature of the reaction, increases the conversion of CO_2. However, there are some limitations for this feed ratio. When this ratio is greater than 2, the Sabatier reaction is more favourable, and converts CO_2 into CH_4. In addition, the preferred ratio of syngas is 2 for CO to H_2 [5]. In order to obtain this ratio in the product stream at 1 atm of pressure with a H_2/CO_2 ratio of 2 in the feed, the reaction would need to take place at approximately 750 °C or greater [4]. Under these conditions, and from 750 °C onward, CO_2 conversion can reach anywhere from 60 to 80 % [4].

Since CO_2 is not completely consumed in this reaction, there exists a need to recycle the unreacted CO_2 back into the RWGS reactor to increase its overall conversion. By assuming complete removal of H_2O, this would leave only CO and H_2 gases to exit the reactor. These components make up syngas or synthesis gas, which can be used to make products such as methanol, ammonia, electricity and even liquid synthetic fuels utilizing the Fischer-Tropsch process [6,7]. Refer to Figure 3-1 for an overview of the RWGS reaction and proposed separation process. This diagram neglects any unwanted by-products and focuses only on the gases involved in the RWGS reaction, assuming incomplete conversion of CO_2. Hydrogen could be recycled individually or with CO_2 from the product stream, which would further increase the overall conversion of CO_2 [3,4]. However, syngas is a valuable combination because it can be used as a feedstock for a variety of other processes and would be readily available after this separation after the reactor.

Membrane processes are cost effective and operate with ease at steady state conditions in comparison to alternative processes such as adsorption, distillation and absorption. From a thermal

efficiency standpoint – in comparison to other separation processes – membranes have greater energy efficiency [8–10]. Membrane separation can also reach steady state in a short time-frame. In this case, membrane separation would facilitate separation of either CO_2 or H_2 as a penetrant gas. H_2 separation is achieved easily when gas molecules are separated on the basis of size, which would leave a combination of CO_2 and CO exiting the separation in the retentate stream. Since the combination of CO_2 and CO is not beneficial for either downstream or RWGS recycle purposes, this type of membrane separation is not ideal. However, dense polymeric membranes would promote the separation of CO_2 from H_2 and CO, which is a more advantageous separation for this proposed process. Therefore, CO_2 will be investigated as the individual recycle gas.

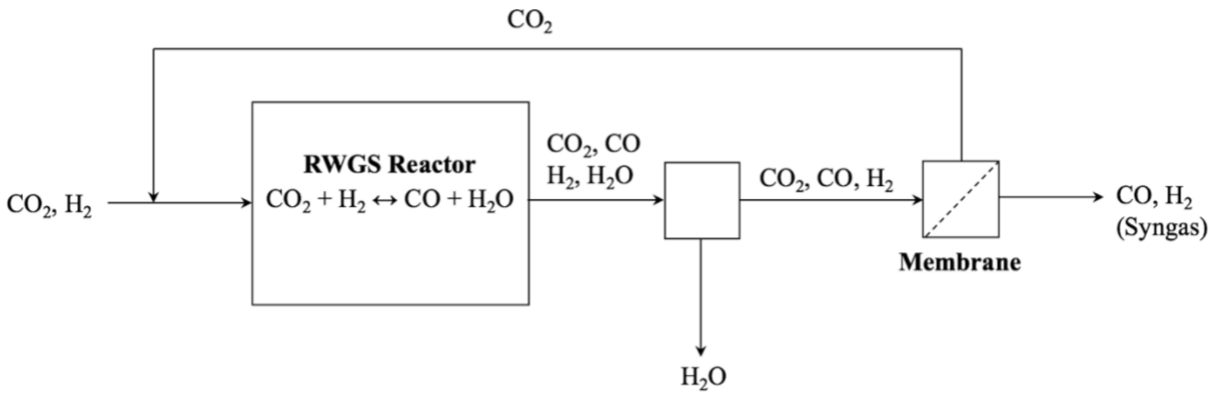

Figure 3-1: Overview of RWGS reaction and proposed post-reactor separations assuming no side reactions and by-products in product stream

3.2.2 Membranes

Membranes operate as an interface that controls the mass exchange between two fluid bulk phases by means of a driving force. The fluid that passes through the membrane material is referred to as the permeate where the retentate stream is the fluid that is retained by the membrane, as seen in Figure 3-2. A driving force is required to facilitate transport across the membrane, which for gas separation in this work is a positive pressure difference across the membrane surface from feed to permeate [11].

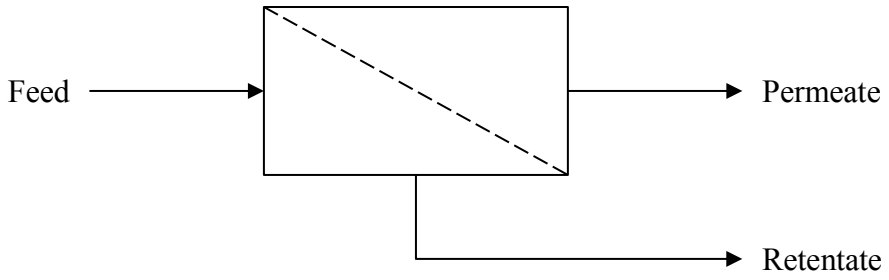

Figure 3-2: Membrane process stream identification [11]

The transport mechanism governing gas separation in polymeric membranes is the product of solubility and diffusivity properties of gases in the polymer. This is referred to as the Solution-Diffusion model, where gas permeability (*P*) can be expressed as a product of a gas diffusivity (*D*) and solubility (*S*). Therefore, both properties for each gas play a large role in determining which molecule the material will selectively allow to permeate more. This allows rubbery polymeric materials to pass larger gas molecules over smaller molecules, as high diffusivity can be overruled by high gas solubility [11–13]. CO_2 often possesses high solubility in these materials, making it favourable for separation over other gases like H_2 and CO [13].

PDMS (polydimethylsiloxane) was proven to be a suitable, rubbery polymeric material for separation of CO_2 over both CO and H_2 from a literature review, outlined in Chapter 2 [14–19]. It is a widely known polymer for its inert and hydrophobic properties [20–22]. Table 3-1 describes the performance characteristics of PDMS for single and mixed gas feeds from published articles in literature. Single gas experiments proved to exhibit the highest permeabilities, where a CO_2 permeability of 3,800 Barrers was recorded by Merkel et al. for PDMS [15]. When exposed to a synthetic syngas feed (including impurities), Scholes et al. measured a lower CO_2 permeability of 1,993 Barrers but with higher CO_2/H_2 and CO_2/CO selectivities of 7 and 11, respectively [16].

CO_2 can have negative effects on polymers in terms of physical polymer chain structure. This effect is known as plasticization in glassy polymers, or swelling in rubbery type polymers where CO_2, when being sorbed by the polymer, interacts with the polymer chains. In the case of plasticization, the effective glass transition temperature of the polymer is reduced, as a result of increased chain mobility, known to increase all gas permeabilities and decrease the materials' selectivity [23,24]. Membrane swelling is a similar phenomenon where the absorption of a component by the polymer is accompanied by an increase in the linear dimension of the polymer. "The swelling of polymers involves either mutual dissolution of two completely miscible substances

(solvent and polymer) or solution of the low molecular weight component into the polymer" [ROYER]. This in turn increase the mobility of the polymer phase and changes the membranes performance much like plasticization [25].

However, due to the softer nature of polymer materials, membrane compaction is a competing concern; high operating feed pressures take effect by physically compacting the polymer chains, increasing polymer density and decreasing gas diffusivities. This increase in density creates a higher resistance for gas transport and causes a reduction in overall gas permeability [26]. Plasticization, swelling or compaction can alter the performance characteristics of polymeric membranes.

Table 3-1: PDMS permeabilities and selectivities from literature for CO_2, CO and H_2 separation

CO_2 Permeability [Barrers]	**H_2 Permeability** [Barrers]	**CO Permeability** [Barrers]	**CO_2/H_2 Selectivity** [-]	**CO_2/CO Selectivity** [-]	**Ref.**
3,800[I]	890[I]		4.3[I]		[15]
3,760[I]	940[I]		4.0[I]		[16,27]
2,848	813		3.5		[14,28]
2,194	617		3.6		[14,28]
1,993	291	181	7.0	11	[16]
1,517	414		3.7		[14,28]

[I] *indicates single gas data (ideal selectivities)*

3.2.2.1 Membrane Characterization

Membranes for gas separation are normally characterized by properties known as permeability and selectivity. Permeability is a standardized way of expressing and normalizing permeate gas flux, while selectivity is a way of describing how well a material can selectively pass one gas over another. Membrane flux (J_i) is described in equation 2 and 3 from Fick's Law of diffusion.

$$J_i = -D_i \frac{dC_i}{dz} \quad (2)$$

$$J_i = -D_i \frac{(\Delta P \cdot S_i)}{\Delta z} \quad (3)$$

where D_i is the diffusivity of component i through the membrane (cm^2/s), C_i is the concentration of component i in the membrane (mol/cm^3), S_i is the solubility coefficient of component i through the membrane ($cm^3/cm^2 \cdot cmHg$), ΔP is the partial pressure difference of component i across the

membrane (cmHg) and z is the selective membrane thickness in the direction of transport (cm). From Fick's Law, membrane permeability (P_i), can be described in equation 4 as the combined product of diffusivity (D_i) and solubility (S_i) coefficients of a given penetrant in the membrane. It is most often expressed in the unit of Barrer, which is shown in equation 5. The equations for permeability presented here were used for the data analysis discussed in this work, assuming negligible external mass transfer resistance in comparison to the diffusion for each component.

$$P_i = D_i \cdot S_i = \frac{J_i \cdot \Delta z}{\Delta P} \tag{4}$$

$$1\ Barrer = 10^{-10}\ \frac{cm^3(STP) \cdot cm}{cm^2 \cdot s \cdot cmHg} \tag{5}$$

Lastly, selectivity is a crucial property of any membrane performance. Ideal selectivity, $\alpha^*_{A/B}$, is defined from single gas experiments by the permeability ratio of components A to B (as shown in equation 6). For mixed gas processes, actual selectivity ($\alpha_{A/B}$) is defined with respect to the composition of components A and B in the permeate (y) and feed (x) streams, seen in equation 7. These equations were used for the data presented in this work.

$$\alpha^*_{A/B} = \frac{P_A}{P_B} \tag{6}$$

$$\alpha_{A/B} = \frac{y_A / y_B}{x_A / x_B} \tag{7}$$

Composite membranes are often used for gas separation, where a thin layer of a selective material is layered onto a more porous support, specifically to maintain high gas flux through the membrane. The selective layer, usually a dense/nonporous polymer, causes significant resistance to gas flow and transport through the material. Therefore, thin layers or films of this dense material are layered on a more porous support to provide structural support without a massive reduction in gas permeability [11].

PDMS (polydimethylsiloxane) was selected as the polymer to test as a selective membrane for CO_2 separation from CO and H_2. It was examined previously, in Chapter 2, for this specific separation, amongst a multitude of other polymers. It is a well-known material in the polymer world because of its desirable properties like biocompatibility, straightforward synthesis, and flexibility [20–22]. These properties, coupled with reported high CO_2 permeabilities and selectivities over H_2 and CO, make this polymer of interest for this separation and membrane application. A commercially available PDMS membrane and two synthesized PDMS membranes on different PAN

(polyacrylonitrile) supports have been investigated in this work. PAN was selected as a support layer due to availability, low cost and chemical resistance [29,30].

3.3 EXPERIMENTAL

3.3.1 Materials and Membrane Preparation

CO_2, CO and H_2 gas cylinders from Linde Canada Ltd. (Mississauga, ON, Canada) were used for experiments and the grades and purities used are displayed in Table 3-2. The commercial PDMS membrane (PERVAP™ 4060) had a selective layer thickness of approximately 7 µm on a PAN (polyacrylonitrile) porous layer (nanofiltration flat-sheet material with a nominal pore size of 20 nm), mechanically supported by a polyester layer. The nominal pore size represents the filter's degree of filtration or its ability to prevent passing a minimum weight percentage of solute larger than the nominal particle size. This product was purchased from Sulzer Chemtech (Tulsa, OK, USA).

The synthesized PDMS membranes (PDMS-PAN I and PDMS-PAN II) utilized two PAN (polyacrylonitrile) ultrafiltration flat-sheet materials with different MWCOs (30 and 300 kDa molecular weight cut-offs, respectively), each backed on polyester from Sterlitech™ Corp. (Kent, WA, USA). The MWCO is the lowest molecular weight where 90% or more of a solute is retained by the membrane [31,32]. It is expressed in the unit of Dalton (Da) or kiloDalton (kDa), which is defined as 1/12th of the weight of a carbon-12 atom [33]. The MWCO used for PDMS-PAN II (300 kDa) is ten times greater than the support used for PDMS-PAN I (30 kDa), as seen in Table 3-3. The PDMS and curing agents used for PDMS-PAN I and PDMS-PAN II were purchased from Gervais Electronics (Ottawa, Ontario, Canada). The toluene solvent used during synthesis of these two membranes was purchased from Fisher Scientific (Ottawa, ON, Canada).

Prior to synthesizing the selective layer, each PAN support (a small sheet roughly 8" x 6") was soaked in distilled water for 30 seconds. This soaking fills the pores of the support with water, preventing any PDMS solution from seeping into the PAN pores, increasing the effective thickness of the membrane and making the membrane less permeable [29,30]. The wetted PAN sheets were then taped to a glass or metal plate, securing all edges and ensuring no gaps of air between the support sheet and the plate.

The first layer applied to the support sheet was a diluted 1 wt % PDMS in toluene layer, to improve adhesion between the selective PDMS layer and the PAN support. With better adhesion,

this diluted PDMS layer could help maximize the flux through the finished synthesized membranes. However, because of its low concentration in toluene, the thickness of this layer will be negligible in comparison to the PDMS selective layer applied after. This diluted mixture involved mixing PDMS:curing agent in a 10:1 mass ratio in a 50 g toluene solution and agitating the mixture with a basic two-blade impeller at 500 RPM and at room temperature for 15 minutes. The selective PDMS layer was synthesized by mixing the PDMS and curing agent in a 10:1 mass ratio in a 20 g toluene solution and was then agitated with the same two-blade impeller at 500 RPM and at room temperature for 15 minutes. A single layer of the diluted 1 wt % PDMS solution was applied to the support. There was a total wait time of 1 hour before continuing. The two selective PDMS layers were then applied, waiting 1 hour between these layers. These two layers were applied perpendicularly to each other, as seen in Part B of Figure 3-3. All casting onto the PAN sheets was performed with an airbrush spray gun (Paasche Airbrush Co.: Chicago, IL, USA) using steady movement (spraying approximately 1 foot above the support) to create a uniformly dispersed layer (Part A of Figure 3-3).

After 1 hour, the membrane was inserted into a vacuum oven, where it was exposed to vacuum pressure (0.8 bar) for 30 minutes. After 30 minutes, the oven began pre-heating to 90 °C and the membranes were cured under vacuum for a total of 3 hours (including pre-heat). At the end of this time, the oven and vacuum were turned off and the oven door was opened slightly to introduce the membranes to atmospheric pressure and room temperature for complete cooling before use. The measured PDMS thicknesses of each membrane are shown in Table 3-3, using SEM imaging. The commercial PDMS membrane was manufactured to have a thin PDMS film only a 7 µm thick, while the PDMS-PAN I and PDMS-PAN II membranes synthesized in house were observed to have PDMS films 75 and 55 µm thick, respectively.

Table 3-2: Feed gas cylinder grade and purity used in this work from Linde Canada Ltd.

Gas	Grade	Purity (%)
CO_2	4.0	99.99
H_2	4.0	99.99
CO	2.5	99.5
He	5.0	99.999

Table 3-3: PDMS membrane supports and thicknesses

Membrane Name	PDMS Thickness [µm]	Support Layer Name	Support MWCO [kDa] [34]
Commercial PDMS	7	PAN	20*
PDMS-PAN I	75	PAN	30
PDMS-PAN II	55	PAN	300

**indicates nominal pore size in nanometers*

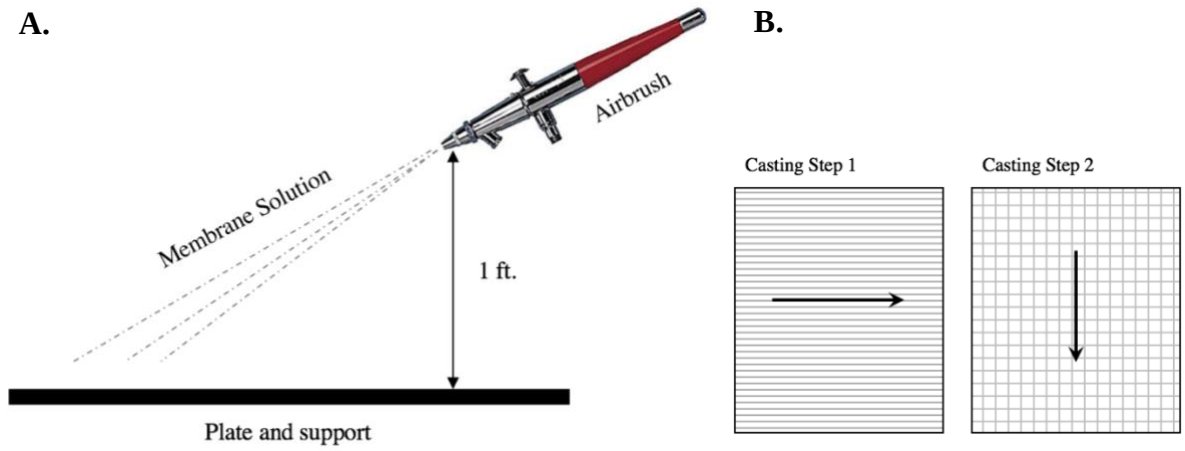

Figure 3-3: A – Membrane casting technique; B – Direction of application to PAN support for PDMS-PAN I, PDMS-PAN II

3.3.2 Experimental Set-up

A laboratory scale, flat-sheet membrane system was constructed from stainless steel piping, including stainless steel Swagelok® (Ottawa, ON, Canada) fittings. The design goals included minimal gas travel (to reduce pressure loss), safe venting, accurate feed gas control with easy sampling and volumetric flow measurements of the feed, retentate or permeate streams to the gas chromatograph.

An integral piece of equipment to this system was a Varian Aerograph 1400 series gas chromatograph (GC) equipped with a thermal conductivity detector, utilizing an 8-port sampling valve (allowing easier and faster injections). A ShinCarbon 1/8" OD x 2 m packed column from Chromatographic Specialties Inc. (Brockville, ON, Canada) was used as the column unit in the GC to efficiently separate each gas and enable analysis of the sample injections (CO_2, CO and H_2 mixtures). Appendix A includes images of the configuration of the 8-port injection valve (Figure 6-6), as well as the peak order for different gas components (H_2, O_2, N_2, CO, CO_2 listed in order of the least time to the longest time from left to right) with the ShinCarbon column used in the GC

with the LabView program (Figure 6-5). Hydrogen peaks were displayed with negative polarity since its thermal conductivity was greater than the carrier gas (Helium), used in this work. CO_2, CO, O_2 and N_2 gases all have thermal conductivities smaller than He, meaning their peaks were displayed with positive polarity.

Three OMEGA® (Laval, QC, Canada) rotameters were purchased and calibrated for their respective gas feeds (CO_2, CO and H_2). A 1L glass bubble flow meter from Sigma Aldrich was used to measure the volumetric flow rates of the retentate and/or the feed gas flow rate. A 25 mL and 500 µL glass bubble flow meters were used to measure the volumetric flow rate of the permeate stream.

To better understand the configuration of the membrane cell used in the experimental system, detailed figures in Appendix A (Figure 6-1 to Figure 6-4) can be viewed for a more in depth look as to how gases entered and exited the cell. As a general overview, the membrane cell was composed of two sections (top and bottom). The bottom section was where the feed entered and contacted the selective side of the membrane, and where the retentate exited the cell. The top was where the permeate exited the cell and also housed two O-rings, which created a sufficient seal under compression to ensure no gases leaked during experimental operation.

Fittings, valves and 1/8" OD tubing were purchased from Swagelok® to ensure stainless steel unity, safety at high operating pressures and insignificant gas interaction with the internal surface of the system. Pressure gauges were positioned just before and after the membrane cell on the feed and permeate streams to monitor the trans-membrane pressure drop. Valves were configured after the membrane cell to allow the user to measure volumetric flow rates of the feed, retentate and permeate, and inject samples of each of these streams into the gas chromatograph to measure their compositions. Figure 3-4 displays an overview of the entire laboratory scale system used to test the flat-sheet polymeric membranes. A summary of the individual processing parts of the membrane system is presented in Table 3-4 as a reference.

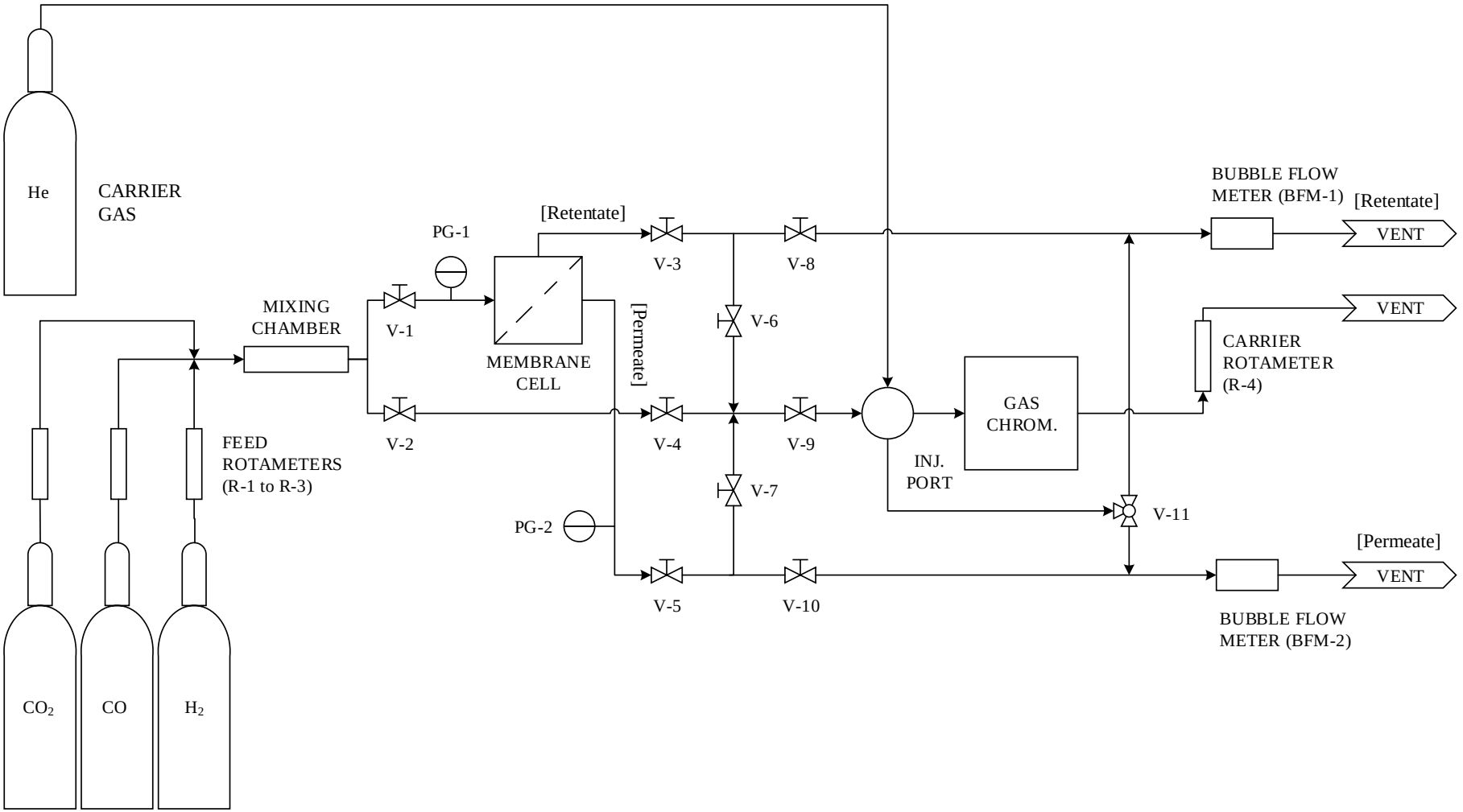

Figure 3-4: Schematic diagram of the experimental set-up used in this work

Table 3-4: Equipment description for entire laboratory experimental schematic

Equipment ID.	Description	Use
CO_2, CO, H_2, He	Gas cylinders	Feed and carrier gases
BFM-1, BFM-2	Bubble flow meters	Measures volumetric flow with timed measurements of quantified bubble travel
Gas Chrom.	Gas chromatograph (Varian Aerograph 1400)	Houses ShinCarbon packed column to analyze sample injection gas concentrations
Inj. Port	Injection sample port for GC (8-port)	Manual injections of samples into GC for analysis
Membrane cell	Module to house flat-sheet membrane	Keeps membrane in correct and stable position for separation
Mixing Chamber	Enlarged tubing	Provides mixing space for feed gases
PG-1, PG-2	Pressure gauges	Measure feed and permeate gauge pressure up to 160 psig
R-1, R-2, R-3	Feed rotameters	Controlling gas feed flows
R-4	Carrier gas rotameter	Controls volumetric flow of He to the GC
Vents	Tubing to fume hood in laboratory	Bring flammable and poisonous gases to fume hood for proper venting
V-1, V-2, V-11	Two-way valves	Control direction of gas flow
V-3 to V-10	Screw down valves	Control direction and resistance of gas flow

3.3.3 Permeation Measurements

Gases were fed from gas cylinders to their respective rotameters and then entered a mixing chamber prior to being fed to the membrane to allow enough time and space for each component to become well integrated. Total gas feed flowrates were maintained at 4.5 L/min. Binary experiments were carried out with 25:75, 50:50 and 75:25 molar ratios of CO_2 with H_2 and CO. Ternary experiments were carried out with equal molar concentrations of each component in the mixture (1:1:1). To accurately represent the range of product stream composition possibilities (depending on reaction temperature, H_2/CO_2 feed ratio and ultimately CO_2 conversion) it was assumed that the water produced would be completely condensed and/or removed. If water was present in the feed to the PDMS membranes studied in this work, it would act as a competitive penetrant, decreasing CO_2 permeability. This is due to strong Flory-Huggins interactions between H_2O and CO_2 in comparison to PDMS, meaning water energetically favours occupying volume within PDMS alone [35]. However, the equimolar mixture of all three gases would serve as an acceptable starting point to

observe how each membrane would perform when exposed to a combination of each gas (CO_2, CO, H_2) in the presence of the other gases.

The feed pressure was controlled with a valve along the retentate line (inducing backpressure) to increase resistance of gas flow in the feed stream. During experiments the permeate flow rate was observed to be much smaller than the feed flow rate (a maximum of 2.5 vol % of the feed flow rate). Using the rotameter controls and retentate valve, the correct feed flow rate was obtained at the desired feed pressure, measured on pressure gauge PG-1. Permeate pressure was measured using pressure gauge, PG-2. To efficiently and clearly analyze the gases in a GC injection for experiments, the column temperature in the GC was set to 40 °C and a carrier flow rate of 40 mL/min of helium was used. This produced well separated peaks of all components to be analyzed for concentration.

Two glass bubble flowmeters (BFM-1: 1L and BFM-2: 25mL or 500 µL) were used to measure the retentate and permeate volumetric flow rates during operation, respectively. To analyze the permeate stream composition, a permeate gas sample was injected into the GC. Sample injections and gas flow measurements (feed, retentate and permeate) were taken approximately every 5 minutes for up to an hour to verify the system had reached steady state. This included permeate gas flow measurements within 5 % error, and gas peak areas from GC injections that were reproducible in area size with 5 % difference or less. Permeabilities of each gas were calculated and then graphed with respect to a standard error calculation, a function of standard deviation across the samples. For all experiments, the stage cut (ratio of permeate to feed flow rate) was 0.006 or less. Only one of each commercial PDMS membrane, PDMS-PAN I and PDMS-PAN II membrane were used for the entirety of single, binary and ternary experiments from start to finish. The sequence of experiments for each membrane was carried out as described in Table 3-5 (beginning with 1. Single Gas Experiments from CO_2 to CO and so forth). This is important for reference, as testing membranes in the presence of CO_2 could change the physical structure of the membranes through swelling.

Table 3-5: Order of gas experiments (single, binary and ternary) for all PDMS membranes from top to bottom

1) Single Gas Experiments	2) Binary Gas Experiments	3) Ternary Gas Experiments
CO_2	CO_2:H_2 (25:75)	CO_2:H_2:CO (1:1:1)
H_2	CO_2:H_2 (50:50)	
CO	CO_2:H_2 (75:25)	
	CO_2:CO (25:75)	
	CO_2:CO (50:50)	
	CO_2:CO (75:25)	

3.4 RESULTS AND DISCUSSION

3.4.1 SEM Imaging

SEM (scanning electron microscope) imaging was performed on the three membranes to provide insight on how thick the selective layers were and what the interface was like between the support and this selective layer. Each image described is shown at a 50 µm scale. The SEM used was a JEOL JSM-6610 series operated with 15 kV electron beams and under 30 Pa of vacuum. Samples of each membrane were mounted (backed with tape and epoxy) perpendicularly to the camera on a seven-sample specimen holder.

The first image in Figure 3-5 is of the commercial PDMS membrane, where the PDMS layer is measured to be approximately 7 µm thick. The second image is PDMS-PAN II where the PDMS layer is much more evident because it is lighter in colour. The selective layers are indicated with arrows in Figure 3-5 and the darker layer above the PDMS in all the images is the porous PAN/polyester support. PDMS-PAN II is significantly thicker (an average of 55 µm) than the commercial PDMS membrane layer. The third image is of PDMS-PAN I, which resembles PDMS-PAN II in terms of visual PDMS thickness. PDMS-PAN I measured a selective PDMS thickness of approximately 75 µm, which is 20 µm thicker than PDMS-PAN II and 68 µm thicker than the commercial PDMS membrane. Every membrane exhibited uniform distribution on the support layer. From these images (specifically 2 and 3), there is no visible evidence of PDMS penetrating the PAN support layer, where the lighter PDMS layer remains on the surface of the darker support.

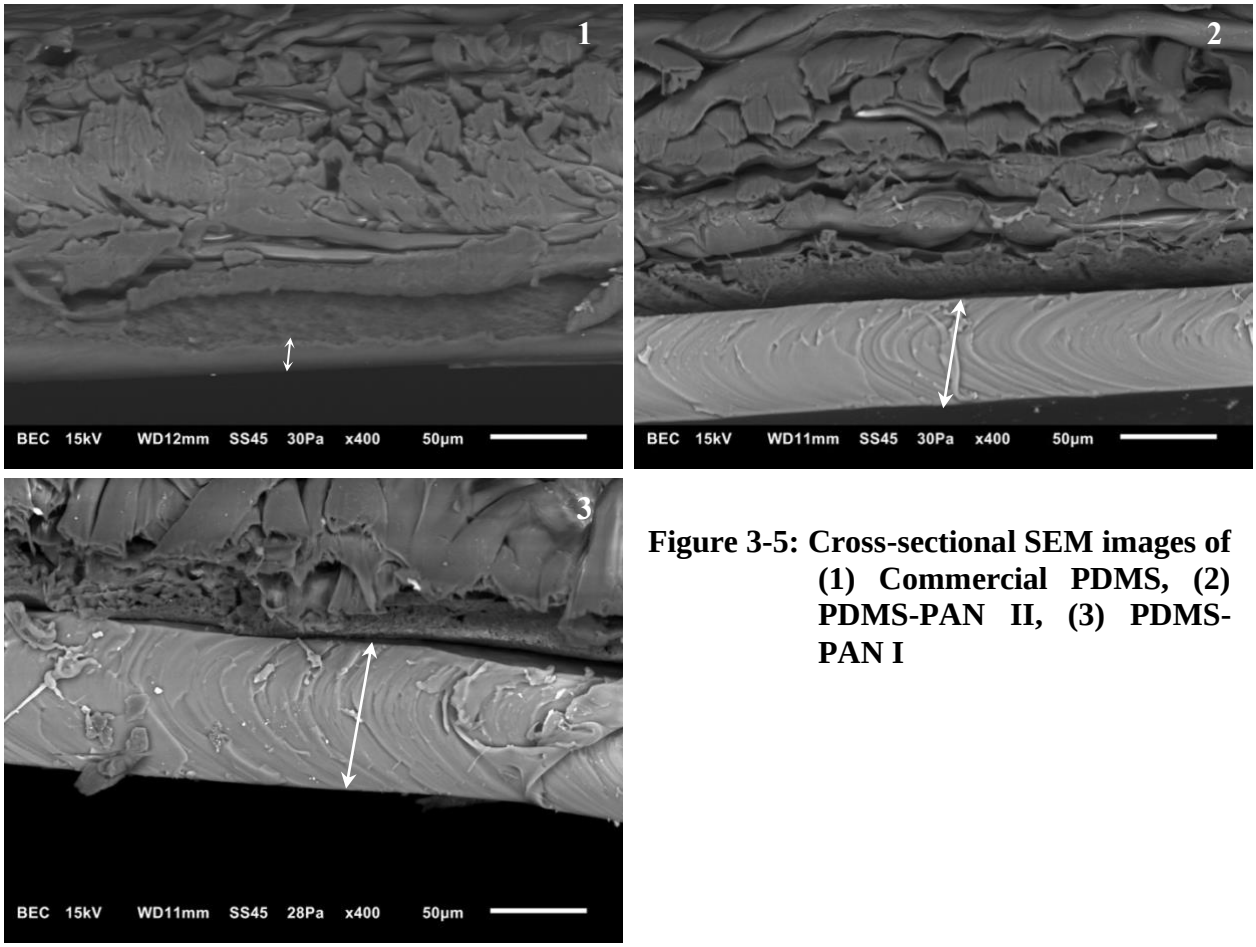

Figure 3-5: Cross-sectional SEM images of (1) Commercial PDMS, (2) PDMS-PAN II, (3) PDMS-PAN I

3.4.2 Single Gas Results and Discussion

3.4.2.1 Commercial PDMS

Single gas permeabilities of all three gases through the commercial PDMS membrane, with respect to pressure differential across the membrane, are presented in Figure 3-6:A. This membrane favoured CO_2 over both H_2 and CO, with permeabilities that approached values from the literature. Gas permeabilities – assuming no physical changes to the membrane – were expected to stay constant with respect to pressure differential. However, CO_2 permeability increased from low to higher pressure differentials. Merkel et al. [15] examined the solubility of CO_2 in PDMS at 35 °C for pressures up to 25 atm. They determined that CO_2 experienced an increase in solubility and permeability with increasing pressure, which was noticeable at pressures up to 11 atm. However, it is also possible for permeability to increase because of polymer swelling. Continued exposure to CO_2 can increase polymer chain mobility, especially at elevated pressures where concentration of CO_2 in the polymer is greater. The increase in chain mobility creates greater fractional free volume

within the polymer that facilitates permeability increases of all penetrating gases [36,37]. To expand on this point, unused and used commercial PDMS membranes were tested to determine any differences in CO and H_2 permeabilities. A used commercial PDMS membrane was exposed to all three gases (CO_2, CO, H_2) for several hours during troubleshooting experiments. The unused membrane had never been exposed to these gases before and was exposed to the same conditions as the used membrane to observe differences in permeability with respect to differential membrane pressure. CO experienced a 12.3% increase in permeability while H_2 experienced a 15.6% increase in permeability when comparing unused to used membranes. Therefore, the effects of swelling are likely to affect the performance of all gases with the commercial PDMS membrane. For these reasons, ideal CO_2 selectivity over CO and H_2 increased with total feed pressure because of the increases in CO_2 permeability from low to high pressure. These trends are seen in parts B of Figure 3-6.

Table 3-6 displays permeability values from literature in comparison to the single gas permeabilities observed in this work. Separation potential of CO_2 over CO and H_2 can be expressed in terms of ideal selectivity, where the ratio of single gas permeabilities dictates how well the membrane material can permeate one component over another. Table 3-6 compares the ideal selectivities with commercial PDMS presented in this work to other published PDMS materials and their published selectivities found in the literature. Merkel et al. [15] and Scholes et al. [16] reported CO_2 permeabilities for single gas data with PDMS membranes up to 3,800 Barrers. Scholes et al. claimed to use the same commercial PDMS membrane used in this work. Their reported CO_2 permeabilities were higher than the single gas CO_2 permeability observed in this work of 2,899 Barrers. However, these permeabilities were reported at temperatures at least 10 °C higher than the experiments performed in this study, which would dictate larger permeabilities overall. Increases in temperature lead to a general increase in gas permeability, as diffusion coefficients increase [16,17]. The CO_2/H_2 ideal selectivity observed in this work at 4.0 is close to the CO_2/H_2 ideal selectivities published by Merkel et al. [15] and Scholes et al. [16] at 4.3 and 4.0, respectively.

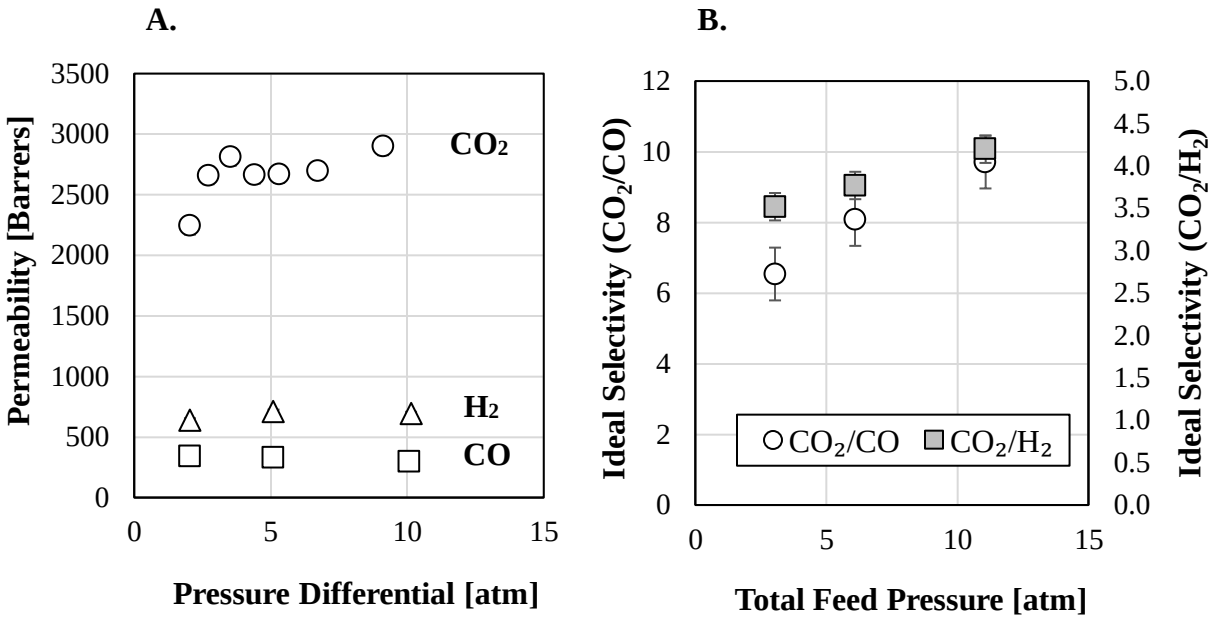

Figure 3-6: A – CO_2, CO, H_2 single gas permeabilities with respect to pressure differential for commercial PDMS 23 °C; B – CO_2/CO and CO_2/H_2 ideal selectivities with respect to feed pressure

Table 3-6: Single gas permeabilities and selectivities of commercial PDMS in comparison to literature PDMS membrane data

PDMS Thickness	**Unit**	**35 µm** **Merkel et al.** [15]	**10 µm** **Scholes et al.** [16]	**7 µm** (this work)
CO_2 Permeability	Barrer	3,800	3,760	2,899
CO Permeability	Barrer	-	-	299
H_2 Permeability	Barrer	890	940	691
CO_2/CO	-	-	-	10
CO_2/H_2	-	4.3	4.0	4.0
Temperature	°C	35	3 – 112	23
Pressure	atm	2 – 17	3 – 29	11

3.4.2.2 PDMS-PAN II

Single gas permeabilities are shown as a function of membrane pressure differential in Figure 3-7:A, for the synthesized PDMS-PAN II. This synthesized membrane utilized a more porous PAN support with a MWCO of 300 kDa [34] and the deposited PDMS film was 20 µm thinner than the PDMS-PAN I membrane. This was a consequence of the synthesis method, where variations in speed of application are expected. As can be seen in Figure 3-7, H_2 permeability increased across the pressure range studied. This is probably a result of defects within the membrane where pinholes or voids exist that allow small gas molecules with high diffusivity to exhibit higher gas permeability with feed pressure. This would not affect CO_2 or CO as greatly with respect to pressure as their diffusivities are significantly less than H_2, and their solubilities in PDMS are significantly greater [15]. These larger gas molecules therefore cannot take advantage of these defects within the PDMS to the same degree as H_2. CO_2 selectivity over CO (seen in Figure 3-7:B) does not vary as greatly as CO_2/H_2 ideal selectivity with respect to feed pressure. There is also a clear decrease in selectivity with feed pressure due to the previously discussed increase in H_2 permeability with membrane pressure differential.

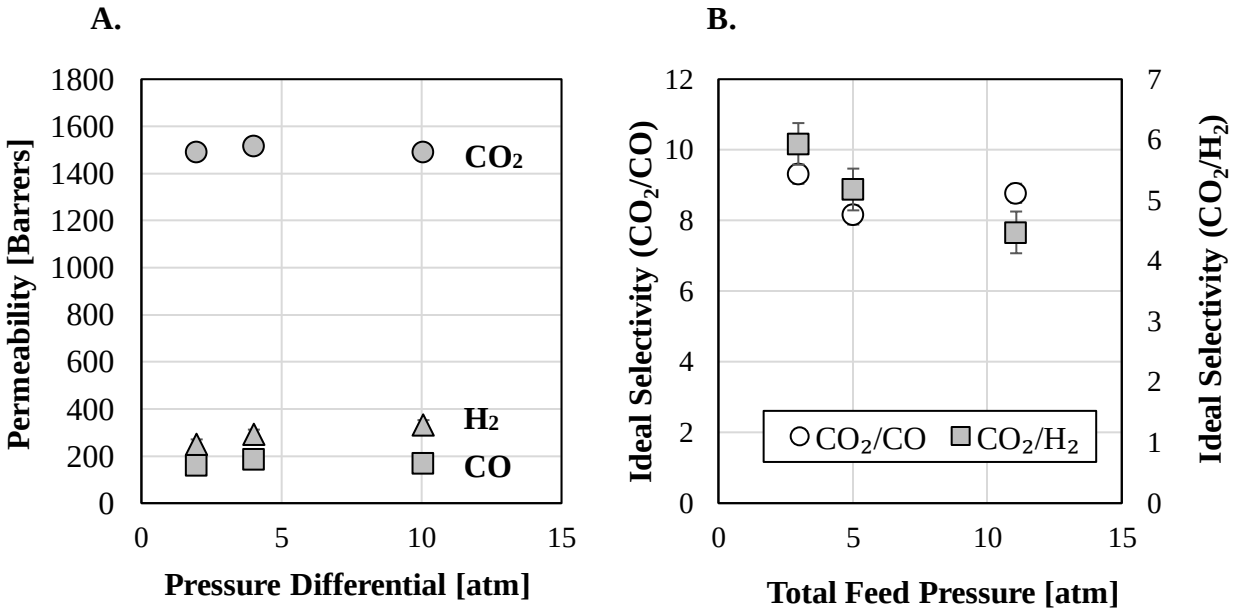

Figure 3-7: A – CO_2, CO, H_2 single gas permeabilities with respect to pressure differential for PDMS-PAN II at 24 °C; B – CO_2/CO and CO_2/H_2 ideal selectivities with respect to feed pressure

3.4.2.3 PDMS-PAN I

Single gas permeability is plotted against membrane pressure differential in Figure 3-8:A for PDMS-PAN I. This membrane used the PAN support with a MWCO of 30 kDa [34]. Overall, this membrane was much less permeable for every gas in comparison to the commercial PDMS membrane. Figure 3-8:A shows increasing permeability values of CO_2 and H_2 with higher pressure differentials, while CO observes a slight decrease. The increase in CO_2 permeability is probably the result of membrane swelling, induced by CO_2 sorption in the PDMS phase. The increases in H_2 permeability are a reflection of the results from PDMS-PAN II. Defects or pinholes in the PDMS layer are a probable cause for H_2 permeability increasing with feed pressure. The reduced permeability of CO at the highest tested feed pressure is likely within experimental error. However, based on the current data set, selectivities in Figure 3-8:B are explainable as increases in H_2 permaebility would decrease this particular membrane's selectivity. Selectivity increase for CO_2/CO in Figure 3-8:B can also be explained by the increase in CO_2 permeability as tested feed pressure increases, which in turn drives a greater selectivity with little to no change in CO permeability.

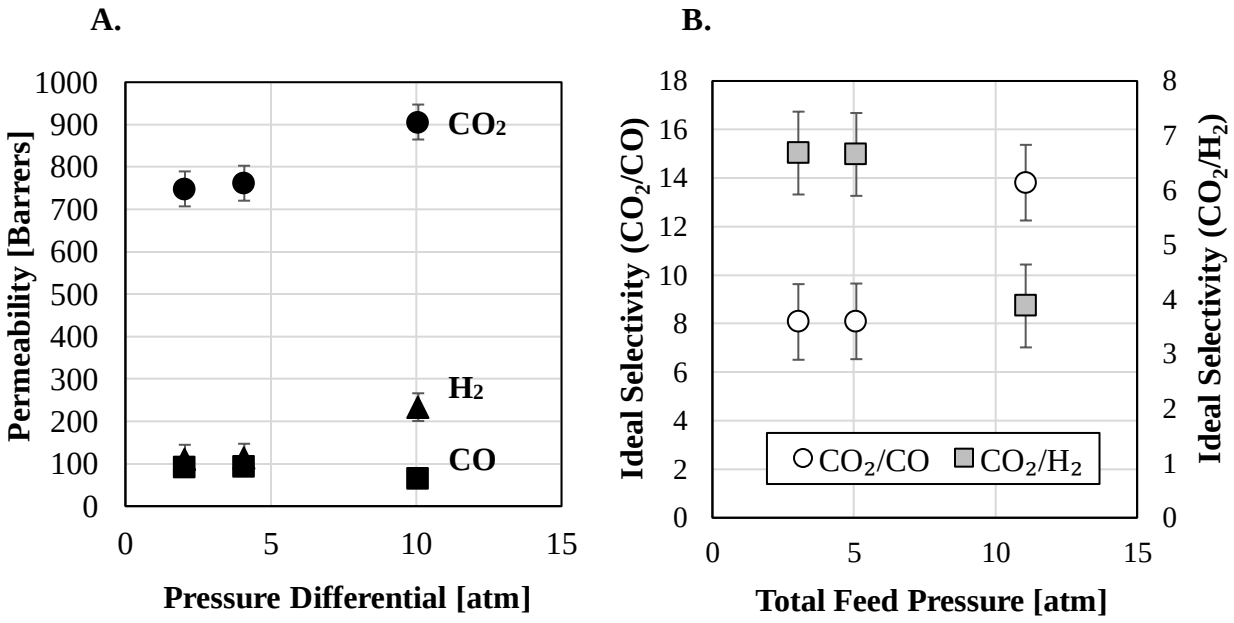

Figure 3-8: A – CO_2, CO, H_2 single gas permeabilities with respect to pressure differential for PDMS-PAN I at 25 °C; B – CO_2/CO and CO_2/H_2 ideal selectivities with respect to feed pressure

In summary, single gas experiments for CO_2, H_2 and CO were performed with each membrane. Commercial PDMS was observed to have the largest gas permeabilities across single gas experiments, followed by PDMS-PAN II and PDMS-PAN I. Due to speculated swelling and the presence of defects within PDMS, ideal selectivity of CO_2 over H_2 and CO changed with respect to feed pressure during single gas experiments. Increasing CO_2 permeability benefited commercial PDMS as CO_2 selectivities over H_2 and CO were larger at higher feed pressures. The opposite was true for CO_2/H_2 selectivity over PDMS-PAN II where CO_2 permeability remained stable in comparison to H_2 permeability and increasing feed pressure decreased this selectivity. However, both synthesized membranes reported similar CO_2/CO selectivities on average, as PDMS-PAN I saw a significant increase in this separation at high feed pressure.

3.4.3 Binary Gas Results and Discussion

3.4.3.1 CO_2:H_2

Binary permeability experimental data for all studied PDMS membranes with CO_2:H_2 feed ratios of 25:75, 50:50 and 75:25 at 23°C are shown in Figure 3-9, 3-10 and 3-11, respectively. These permeabilities were graphed as a function of partial pressure differences for each respective gas across the membrane. Overall, binary experiments proved CO_2 permeability to exceed H_2 permeability, and all membranes tested under these conditions were selective for CO_2. PDMS-PAN II and commercial PDMS were the most permeable for CO_2, while PDMS-PAN I was the least permeable for both gases.

Permeabilities observed for each gas across the tested pressure range were not always constant. Should no chemical or physical changes occur to the membrane, it was expected to see little or no change in permeability of each gas across the tested pressure range; increasing permeate flux is normalized to the partial pressure differential across the membrane. However, if a membrane experiences physical or chemical changes throughout a separation, noticeable differences in permeability may be observed. When an increase in gas permeability is observed at higher operating pressures, swelling from CO_2 may be the cause. Exposure to CO_2 during experiments can have a physical effect on the structural properties of a polymer (as discussed in single gas trends), increasing the fractional free volume allowing greater quantities of gas to diffuse through the material [36,37]. In addition to this, defects in the membrane such as pinholes or areas of void space cause gas permeabilities to increase with increasing pressure. However, at higher feed pressures (up

to 11 atm in this work), membrane compaction can cause permeabilities to drop rather than remain stable. A higher pressure is then required to maintain constant permeability to combat the effects of compaction. It should be noted that the driving force for separation of CO_2 and H_2 across each membrane changes due to differences in applied feed pressures, feed compositions and permeate compositions. These properties dictate where each permeability measurement falls along the x-axis of the figures presented below for CO_2:H_2 experimental data.

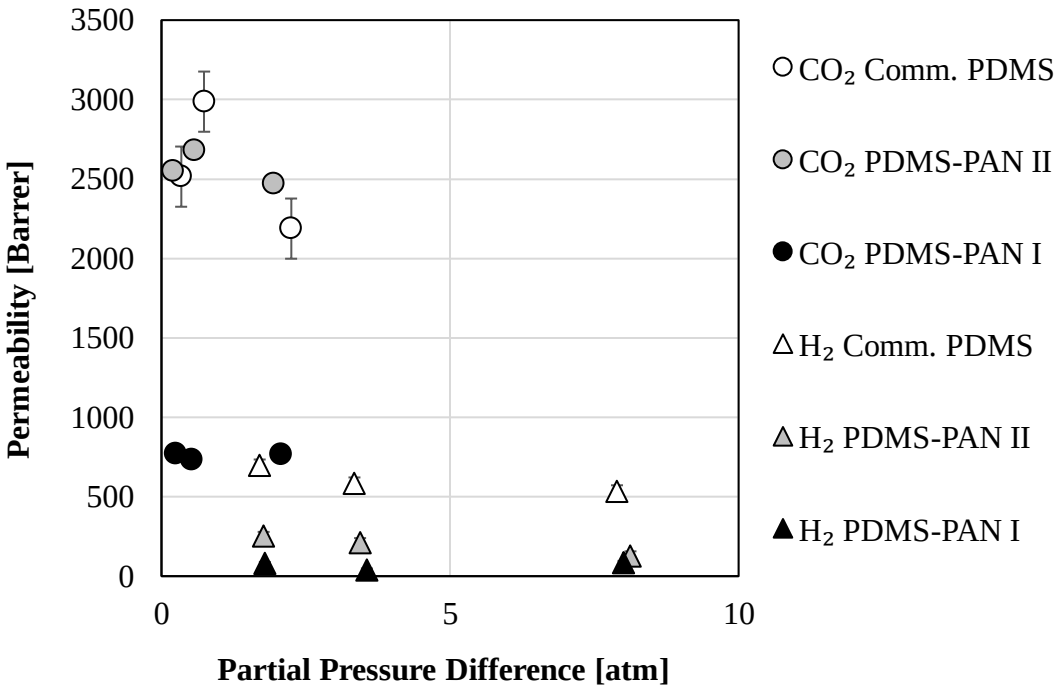

Figure 3-9: CO_2, H_2 binary gas permeabilities with respect to individual gas transmembrane partial pressure difference (25:75 CO_2:H_2) at 23 ºC and 3 – 11 atm total feed pressures

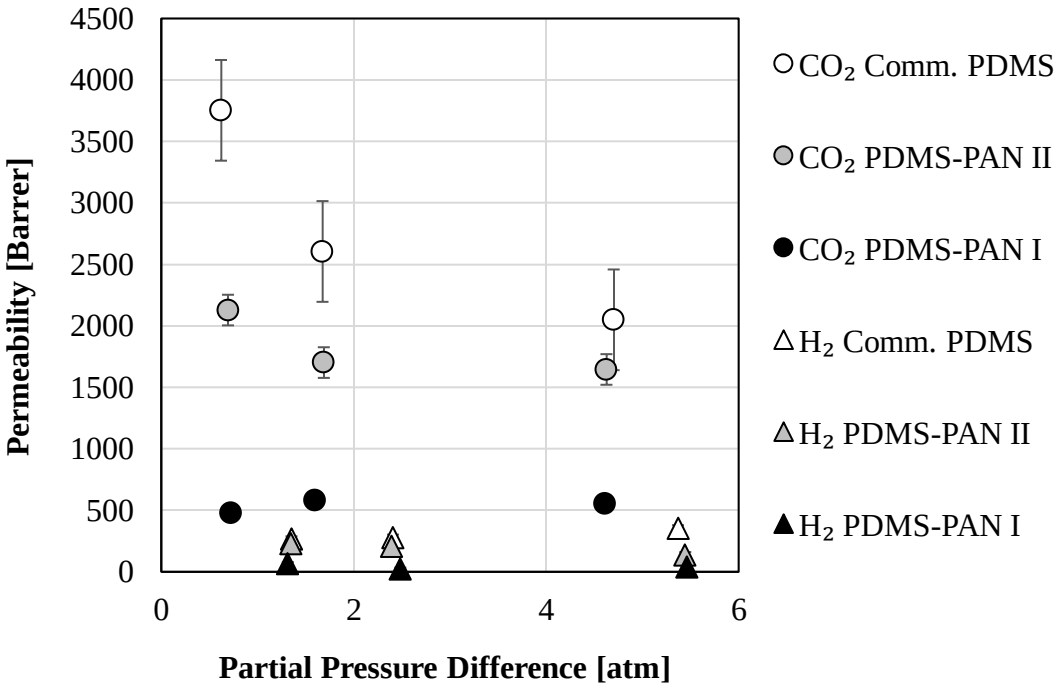

Figure 3-10: CO_2, H_2 binary gas permeabilities with respect to individual gas transmembrane partial pressure difference (50:50 CO_2:H_2) at 23 ºC and 3 – 11 atm total feed pressures

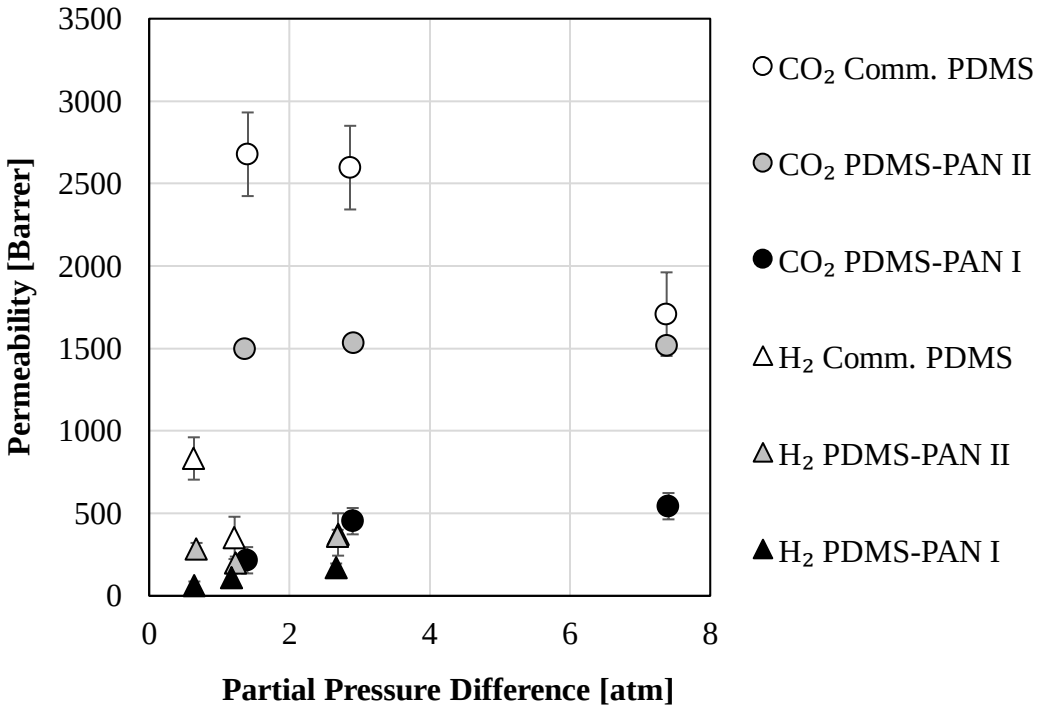

Figure 3-11: CO_2, H_2 binary gas permeabilities with respect to individual gas transmembrane partial pressure difference (75:25 CO_2:H_2) at 23 ºC and 3 – 11 atm total feed pressures

Commercial PDMS showed rather significant decreases in CO_2 permeabilities as CO_2:H_2 experiments progressed to higher partial pressures. It is reasonable to assume that change in CO_2 permeabilities for 25:75, CO_2:H_2 data for this membrane may be a result of experimental error or may be the result of decreasing permeability with greater pressure differential. However, Figure 3-10 and 3-11 show definitive decreases in CO_2 permeability for the commercial membrane, which can be attributed to membrane compaction. Compaction would affect the gases permeating the most through a dense PDMS polymer, where solubility is the primary separating component. The effects of membrane compaction will be observed first for a larger molecule like CO_2, with low diffusivity in comparison to H_2. When the polymer is compacted, the larger molecules will experience a significant reduction in diffusivity in comparison to H_2. Hydrogen permeability did show decreasing trends for the commercial membrane, with the exception of Figure 3-10, where H_2 permeability actually increases by roughly 90 Barrers (from a feed pressure of 3 to 11 atm) for the commercial membrane. Accounting for error, this difference is minimal in comparison to the variation in CO_2 permeabilities on the same plot.

In the case of single gas experiments for commercial PDMS, swelling was speculated to be the reason for increasing CO_2 permeability. However, the commercial membrane was the thinnest PDMS membrane tested in this work, meaning it would not have as much structural integrity as the thicker, synthesized PDMS membranes (PDMS-PAN I and PDMS-PAN II) which would allow it to be more easily compressed. So, after exposure to more high-pressure experiments, compaction is reasoned to cause decreases in both CO_2 and H_2 permeabilities for commercial PDMS.

Much like the commercial membrane, PDMS-PAN II observed some decreasing CO_2 and H_2 permeabilities with respect to partial pressure difference. This began in Figure 3-9 with H_2 and continues into Figure 3-10 where both CO_2 and H_2 permeability decrease with increasing feed pressure. This is likely due to membrane compaction as the trends end up affecting both components, rather than singly H_2 individually. Competitive mass transport from the introduction of a binary gas feed could dictate that CO_2 would occupy more volume within PDMS and prevent H_2 from transporting to the permeate. However, in the case of 50:50, CO_2:H_2 experiments, both CO_2 and H_2 observe a decrease. The measured selective layer of PDMS-PAN II was thicker than commercial PDMS, however it was not as thick as PDMS-PAN I – which did not observe decreasing gas permeabilities for CO_2:H_2 binary gas experiments, discussed later. It was probable that commercial PDMS was significantly affected by compaction, which is speculated to be a result of

how thin the selective layer is, in comparison to the synthesized membranes. PDMS-PAN II was measured to be 20 µm thinner than PDMS-PAN I, so compaction could be expected with this thinner PDMS layer. However, in Figure 3-11 permeabilities of both gases remained stable for PDMS-PAN II. Therefore, one could assume that the effects of compaction no longer persisted for 75:25, CO_2:H_2 experiments.

PDMS-PAN I exhibited CO_2 and H_2 permeabilities that were stable for all CO_2:H_2 binary experiments with the exception of experimental data shown in Figure 3-11 for 75:25 CO_2:H_2 feed ratio. The set of experiments for this membrane for binary mixture of CO_2:H_2 showed an increase with increasing partial pressure in both CO_2 and H_2 permeabilities due to probable membrane swelling. PDMS-PAN I was the thickest PDMS membrane synthesized, so a greater volume of CO_2 could be sorbed in the polymer at any given time during binary experiments. Binary experiments were performed with ascending order of CO_2 concentration in the feed (25, 50 and then 75 mol % of CO_2 in H_2), meaning greater amounts of CO_2 could sorb in PDMS with greater CO_2 concentration in the feed. For this reason, the effects of swelling could increase with each corresponding binary feed experiment, which is seen from the progression of CO_2:H_2 experiments (no increase in permeability with increasing partial pressure at 25 mol % CO_2 to increasing permeability with respect to pressure differential at 75 mol %). Therefore, CO_2 and H_2 permeabilities increase more with respect to partial pressure difference as overall CO_2 concentration and partial pressure increases in the feed for PDMS-PAN I.

A CO_2/H_2 selectivity versus CO_2 permeability plot from Lin et al. [36] was used for additional data analysis. Figure 3-12 presents CO_2/H_2 selectivities as a function of CO_2 permeabilities from this binary work in comparison to the literature data (noted in the legend as 'Literature Ref.') specific to polymeric membrane separation. The better performing membranes on this graph approach the upper right corner where both selectivity and permeability values are maximized, a challenging feat in the membrane world. All the membranes tested in this work land towards this area of the graph.

The most notable separations on this graph are PDMS-PAN I and PDMS-PAN II with feed compositions less than or equal to 50 mol % CO_2 (the greatest selectivity of 16). The stage cut of these experiments approached 0, meaning the ratio of permeate to feed flow was negligible. This, coupled with the fact that this is a single stage membrane separation, means that as the CO_2 concentration in the feed increases (in this case, past 50 mol %), it becomes more difficult to achieve

a high purity of CO_2 in the permeate in comparison to the feed concentrations. For example, commercial PDMS achieved a 10 % increase in CO_2 permeate concentration from 50:50 to 75:25, CO_2:H_2 experiments. However, because the feed compositions were also increasing in CO_2 composition, small differences in the permeate stream ratios can dictate a large drop in separation. To overcome this, a multi-stage membrane separation would be suggested.

PDMS-PAN I and PDMS-PAN II achieved the highest binary CO_2/H_2 selectivity values. In reference to this graph, these membranes did show lower permeability. While small advances across a logarithmic scale can be amplified because of the nature of the graph, these two membranes are not far off the permeability rates that commercial PDMS achieved in CO_2:H_2 binary experiments (highest permeability of 3,753 Barrers). This is promising, as maintaining separation while striving to increase permeability would mean simply optimizing the PDMS on a 300 kDa PAN support.

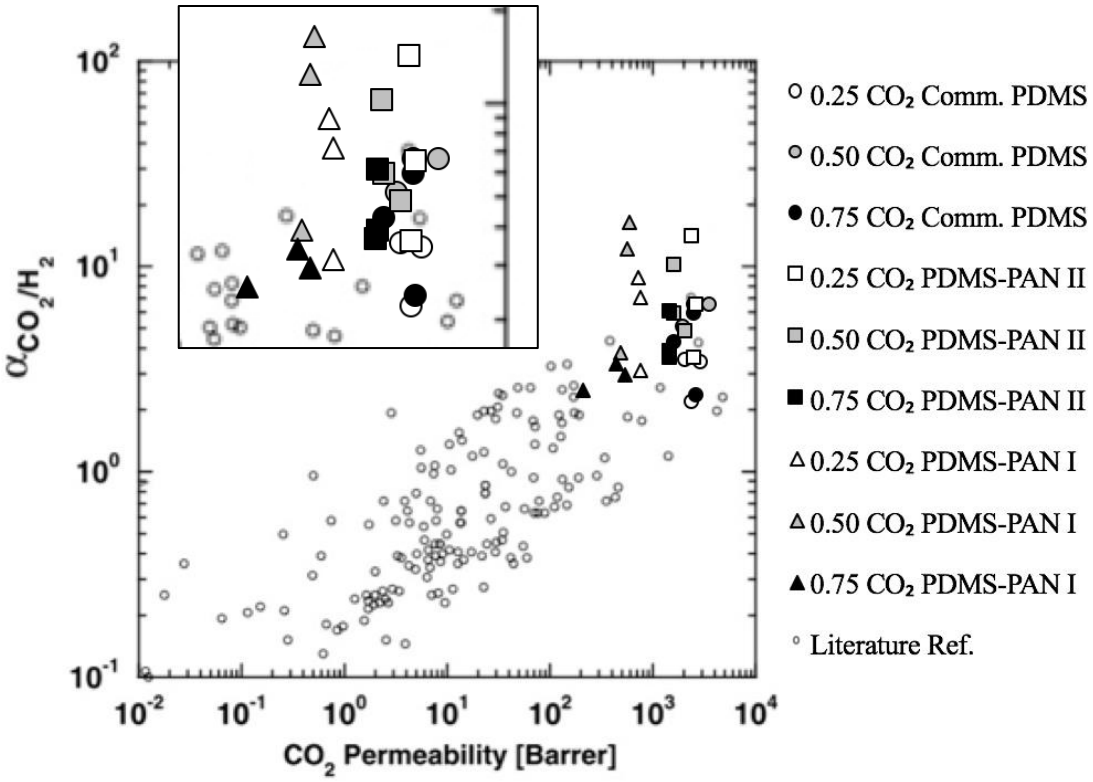

Figure 3-12: CO_2/H_2 selectivity with respect to CO_2 permeability binary data from Figure 3-9 to Figure 3-11, plotted in comparison to literature data (0.25, 0.50, 0.75 refers to CO_2 mole fraction in CO_2:H_2 feed) [36]**; the insert shows an enlarged version of the same data of the upper right corner of the figure.**

3.4.3.2 CO_2:CO

The results of binary permeability experiments for all studied PDMS membranes are shown for CO_2:CO feed ratios of 25:75, 50:50 and 75:25, in Figure 3-13, 3-14 and 3-15, respectively. CO_2 and CO permeabilities were graphed as a function of partial pressure differences for each respective gas across the membrane. Much like the CO_2:H_2 binary experiments, CO_2 permeability was greater than CO across the partial pressure range studied, and every membrane was selective for CO_2 over CO. Commercial PDMS remained the most permeable and PDMS-PAN I was again the least permeable.

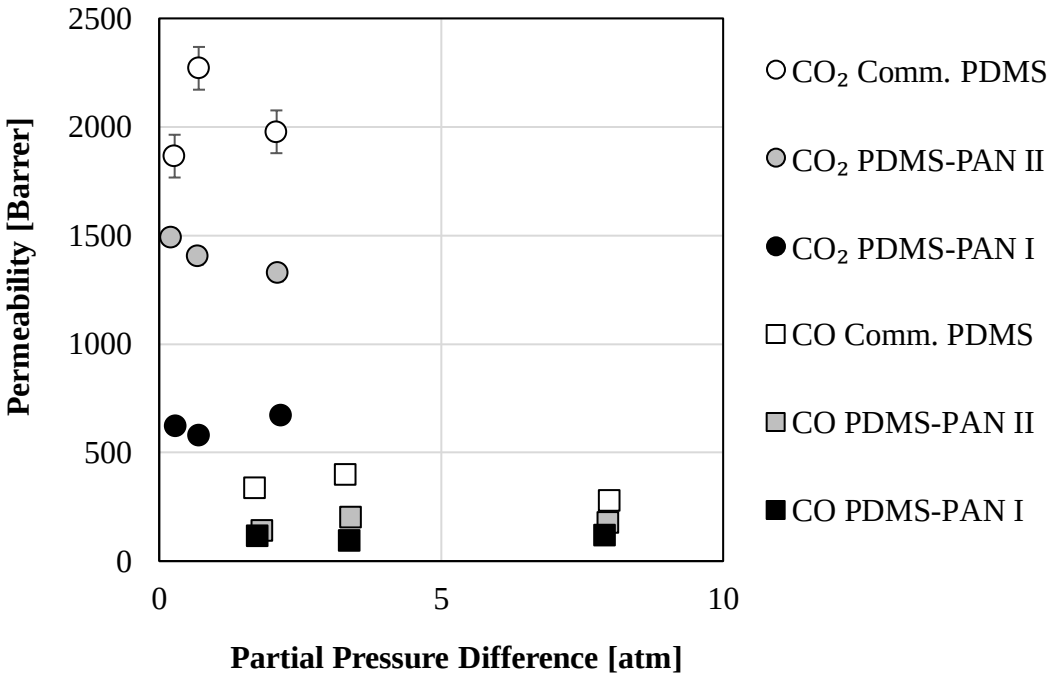

Figure 3-13: CO_2, CO binary gas permeabilities with respect to individual gas transmembrane partial pressure difference (25:75 CO_2:CO) at 24 ºC and 3 – 11 atm total feed pressures

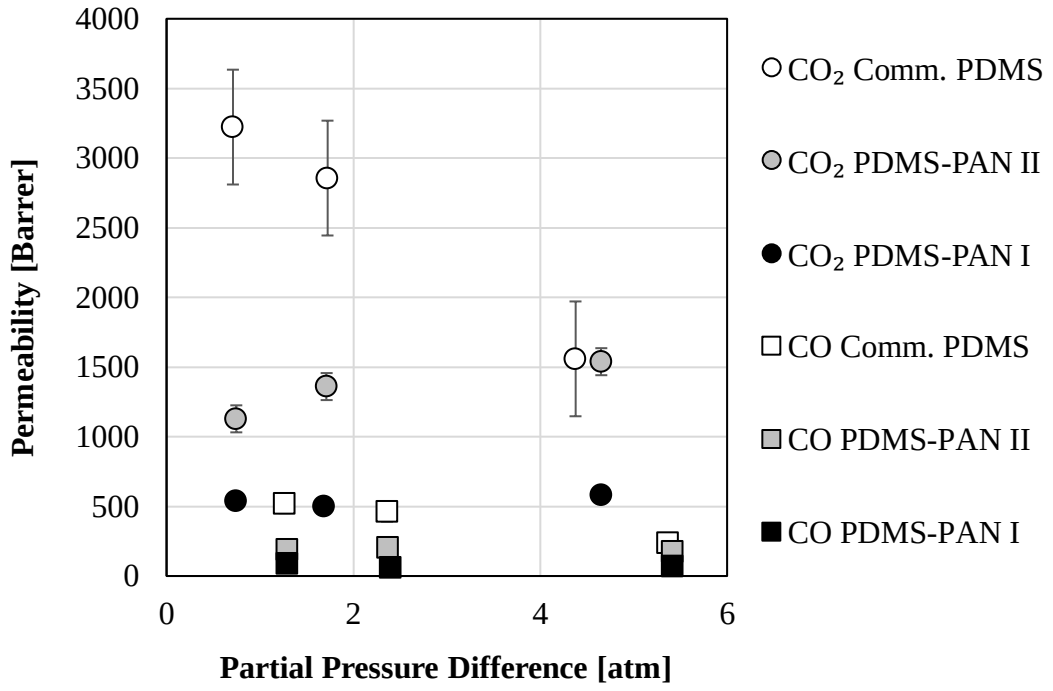

Figure 3-14: CO_2, CO binary gas permeabilities with respect to individual gas transmembrane partial pressure difference (50:50 CO_2:CO) at 24 ºC and 3 – 11 atm total feed pressures

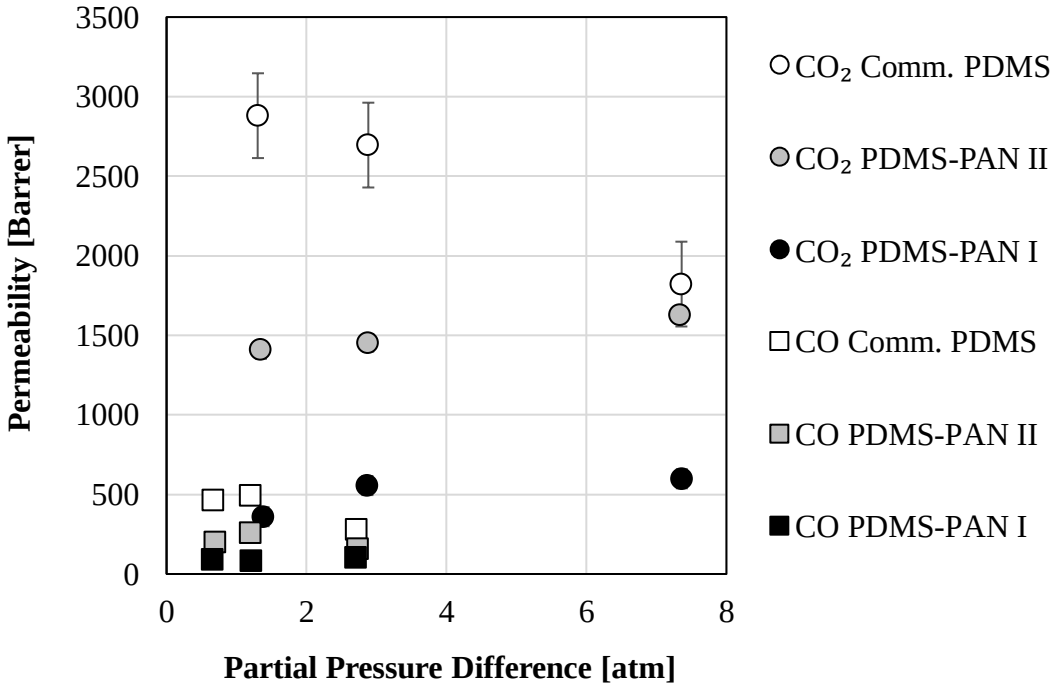

Figure 3-15: CO_2, CO binary gas permeabilities with respect to individual gas transmembrane partial pressure difference (75:25 CO_2:CO) at 24 ºC and 3 – 11 atm total feed pressures

As seen in CO_2:H_2 binary experiments, CO_2:CO data showed similar trends regarding CO_2 and CO permeabilities with respect to partial pressure difference through the commercial PDMS membrane. The deviation in CO_2 permeability across the tested pressure range in Figure 3-13 is not insignificant, but it does not define a clear trend for this membrane. Much like Figure 3-9, it is reasonable to assume that these differences may be a result of experimental error or may in fact be the result of compaction with a greater partial pressure differential. However, Figure 3-14 and 3-15 show definitive decreases in both CO_2 and CO permeabilities for the commercial PDMS, which can again be attributed to probable membrane compaction. Compaction is likely a continuous trend that commercial PDMS experiences for all binary experiments performed in this work, where compressing of the polymer chains increases the density, reducing gas diffusivities.

Permeability trends were not consistent for PDMS-PAN II. At first in Figure 3-13, PDMS-PAN II showed decreasing CO_2 permeability with respect to partial pressure differential. This trend was an extension of what was observed in CO_2:H_2 binary experiments. In Figure 3-14 and 3-15, the opposite trend was observed from Figure 3-13, where CO_2 permeability increased with increasing partial pressure difference for the PDMS-PAN II membrane. As these binary experiments were conducted, CO_2 concentration and partial pressures were increasing from a 25 mol % to a 75 mol % feed concentration, mirrored from Figure 3-13 to 3-15, respectively. For this reason, it could be speculated that a molar CO_2 feed concentration of 25 % or below in combination with CO, is not able to swell PDMS-PAN II. Instead, it observes compaction, with decreasing permeability with increasing partial pressure difference, as it may not be thick enough to withstand the same physical forces as PDMS-PAN I. However, CO_2 molar feed concentrations of 50 % in CO and up are speculated to cause PDMS-PAN II to swell, with higher CO_2 partial pressures over the same feed pressure range, as permeability increases with increasing partial pressure difference. From this data analysis, it is reasonable to assume that PDMS-PAN II could observe both compaction and membrane swelling, depending on the concentration of the CO_2 in the mixture with CO.

The trend for gas permeabilities throughout CO_2:CO binary experiments for PDMS-PAN I was generally stable. The exception to this trend was the data presented in Figure 3-15, where both CO_2 and CO permeabilities see a distinct increase with respect to partial pressure difference. This was also observed in binary experiments with CO_2:H_2 (with respect to the order of experiments, seen in Figure 3-11), meaning this trend was repeated in CO_2:CO binary data. This suggests that after previous exposure to single and binary gas feeds, PDMS continued experiencing membrane

swelling, which increases when there are greater concentrations of CO_2 present in the feed. With larger feed compositions of CO_2, a greater amount of CO_2 can be sorbed in PDMS and effectively increase the fractional free volume in the polymer. This justifies why permeabilities of CO_2, H_2 and CO gases (for CO_2:H_2 and CO_2:CO experiments) can see an increase with respect to partial pressure difference when the concentration of CO_2 in the feed is 75 mol % (as seen in Figure 3-11 for CO_2:H_2 and Figure 3-15 for CO_2:CO).

In the case of CO_2 separation from CO (seen in Figure 3-16), the permeability and selectivity for CO_2:CO binary experiments were plotted on the same graph axes as Figure 3-12, however the reference literature data points were collected from different sources, specific to this separation [16,17,36,38]. The literature reference points are outlined in the legend as 'Literature Ref.' and include single and mixed gas data. Since the separation of CO_2 from H_2 has been studied more widely than CO_2 from CO, the amount of data collected from literature to compare to the data collected in this work is limited. However, Figure 3-16 serves as a starting point for CO_2/CO selectivity-permeability analysis. Like Figure 3-12, the best suited membranes exhibit high permeability and selectivity, meaning this data would approach the upper right corner of this selectivity-permeability plot.

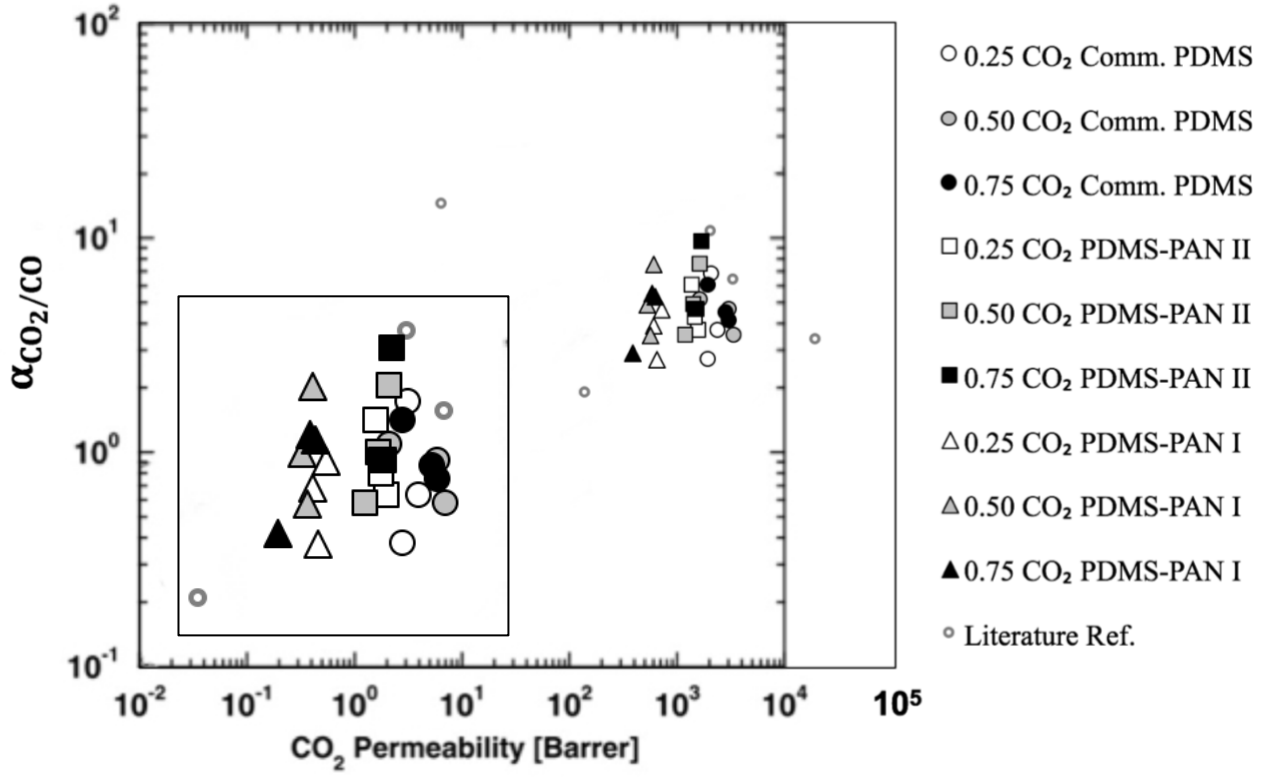

Figure 3-16: CO_2/CO selectivity with respect to CO_2 permeability binary data from Figure 3-13 to Figure 3-15, plotted in comparison to literature data (0.25, 0.50, 0.75 refers to CO_2 mole fraction in CO_2:CO feed) [16,17,36,38]**; the insert shows an enlarged version of the same data of the upper right corner of the figure.**

CO_2/CO selectivity did not vary as greatly between membranes as CO_2/H_2 selectivity did for binary experiments. Commercial PDMS was still the most permeable for CO_2. While PDMS-PAN I remained the least permeable, it was not as selective as PDMS-PAN II overall, making it the least favourable candidate for CO_2 separation from CO. None of the membranes from this work surpassed any of the literature reference data plotted in Figure 3-16 for selectivity, although the general trend of CO_2:CO binary data was towards the upper right quadrant of the graph. PDMS-PAN II exhibited the best separation over CO (selectivity of 9) with minimal difference in permeability in comparison to commercial PDMS (largest permeability of 3,222 Barrers). Therefore, in the case of CO_2:CO binary experiments, PDMS-PAN II was the most suitable membrane with permeabilities comparable to commercial PDMS and the greatest separation of CO_2 from CO. In conclusion from the binary experiments, although CO_2 permeability was the highest

for commercial PDMS, PDMS-PAN II maintained greater separation and higher CO_2 permeabilities than PDMS-PAN I across the binary feed concentration range.

3.4.4 Ternary Gas Results and Discussion

Ternary gas feeds were introduced to the three membranes tested in this study and the corresponding permeability data as a function of partial pressure differences can be viewed in Figure 3-17. Permeability was plotted on a logarithmic scale to allow for easier analysis between the three membranes. Much like the binary and single gas data, CO_2 permeated more than CO and H_2 for all membranes tested and each membrane tested with ternary gas feeds could successfully separate CO_2 from both syngas components (CO and H_2). Also, H_2 permeability for each PDMS membrane was lower on average for ternary gas experiments than single gas experiments. When more than one gas is present in a membrane feed, there can be competitive gas transport. This is the case for H_2 permeability, where CO_2 and CO compete to permeate over H_2. CO_2 and CO are more soluble in PDMS than H_2, due to properties like higher condensability [15]. A rubbery polymer like PDMS has difficulty sieving molecules based purely on gas penetrant size, so differences in solubility take precedence when multiple gases are being separated. This causes CO_2 and CO to compete for transport over H_2, and decreases H_2 permeability for ternary gas feeds [39].

Many of the permeability trends with respect to pressure difference from single and binary gas experiments continued into ternary gas experiments as can be seen in Figure 3-17. Commercial PDMS continued to experience membrane compaction with decreasing CO_2 and CO permeability with respect to partial pressure difference. H_2 permeability, however, increased with increasing partial pressure difference and surpassed CO permeability at the highest tested feed pressure for this membrane. It can be speculated that compaction could begin to favour permeation of H_2 over larger molecules like CO and CO_2, as the membrane begins to become more and more compressed (acting like a size sieving material). In order to counteract compaction, adsorbent particles can be added into the PDMS matrix (forming mixed matrix membranes) to increase the strength of the membrane to outward pressure forces [40,41]. Additionally, the particles can have capabilities for separation of CO_2 from CO to enhance the separation in a mixed matrix membrane format [42].

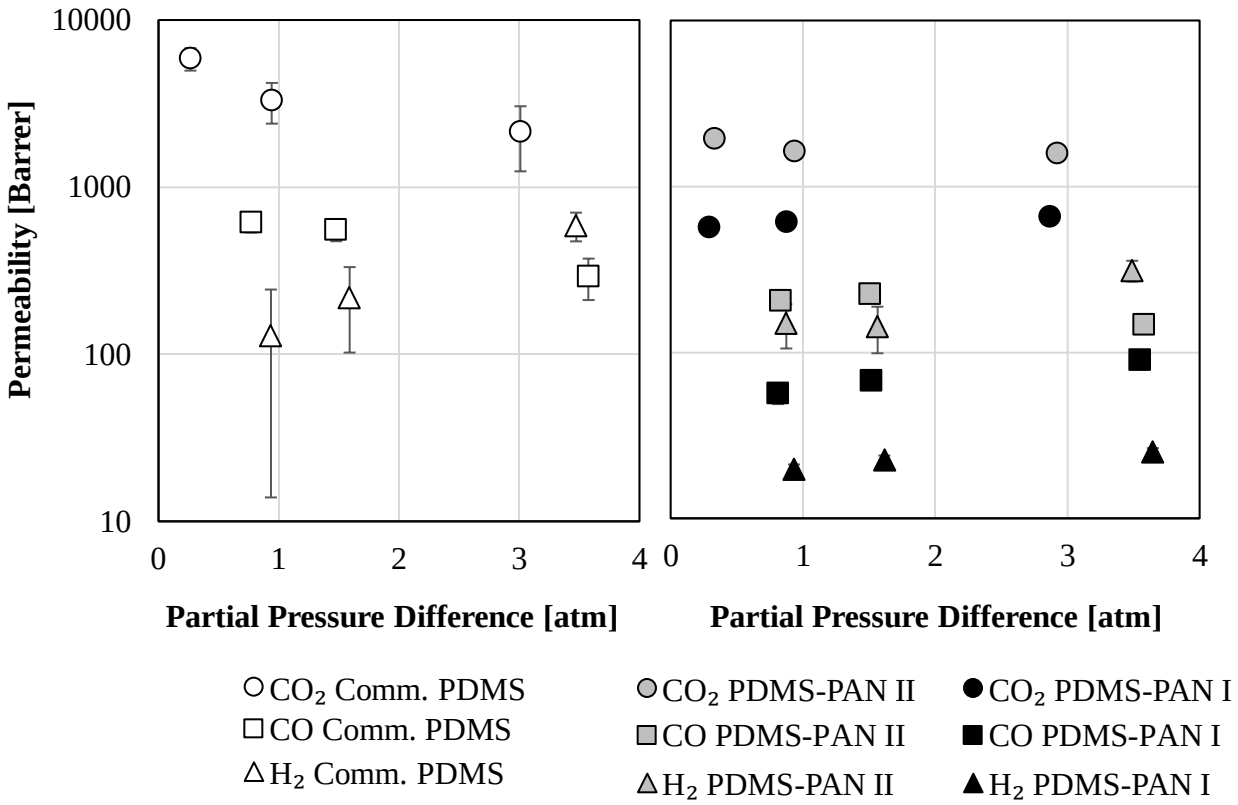

Figure 3-17: CO_2, CO, H_2 ternary gas permeabilities with respect to individual gas transmembrane partial pressure difference (1:1:1 CO_2:CO:H_2) at 24 °C

PDMS-PAN I continued to observe increasing permeability for all gases with partial pressure differential, suggesting that membrane swelling was still responsible for this trend after prolonged exposure to CO_2. Stabilizing additives have been studied and published in literature to counteract this issue and could be incorporated into a PDMS matrix to help prevent CO_2 from affecting the structural nature of the membrane [43]. PDMS-PAN II observed decreasing CO_2 and CO permeabilities with respect to partial pressure differential, while H_2 increased with respect to partial pressure difference – similarly to commercial PDMS. H_2 permeability also surpassed CO permeability at the highest tested feed pressure for this membrane. Again, hydrogen is a much smaller molecule than both CO and CO_2, meaning it has a diffusivity advantage over larger molecules. This may be amplified after a certain degree of compaction with high partial pressure differences.

Ternary data was plotted on a CO_2/H_2 selectivity versus CO_2 permeability graph in Figure 3-18 which is adapted from Lin et al. [36], to observe where the tested membranes fell with respect

to published literature (reference data denoted by "Literature Ref." in the legend). On this plot, PDMS-PAN I clearly exhibited the highest CO_2/H_2 selectivity of 21 in comparison to the other membranes tested, including literature data. Competitive sorption proved to benefit the separation of this membrane with the most significant decrease in H_2 permeability in comparison to PDMS-PAN II and commercial PDMS. Commercial PDMS and PDMS-PAN II fell in the general trend area of the reference membranes from the literature with higher CO_2 permeabilities than PDMS-PAN I; with the largest ternary CO_2 permeability of 5,883 Barrers. Ideally, with a reduction in PDMS thickness, an optimized membrane would create permeabilities and selectivities that would land in the region between PDMS-PAN I and commercial PDMS in Figure 3-18.

Figure 3-19 outlines the comparison between CO_2 permeability and CO_2/CO separation for ternary gas data. In this figure it is clear to see that the varation in separation is not as great as Figure 3-18; CO_2/CO selectivities varied between 3 and 9, where CO_2/H_2 selectivities varied between 3 and 21. It is reasonable to assume that PDMS thicknesses between 7 and 75 μm do not have as significant of an impact on CO_2/CO selectivity, in comparison to CO_2/H_2 selectivity. Of all three membranes, PDMS-PAN II achieved the highest CO_2/CO selectivity of 9, as was the case in binary data.

With a 60 to 80 % reaction conversion of CO_2 in the RWGS, Table 3-7 outlines the product stream molar compositions assuming no side reactions. There are many variables associated with the RWGS reaction (i.e., operating conditions, changing feed composition, catalyst) that make it hard to predict the exact product stream compositions a separation unit downstream would face. While the ternary experiments in this work do not completely represent the RWGS product stream scenarios, they provide insight into a membrane's capabilities when faced with the gases in question. After characterizing PDMS as a membrane material for this separation, the intention of this work is to determine the best possible way to utilize PDMS as a membrane material to perform a recycle stream separation for the RWGS reaction. In reality, it would be necessary to use a series of these membranes (such as a spiral wound format) to maintain this separation quickly and efficiently. Of the three membranes examined, the maximum molar concentration of CO_2 in the permeate stream was 82 % from a ternary gas feed. This could be further optimized, with a larger membrane surface area.

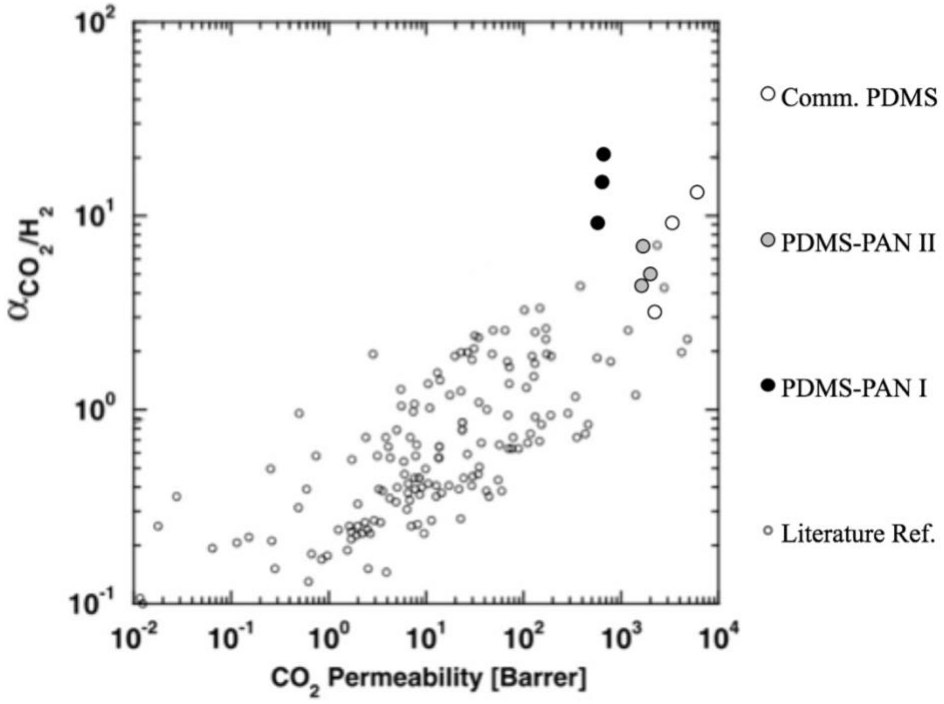

Figure 3-18: CO_2/H_2 selectivity with respect to CO_2 permeability ternary data from Figure 3-18, plotted in comparison to literature data [36]

Table 3-7: Breakdown of RWGS product stream molar compositions assuming a H_2/CO_2 ratio of 2 at 750 ºC to 1200 ºC [4]

CO_2 Conversion	60 % Product Stream	80 % Product Stream
CO_2 mol %	17 %	9 %
CO mol %	25 %	36 %
H_2 mol %	58 %	55 %

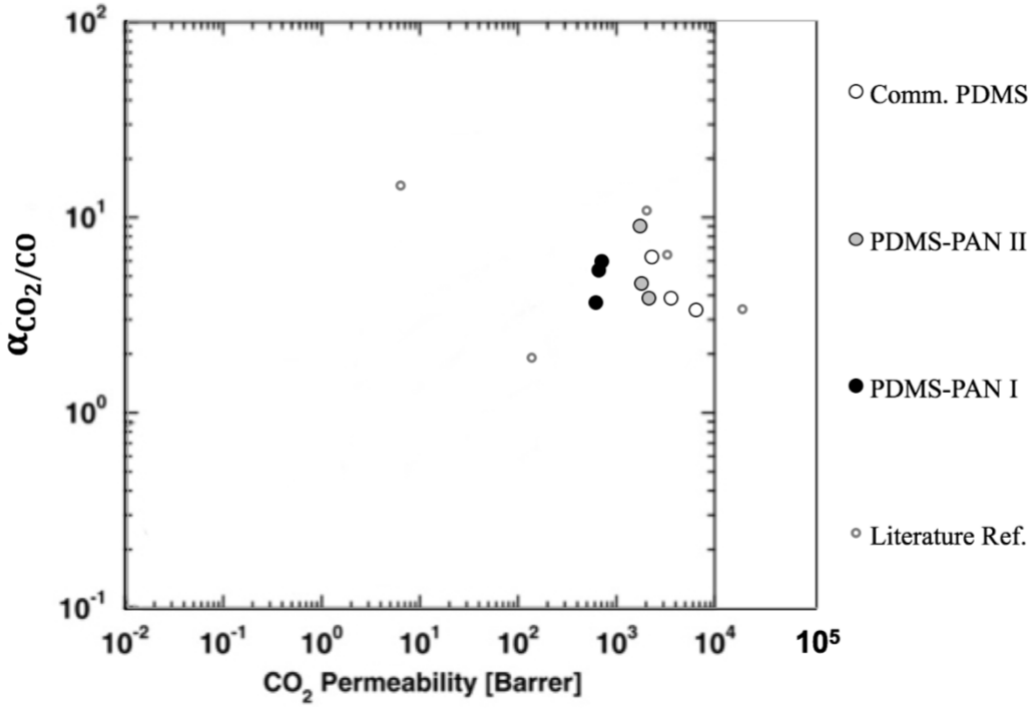

Figure 3-19: CO_2/CO selectivity with respect to CO_2 permeability ternary data from Figure 3-18, plotted in comparison to literature data [16,17,36,38]

3.5 CONCLUSIONS AND FUTURE WORK

Commercial PDMS and two synthesized PDMS membranes were investigated for separation of CO_2 from two syngas components. A flat-sheet membrane system was constructed and used to test the membranes under single, binary and ternary gas feeds up to a total pressure of 11 atm at room temperature (23 to 25 ºC). SEM imaging confirmed selective layer thicknesses (7 to 75 µm) and uniformity of the three PDMS layers. PDMS on a PAN support successfully separated CO_2 from both CO and H_2.

Single gas experiments proved that PDMS was selective for CO_2 over CO and H_2. The commercial PDMS membrane purchased from Sulzer Ltd was confirmed to be the thinnest and exhibited the largest gas permeabilities for all components. The synthesized PDMS-PAN I membrane was the thickest measured and exhibited the smallest gas permeabilities for all components. Selectivities did experience some variation as membrane swelling is speculated to have increased CO_2 and H_2 permeability with respect to feed pressure.

Binary experiments provided some more insight in terms of how each membrane performed when exposed to combinations of CO_2:H_2 and CO_2:CO, in varying compositions. Commercial

PDMS was the most permeable and overall the least selective for CO_2 from both syngas components. It experienced significant membrane compaction. PDMS-PAN I experienced membrane swelling from CO_2 and remained the least permeable membrane with the highest CO_2/H_2 selectivity of 16. Analysis from a selectivity-permeability plot confirmed that PDMS-PAN I and PDMS-PAN II were the leading materials in separation and overall membrane permeability in comparison to the literature. It demonstrated that while commercial PDMS could perform this separation with the highest CO_2 flux, PDMS-PAN I exhibited the highest selectivity for CO_2 over H_2.

Ternary gas experiments provided a realistic look into a RWGS product stream separation. Although an even split of CO_2, CO and H_2 did not exactly represent RWGS product stream compositions, it provided a good first look into how PDMS performed with all three gases. PDMS-PAN I proved to deliver high separation of CO_2 from H_2 (highest selectivity of 21) in a ternary feed environment after CO_2 swelling. However, PDMS-PAN II was the most selective for CO_2 over CO (selectivity of 9) with the highest CO_2 permeability of 1,949 Barrers, comparable to the 1,993 Barrers reported by Scholes et al. [16]. The MWCO of 300 kDa from the PAN support proved to facilitate greater permeability in general for PDMS-PAN II, while maintaining high separation of CO_2.

Membrane compaction and swelling by CO_2 were believed to cause the decreases and increases observed in permeability trends through each membrane with respect to feed pressure. Commercial PDMS experienced the most significant change in permeability with respect to pressure from speculated compaction. This could be overcome by introducing adsorbent particles into to the matrix to increase the strength of the membrane from outward pressure forces. PDMS-PAN I observed the most increases in permeability with respect to pressure due to CO_2 swelling. Stabilizing additives can also be investigated for further support.

Ternary gas experiments proved that the permeabilities reported in this work were similar to those reported in literature. The highest reported CO_2/H_2 selectivity in this work with ternary gas feeds for PDMS-PAN I membrane was 21 at a feed total pressure of 11 atm, which was more than twice as selective as a commercial PDMS membrane reported in literature at 8 atm (mixed gas CO_2/H_2 selectivity of 6.8) [16]. The highest CO_2/CO selectivity in this work achieved with PDMS-PAN II membrane was 9 and was consistent between binary and ternary gas feeds. This was also close to the CO_2/CO selectivity of 10.8 reported by Scholes et al. for a mixed gas feed [16]. PDMS

proved to be a competitive candidate in comparison to the literature data with high permeabilities and selectivities for CO_2 over H_2 and CO.

Future work should begin by repeating and extending the current data sets to develop a broader understanding of the true nature of the permeability trends with respect to partial pressure differences across each membrane. Repeatability should also be validated to solidify the error that is inherent to the experimental system. Three data points along an x-axis provides an initial understanding of the data collected, but the suggestions above would provide a stronger argument in terms of physical changes to each membrane and the error associated with each measurement.

Additionally, there are other operational avenues that could be considered. Should compaction remain an issue, it may be recommended to operate at pressures below 5 atm in feed pressure to minimize decreases in gas permeability. This also aligns with the typical low operating pressure of the RWGS. PDMS also serves as a sufficient polymer matrix to house inorganic materials for mixed matrix membrane fabrication, which would offer mechanical support. With appropriate contact between particle and polymer, inorganic particles can be used to enhance the separation that PDMS can already achieve. Furthermore, to better understand how these materials respond to high pressure and long exposures to gases known to cause membrane swelling (CO_2), more work could be done on the effects of permeability and selectivity. The membranes could be exposed to CO_2 for longer periods, and repeated high-pressure experiments could be performed to note any differences in gas permeabilities and selectivities.

3.6 ACKNOWLEDGEMENTS

The authors would like to thank and acknowledge the financial support received from MITACS (Mathematics of Information Technology and Complex Systems), Phoenix Canada Oil Company Ltd., NSERC (Natural Science and Engineering Research Council of Canada) and Natural Resources Canada. The authors would like to thank Hoda Azimi for providing the PDMS-PAN II membrane tested in this work and providing guidance and information for the synthesis method. The authors would also like to thank Glenn Poirier on behalf of the University of Ottawa for the SEM imaging, training and assistance in the Advanced Research Centre (ARC).

3.7 NOMENCLATURE

Term	Definition	Units
C	Concentration in membrane	mol/cm^3
D	Diffusivity coefficient	cm^2/s
J	Permeate flux	$cm^3\ (STP)/s \cdot cm^2$
MWCO	Molecular weight cut-off	Da, kDa
P	Permeability	$10^{-10}\ \frac{cm^3\ (STP) \cdot cm}{s \cdot cm^2 \cdot cmHg}$ = 1 Barrer
ΔP	Partial pressure differential	cmHg, atm
R	Molar ratio of H_2 to CO_2	mole:mole
S	Solubility coefficient	$\frac{cm^3\ (STP)}{cm^3 \cdot atm}$
$\mathbf{x_A}$, $\mathbf{x_B}$	Mole fraction of component A, B in feed	Dimensionless
$\mathbf{X_{CO2,equil}}$	Equilibrium conversion of CO_2 in RWGS	%
$\mathbf{y_A}$, $\mathbf{y_B}$	Mole fraction of component A, B in permeate	Dimensionless
z	Selective membrane thickness	cm
$\mathbf{\alpha^*_{A/B}}$	Ideal selectivity of A over B	Dimensionless
$\mathbf{\alpha_{A/B}}$	Actual selectivity of A over B	Dimensionless

3.8 ABBREVIATIONS AND SYMBOLS

Symbol	Description
CO_2	Carbon dioxide
CO	Carbon monoxide
H_2	Hydrogen
He	Helium
GC	Gas chromatograph
GPU	Gas permeation unit
OD	Outer diameter
PAN	Polyacrylonitrile
PERVAP™ 4060	PDMS commercial membrane (Sulzer)
PDMS	Polydimethylsiloxane
RWGS	Reverse Water Gas Shift
SEM	Scanning electron microscope
STP	Standard temperature and pressure (0 °C, 1 bar)

3.9 REFERENCES

[1] S.A. Rackley, Carbon Capture and Storage, 1st ed., Butterworth-Heinemann, 2009.

[2] K. Zickfeld, M. Eby, H.D. Matthews, A.J. Weaver, Setting cumulative emissions targets to reduce the risk of dangerous climate change., in: Proc. Natl. Acad. Sci. U. S. A., 2009: pp. 16129–16134.

[3] F. Abdollahi, F.H. Tezel, S. Aplin, Increasing Conversion of CO_2 To CO Via RWGS Reaction: Simulation and Process Design, Altern. Energy. 2 (2013) 1–6.

[4] U.R. Bajirao, Kinetics and Reaction Engineering Aspects of Syngas Production by the Heterogeneously Catalysed Reverse Water Gas Shift Reaction, Ph.D. Thesis, University of Bayreuth, 2012.

[5] W.L. Luyben, Control of parallel dry methane and steam methane reforming processes for Fischer-Tropsch syngas, J. Process Control. 39 (2016) 77–87.

[6] D. Bell, B. Towler, M. Fan, Coal Gasification and It's Applications, in: 1st ed., William Andrew (Elsevier), Great Britain, 2011: pp. ix–xi.

[7] A. Steynberg, M. Dry, Studies in Surface Science and Catalysis, in: M. Dry (Ed.), Stud. Surf. Sci. Catal., Science Direct (Elsevier), 2004: pp. 1–63.

[8] P. Bernardo, E. Drioli, G. Golemme, Membrane Gas Separation: A Review / State of the Art, Ind. Eng. Chem. Eng. Res. 48 (2009) 4638–4663.

[9] S. Shelley, Capturing CO_2: Membrane Systems Move Forward, Chem. Eng. Prog. 105 (2009) 42–47.

[10] W.J. Koros, Evolving Beyond the Thermal Age of Separation Processes: Membranes Can Lead the Way, AIChE J. 50 (2004) 2326–2334.

[11] J.D. Seader, E.J. Henley, K.D. Roper, Separation Process Principles: Chemical and Biochemical Operations, in: 3rd ed., Wiley, 2010: p. 848.

[12] R.W. Baker, Membrane Technology and Applications, in: 3rd ed., John Wiley & Sons Ltd., 2012: pp. 15–84.

[13] J.G. Wijmans, R.W. Baker, The solution-diffusion model: a review, J. Memb. Sci. 107 (1995) 1–21.

[14] M.K. Barillas, R.M. Enick, M. O'Brien, R. Perry, D.R. Luebke, B.D. Morreale, The CO_2 permeability and mixed gas CO_2/H_2 selectivity of membranes composed of CO_2-philic polymers, J. Memb. Sci. 372 (2011) 29–39.

[15] T.C. Merkel, V.I. Bondar, K. Nagai, B.D. Freeman, I. Pinnau, Gas sorption, diffusion, and permeation in poly(dimethylsiloxane), J. Polym. Sci. Part B Polym. Phys. 38 (2000) 415–434.

[16] C.A. Scholes, J. Bacus, G.Q. Chen, W.X. Tao, G. Li, A. Qader, et al., Pilot plant performance of rubbery polymeric membranes for carbon dioxide separation from syngas, J. Memb. Sci. 389 (2012) 470–477.

[17] T.C. Merkel, R.P. Gupta, B.S. Turk, B.D. Freeman, Mixed-gas permeation of syngas components in poly(dimethylsiloxane) and poly(1-trimethylsilyl-1-propyne) at elevated temperatures, J. Memb. Sci. 191 (2001) 85–94.

[18] V.I. Bondar, B.D. Freeman, I. Pinnau, Gas transport properties of poly (ether-b-amide) segmented block copolymers, J. Polym. Sci. Part B Polym. Phys. 38 (2000) 2051–2062.

[19] C.J. Orme, M.L. Stone, M.T. Benson, E.S. Peterson, Testing Of Polymer Membranes For The Selective Permeability Of Hydrogen, Sep. Sci. Technol. 38 (2003) 3225–3238.

[20] A. Lamberti, A. Virga, P. Rivolo, A. Angelini, F. Giorgis, Easy Tuning of Surface and Optical Properties of PDMS Decorated by Ag Nanoparticles, J. Phys. Chem. 119 (2015) 8194–8200.

[21] A. Lamberti, S.L. Marasso, M. Cocuzza, PDMS membranes with tunable gas permeability for microfluidic applications, R. Soc. Chem. 4 (2014) 61415–61419.

[22] D. Sun, M.Q. Liu, J.H. Guo, J.Y. Zhang, B.B. Li, D.Y. Li, Preparation and characterization of PDMS-PVDF hydrophobic microporous membrane for membrane distillation, Desalination. 370 (2015) 63–71.

[23] N.R. Horn, D.R. Paul, Carbon dioxide plasticization and conditioning effects in thick vs. thin glassy polymer films, Polymer. 52 (2011) 1619–1627.

[24] A. Bos, I.G.M. Pünt, M. Wessling, H. Strathmann, CO_2-induced plasticization phenomena in glassy polymers, J. Memb. Sci. 155 (1999) 67–78.

[25] M.S. Suleman, K.K. Lau, Y.F. Yeong, Plasticization and Swelling in Polymeric Membranes in CO_2 Removal from Natural Gas, Chem. Eng. Technol. 39 (2016) 1604–1616. doi:10.1002/ceat.201500495.

[26] K.W. Lawson, M.S. Hall, D.R. Lloyd, Compaction of microporous membranes used in membrane distillation. I. Effect on gas permeability, J. Memb. Sci. 101 (1995) 99–108.

[27] X. Duthie, S. Kentish, C. Powell, K. Nagai, G. Qiao, G.W. Stevens, Operating temperature effects on the plasticization of polyimide gas separation membranes, J. Memb. Sci. 294 (2007) 40–49.

[28] C. Myers, H. Pennline, D.R. Luebke, J. Ilconich, J.K. Dixon, E.J. Maginn, et al., High temperature separation of carbon dioxide/hydrogen mixtures using facilitated supported ionic liquid membranes, J. Memb. Sci. 322 (2008) 28–31.

[29] P. Li, H.Z. Chen, T.S. Chung, The effects of substrate characteristics and pre-wetting agents on PAN-PDMS composite hollow fiber membranes for CO_2/N_2 and O_2/N_2 separation, J. Memb. Sci. 434 (2013) 18–25.

[30] J. Peter, K.-V. Peinemann, Multilayer composite membranes for gas separation based on crosslinked PTMSP gutter layer and partially crosslinked Matrimid® 5218 selective layer, J. Memb. Sci. 340 (2009) 62–72.

[31] C. Zhao, X. Zhou, Y. Yue, Determination of pore size and pore size distribution on the surface of hollow-fiber filtration membranes: A review of methods, Desalination. 129 (2000) 107–123.

[32] C. Li, Y. Ma, H. Li, G. Peng, A convenient method for the determination of molecular weight cut-off of ultra fi ltration membranes, Chinese J. Chem. Eng. (2016) Article in Press.

[33] A. Barański, The atomic mass unit, the Avogadro constant, and the mole: A way to understanding, J. Chem. Educ. 89 (2012) 97–102.

[34] Ultrafiltration (UF) Flat Sheet Membranes, (n.d.). http://www.sterlitech.com/membrane-process-development/flat-sheet-membranes/ultrafiltration-uf-membrane.html (accessed July 31, 2016).

[35] C.A. Scholes, G.W. Stevens, S.E. Kentish, The effect of hydrogen sulfide, carbon monoxide and water on the performance of a PDMS membrane in carbon dioxide/nitrogen separation,

J. Memb. Sci. 350 (2010) 189–199.

[36] H. Lin, E. Van Wagner, B.D. Freeman, L.G. Toy, R.P. Gupta, Plasticization-Enhanced Hydrogen Purification Using Polymeric Membranes, Science. 311 (2006) 639–642.

[37] E.H. Immergut, H.F. Mark, Principles of Plasticization, Plast. Plasticizer Processes. 48 (1965) 1–26.

[38] O.C. David, Membrane technologies for hydrogen and carbon monoxide recovery from residual gas streams, Ph.D. Thesis, Universidad de Cantabria, 2012.

[39] C. a. Scholes, S.E. Kentish, G.W. Stevens, Effects of Minor Components in Carbon Dioxide Capture Using Polymeric Gas Separation Membranes, Sep. Purif. Rev. 38 (2009) 1–44.

[40] W.F. Yong, K.H.A. Kwek, K.S. Liao, T.S. Chung, Suppression of aging and plasticization in highly permeable polymers, Polym. (United Kingdom). 77 (2015) 377–386.

[41] Y. Zhao, B.T. Jung, L. Ansaloni, W.S.W. Ho, Multiwalled carbon nanotube mixed matrix membranes containing amines for high pressure CO_2/H_2 separation, J. Memb. Sci. 459 (2014) 233–243.

[42] S.M. Wilson, Adsorption Separation of CO_2 from CO in Syngas: Improving the Conversion of the Reverse Water Gas Shift Reaction, M.A.Sc. Thesis, University of Ottawa, 2015.

[43] E.M. Maya, M.L. Sanchez, A. Marcos, J.G. de la Campa, J. de Abajo, Preparation and Properties of Catalyzed Polyimide/ Dicyanate Semi-Interpenetrating Networks for Polymer Gas Membrane with Suppressed CO_2-Plasticization, J. Appl. Polym. Sci. 124 (2013) 713–722.

Chapter 4: Separation of CO_2 from syngas to increase the conversion of the RWGS reaction using mixed matrix membranes

4.1 ABSTRACT

The Reverse Water Gas Shift (RWGS) reaction is becoming an exciting alternative for CO_2 recycling and consumption. On top of CO_2 consumption, it is also a source of syngas (CO and H_2) production, which, as a feedstock, has multitude of uses. To increase the conversion of this reaction and purify the product stream, an effective separation process capable of isolating CO_2 from both CO and H_2 needs to be developed. Membranes, proven to be an energy efficient and effective means of separation, were investigated for their capability to aid in this post-reactor process. PDMS (polydimethylsiloxane) was proven to be a successful polymeric candidate in published literature, and it was of interest to incorporate appropriate adsorbent materials into this polymer matrix to determine if a mixed matrix material would enhance selectivity and potentially permeability of CO_2. In this work, HY zeolite (Y-type zeolite with H ion), silica gel (SG) and activated carbon (AC) adsorbent materials were incorporated into PDMS to form selective membrane materials. These membranes were characterized using single, binary and ternary gas feeds of CO_2, CO and H_2 with feed pressures up to 11 atm, at room temperatures. Experiments were performed over a single-cell flat-sheet membrane system. All membranes were fabricated in-house. Activated carbon in PDMS proved to be the best performing mixed matrix material under ternary gas feeds with high CO_2 permeability (2,447 Barrers) and selectivity over both CO (9) and H_2 (14). Membrane compaction, swelling, and adsorbent-polymer interfaces within the membrane matrix are discussed as causes for permeability trends with respect to pressure driving force.

4.2 INTRODUCTION

4.2.1 RWGS and Recycle

The Reverse Water Gas Shift reaction (equation 1) utilizes carbon dioxide as a reactant to produce CO (a component of syngas) and water.

$$CO_2 + H_2 \leftrightarrow CO + H_2O \qquad (1)$$

This endothermic, equilibrium reaction occurs at high temperatures (700 – 1100 °C) over a catalyst with an enthalpy of reaction of 41 kJ/mol. It is a means to consume CO_2 emissions, however the reaction does not reach complete conversion of CO_2 [1,2]. The product stream is therefore composed of both reactant and product gases. Assuming water can be condensed out of the stream, the reactant stream is pure and no side reactions are present, the remaining gases are CO_2, H_2 and CO. While H_2 can be recycled with CO_2 back into the reactant stream, the combination of CO and

H_2 make-up syngas. These gases together, in the appropriate ratio, would be ready to be used in processes like methanol or ammonia production, electricity generation or the Fischer-Tropsch reaction [3,4]. Additionally, a single membrane separation would typically facilitate separation of either CO_2 or H_2. CO_2 could be separated from CO and H_2, or H_2 may be separated from CO_2 and CO. The latter would not be of interest for the RWGS recycle as the combination of CO_2 and CO prove to not be as advantageous as CO and H_2 (when CO_2 can be removed individually). Figure 4-1 presents the scenario of the RWGS reaction and post-reaction separations, with condensation of water and membrane separation of CO_2 for recycle to the feed gas. If water was present in the feed to the membrane separation, CO_2 permeability would decrease. H_2O would compete for transport based on the differences in interactions between CO_2, CO, H_2 and H_2O with PDMS [5].

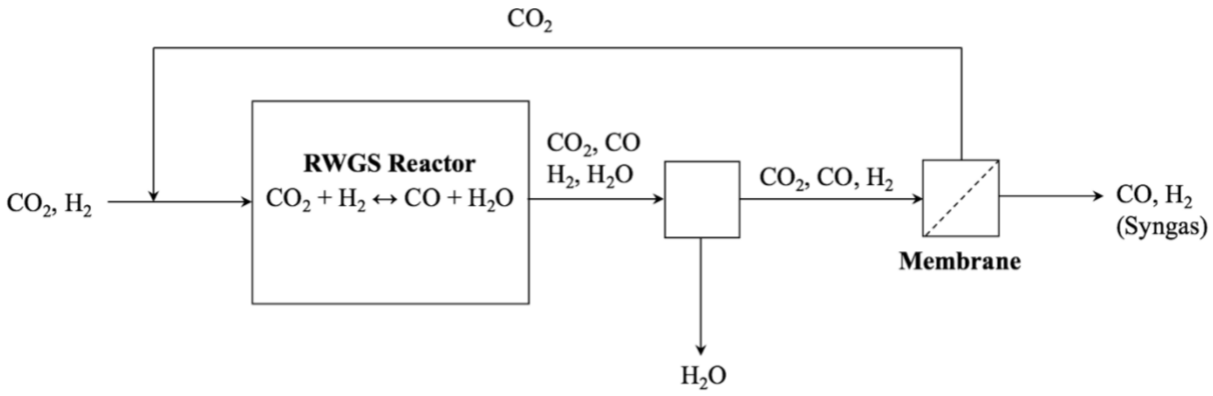

Figure 4-1: RWGS reaction and post-reactor separations assuming no side reactions and by-products in product stream

Side reactions do exist with the RWGS reaction, including the Sabatier, Bosch, Boudouard, methanation, and the WGS (Water Gas Shift) reaction [2]. However, these reactions are minimized by optimizing the reaction conditions and the catalyst. Realistically, there will exist traces of some by-products, such as CH_4 and carbon deposits on the catalyst [6]. For the purposes of this study, CO_2, CO and H_2 will be investigated exclusively as they will comprise the bulk of the product stream.

4.2.2 Membrane Separations

Membranes are used in separation processes that operate on the basis of a multi-component fluid coming into contact with a selective surface (organic or inorganic) accompanied with a driving force to provide a means of separation. This process is outlined in Figure 4-2.

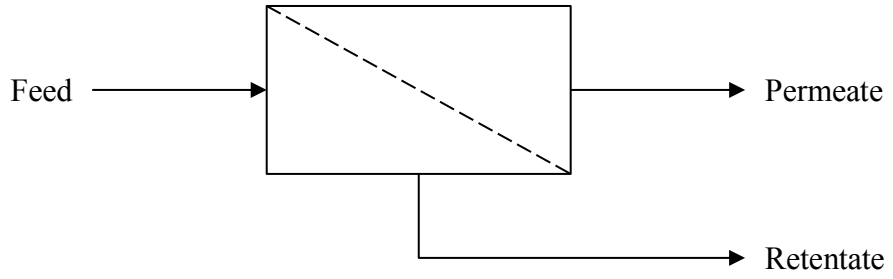

Figure 4-2: Membrane process diagram

In the case of gas separation, the driving force is a pressure gradient across the membrane [7,8]. Membranes can be fabricated from organic materials, inorganic materials and a combination of the two. When polymeric (organic) membranes, are combined with inorganic adsorbent particles (such as zeolites), mixed matrix membranes (MMM) are formed. Inorganic membranes are resistant over a larger range of temperatures and pressures than their polymeric counterparts. In practice, however, inorganic membranes can be more expensive and difficult to synthesize [9,10]. Combining the two material types into a matrix can produce a better performing membrane. The inorganic material, in particle form, is dispersed uniformly within a polymer matrix and has the potential to reach higher selectivities and permeabilities than purely polymeric membranes [9,11,12].

Membranes have gained traction in the separation industry. Compared to processes like adsorption, absorption and distillation, membrane separation is more energy efficient, simple to operate and cost effective. Their design also facilitates easy replacement and they can reach steady state more efficiently [12–15]. Polymeric membrane separation is governed by both solubility and diffusivity properties of the gas components. This is known as the Solution-Diffusion model (equation 2) where permeability (P_A) can be represented as the product of solubility (S_A) and diffusivity (D_A) coefficients of a gas in a polymer [7].

$$P_A = S_A \cdot D_A \qquad (2)$$

Most polymers used for gas membrane separations fall into the class of dense or nonporous materials based on the way their molecular chains stack and layer. CO_2 is a larger molecule than H_2

and CO is even larger than CO_2. As shown in Table 4-1, H_2 has a smaller kinetic diameter than CO_2 and CO. Given these physical properties, one could assume separation of CO from CO_2 and H_2 would be achieved based purely on size exclusion (smaller molecules permeate more quickly through a given pore). However, CO_2 is highly soluble in certain polymers and can competitively permeate over both CO and H_2 [11,16]. Typically, the more condensable a gas is (such as those with higher boiling points at standard atmospheric pressure), the more soluble it will be in a polymer. Dense, nonporous polymeric membranes used for gas separations (often rubbery, amorphous polymers) have weak size sieving abilities [16], and gases with higher solubilities (CO_2, CO) have precedence over smaller, more diffusive gases (H_2).

Table 4-1: Feed gas kinetic diameter and normal boiling points

Chemical	Kinetic Diameter [Å]	Normal Boiling Point [ºC]
CO	3.76	-192
CO_2	3.30	-78.5
H_2	2.89	-253

Transport within inorganic and adsorptive materials is governed by similar properties to polymeric membranes. Under the assumption that the gas particles are smaller than the pore size of the inorganic membrane, gas transport occurs with adsorption, followed by diffusion through the pore, and then desorption into the permeate stream. More condensable components like CO_2 with higher heats of adsorption, have preferential adsorption capabilities over lighter, smaller gases, such as H_2 [11].

The Maxwell model is an accepted way of modeling the permeability of gases through a mixed matrix membrane. It allocates the two materials into dispersed, diluted (inorganic) spherical particles in a continuous, polymer matrix. It is adapted from thermal or electrical conductivity models for composite materials, due to the analogy between these parameters and diffusion [10,12,17]. These inorganic fillers also act as mechanical supports for the polymer, making them more resistant to the irreversible effects of membrane compaction [18].

4.2.2.1 Membrane Characterization

Membrane characterization for gas separation involves permeability and selectivity measurements. Equations 3 – 8 were used to calculate the data presented in this work. Gas

permeability (P, from the Solution-Diffusion model in equation 5) is a normalized and standardized permeate flux (J, in equations 3 and 4) to standard temperature and pressure (STP), expressed in the unit of Barrer (equation 6). These equations are derived from Fick's Law of diffusion, under the assumption of a negligible convective mass transfer resistance and constant properties. The pressure differential used to calculate permeability is defined for binary and ternary gas separations with respect to partial pressure differences. Selectivity can either be defined in terms of single or mixed gas conditions. Ideal selectivity ($\alpha^*_{A/B}$, in equation 7) describes the ideal separation capabilities of a membrane, based on permeability ratios obtained from single gas experiments. Actual selectivity ($\alpha_{A/B}$, in equation 8) describes a membrane's separation capabilities under conditions where there are at least two gases in a feed mixture [7].

$$J_i = -D_i \frac{dC_i}{dz} \tag{3}$$

$$J_i = -D_i \frac{(\Delta P \cdot S_i)}{\Delta z} \tag{4}$$

$$P_i = S_i \cdot D_i \tag{5}$$

$$1\ Barrer = 10^{-10} \frac{cm^3(STP) \cdot cm}{cm^2 \cdot cmHg \cdot s} \tag{6}$$

$$\alpha^*_{A/B} = \frac{P_A}{P_B} \tag{7}$$

$$\alpha_{A/B} = \frac{y_A / y_B}{x_A / x_B} \tag{8}$$

where C_i is the concentration of component i in the membrane (mol/cm^3), z is the position in the membrane (cm), D_i is the diffusivity coefficient of component i in the membrane (cm^2/s), S_i is the solubility coefficient of component i in the membrane (cm^3/cm$^2 \cdot$ cmHg), ΔP is the partial pressure difference across the membrane for component i (cmHg), P_A is the permeability of component A (Barrers), P_B is the permeability of component B (Barrers), y_A is the mole fraction of component A in the permeate, y_B is the mole fraction of component B in the permeate, x_A is the mole fraction of component A in the feed and x_B is the mole fraction of component B in the feed.

When fabricating and testing thin-film composite membranes suited for gas separation, it was desired to achieve both high gas permeability and high selectivity. Robeson has been distinctly known for modeling what is referred to as the upper bound, indicating the maximum combination a membrane can achieve between permeability and selectivity for polymeric membranes [18,19]. CO_2 is often highly soluble in many polymers, which gives it an advantage over smaller molecules like

H_2 that diffuse extremely quickly in general. For this reason, polymeric membranes can simultaneously achieve high permeability and selectivity, such as separation of CO_2 from H_2 [20]. Additionally, adsorbents can selectively adsorb gas molecules with higher heats of adsorption, like CO_2, and increase overall separation. By integrating inorganic, adsorbent materials into a polymer matrix, this study will aim to prove that this combination will be able to overcome permeability and selectivity limits met by polymeric membranes from literature.

PDMS (polydimethylsiloxane) was selected as the polymer for the mixed matrix membranes in this work for a multitude of reasons. It has been proven to selectively separate CO_2 over syngas components with high CO_2 permeability (Chapter 3) [16,22,23]. It is also a widely used polymer with desired properties like cost effectiveness, flexibility and simple fabrication, which makes synthesizing membranes with this material straightforward [24–26]. This work investigates PDMS combined with adsorbent materials that were selected specifically for this separation. From previous research by Wilson, where this specific separation was investigated using adsorption, HY and high-density silica gel (SG) were determined to be promising candidates for bulk separation of CO_2 from syngas [27]. Of the adsorbents investigated in that study (20 zeolites, 2 activated aluminas, 3 activated carbons (AC) and 2 silica gels (SG)), HY and silica gel were determined to have the highest adsorption capacity ratios for CO_2 over CO. It was assumed H_2 was not significantly adsorbed by any of the selected adsorbents because of its small particle size and high diffusivity. For this reason, it was assumed that adsorption capacities for CO_2 were consistently higher over H_2 in comparison to CO. Each of these adsorbents also had pore sizes larger than the kinetic diameter of CO_2, CO and H_2 gases (seen in Table 4-2). PAN (polyacrylonitrile) was used as a support material due to availability, easy processing ability and good chemical resistance [28,29]. Activated carbon and PDMS mixed matrix membranes prepared on a PAN support were synthesized by Hoda Azimi. HY-PDMS and SG-PDMS mixed matrix membranes were prepared by Lauren Rose.

Table 4-2: Size of the gas molecules and physical properties of adsorbents used in this work

Gases		Adsorbents			
Gas	Kinetic Diameter [Å]	Adsorbent	Pore Size [Å]	Particle Size [μm]	Specific Surface Area [m^2/g]
CO	3.76 Å	SG	22 – 26 Å	63 – 200	500 – 600
CO_2	3.30 Å	HY	7.4 Å	≤ 45	700
H_2	2.89 Å	AC	20 – 50 Å	0.02 – 0.04	1,400

4.3 EXPERIMENTAL

4.3.1 Materials and Membrane Preparation

CO_2, CO and H_2 gases were obtained from Linde Canada Ltd. (Mississauga, ON, Canada), and their respective grades can be seen in Table 4-3. The mixed matrix membranes were synthesized in the laboratory using two different flat sheet PAN supports from Sterlitech™, details in Table 4-4 (Kent, WA, USA). The MWCO (molecular weight cut-off) of these supports varied by a factor of 10. PAN I had a MWCO of 30 kDa and PAN II had a MWCO of 300 kDa. The PDMS and curing agent (octamethylcyclotetrasiloxane) used for these membranes was purchased from Gervais Electronics as a kit: RTV615-1P (Ottawa, ON, Canada). HY (CBV 901) was purchased from Zeolyst International (Conshohocken, PA, USA) in a powder-like form with a SiO_2/Al_2O_3 ratio of 80. Particle size information was not provided by the company, so a particle-size analysis was conducted, however agglomeration was an issue. From the analysis, the conclusion would be a maximum particle size of 45 um, outlined in Table 4-2. The measured membrane thickness of HY-PDMS-PAN II would therefore be smaller than the maximum particle size measured. Throughout membrane synthesis the desired membrane thickness was to be thicker than the particle size of the adsorbents. However, upon further analysis, this was not achieved for HY-PDMS-PAN II which was considered during data analysis. Silica gel (catalogue no. 146644, 63 – 200 μm) was purchased from Selecto Scientific (Suwanee, GA, USA). It should be noted that the thickness of the selective membrane layer in Table 4-4 was smaller than the particle size outlined in Table 4-2 for the silica gel. Again, this is considered during data analysis. Activated carbon nano-particles (US-1074, particle size 20 – 40 nm) were purchased from US Research Nanomaterials Inc. (Houston, TX, USA). The class of Y-type zeolites, which HY falls under, have an average pore size of 7.4 Å, where the high-density silica gel used in this work has an average pore size from 22 to 26 Å [29,30]. The activated carbon nano-particles presented in this work reported a pore size from 2 – 5 nm (20 – 50

Å) [31]. Toluene was used as a solvent for the synthesis process (Fisher Scientific: Ottawa, ON, Canada).

Table 4-3: Feed gas grade and purity from Linde Canada Ltd.

Gas	Grade	Purity (%)
CO_2	4.0	99.99
H_2	4.0	99.99
CO	2.5	99.5
He	5.0	99.999

Table 4-4: Mixed matrix membrane and PAN support details from Sterlitech™

Selective Layer (Adsorbent-PDMS)	Adsorbent wt %	Selective Layer Thickness [µm]	Support Layer	Support MWCO [kDa] [33]
HY-PDMS-PAN I′	4	50	Dry PAN I	30
HY-PDMS-PAN I	4	30	Wetted PAN I	30
SG-PDMS-PAN II	4	15	Wetted PAN II	300
AC-PDMS-PAN II	4	55	Wetted PAN II	300

**Adsorbent wt % does not include PAN in total membrane weight, includes curing agent*

The difference between the two HY MMMs (as denoted in Table 4-4) was in the preparation of the PAN supports. The HY-PDMS-PAN I′ membrane was synthesized on a dry PAN I support, where all other membranes discussed in this work were synthesized with a wetted PAN I or PAN II support using distilled water. All mixed matrix membranes reported in this work were made with a 4 wt % loading of adsorbent in the polymer matrix, the remaining 96 wt % being PDMS and the curing agent.

To start the membrane synthesis, a small sheet (roughly 8” x 6”) of each PAN support (PAN I and PAN II) was immersed in distilled water for 30 seconds, to minimize the potential for any unwanted dust, debris or selective membrane material from entering the PAN pores. If this were to occur during synthesis of a purely polymeric membrane, the effective thickness of the membrane would increase and the resistance for gas transport would be higher [28,29]. Therefore, this technique was used as a measure to prevent this. The PAN support was taped to a glass or metal plate, securely around all edges. The first membrane layer applied onto the support was a diluted 1 wt % PDMS in toluene mixture. A 10:1 weight ratio of PDMS:curing agent was mixed in a toluene solution, where 0.5 g of PDMS, 0.05 g of curing agent and 50 g of toluene were combined. This mixture was agitated for 15 minutes using a stirrer at 500 RPM and at room temperature. A single

layer of this 1% diluted PDMS solution was cast onto the PAN sheet (in only one direction), using an airbrush spray gun (Paasche Airbrush Co.: Chicago, IL, USA) as seen in Part A. of Figure 4-3. The technique for applying any membrane layer with this tool involved steady, uniform movements approximately 1 foot above the plates, to cover the entire support.

The selective MMM solution synthesis for HY-PDMS-PAN I′, HY-PDMS-PAN II and SG-PDMS-PAN II involved mixing either HY or SG adsorbents with toluene solvent and PDMS polymer (without the curing agent), respectively. A 4 wt % loading of the adsorbent was used in all syntheses of the mixed matrix membranes in this work; the wt % was calculated from the total membrane weight excluding the PAN support and toluene solvent. Each loading of adsorbent was mixed with a 10:1 weight ratio of PDMS:curing agent in a toluene solution, where 10 g of PDMS, 1 g of curing agent and 0.45 g of adsorbent were combined with 50 g of toluene. Each respective mixture (HY or SG) was agitated using the same stirrer at 500 RPM for 10 minutes and at room temperature. The mixture was sonicated (QSONICA, Part No.Q700, Fullerton, USA) for a total of 2 hours in an ice bath. The frequency of sonication followed a 30 second on, 30 second off schedule over the 2 hours (with a total effective sonication of 1 hour). Due to heating during sonication it was recommended to only sonicate mixtures of adsorbent and solvent (toluene), without PDMS and curing agent components. Sonicating a solution including a polymer and/or curing agent could induce polymerization with added heat and cause the mixture to solidify quickly. However, HY and SG particles were observed to settle when mixed only with toluene, meaning their particle sizes were not small enough to maintain full dispersion without any additional forces. Adding PDMS in advance of sonication to the adsorbent-toluene solution allowed the adsorbent particles to disperse well with no particle settling (PDMS viscosity > toluene viscosity). An ice bath was used during sonication to keep the temperature of the solution as low as possible to combat any heat generation and prevent polymerization. After sonication, the curing agent was added, and the entire solution was agitated again for 15 minutes with the two-blade impeller at 500 RPM and room temperature. Each step of this synthesis is outlined in Figure 4-4.

The synthesis for AC-PDMS-PAN II had slight modifications from the synthesis method discussed above and can be seen in Figure 4-5. The AC nano-particles were sonicated with toluene only (without PDMS polymer or curing agent). This solution was sonicated for 2 hours in an ice bath, following the same 30 second on, 30 second off timeline (with an effective total sonication of 1 hour). After sonication, the PDMS polymer was added to the solution and was agitated for 30

minutes with the two-blade impeller at 500 RPM and room temperature. The curing agent was added last and the mixture was agitated again for 15 minutes under the same RPM and temperature conditions.

Each polymer-adsorbent solution was applied to their respective support layers using the same airbrush spray gun and technique (outlined in Part A and B of Figure 4-3), one hour after applying the single layer of 1 wt % PDMS in toluene. HY was cast onto dry (PAN I′) and wetted PAN I sheets where SG and AC were cast onto wetted PAN II sheets. The application was a two-step process, where two layers were applied in perpendicular directions, each one hour apart – seen in Part B. of Figure 4-3. One hour after the last layer was applied, the membranes were placed in a vacuum oven, where they were exposed to vacuum pressure (0.8 bar gauge). Approximately 30 minutes later, the oven was turned on to 90 ºC and the materials were heated for 3 hours (including pre-heating). After 3 hours, the oven and vacuum pump were turned off and the membranes were cooled to room temperature and exposed to atmospheric pressure with the oven door left ajar.

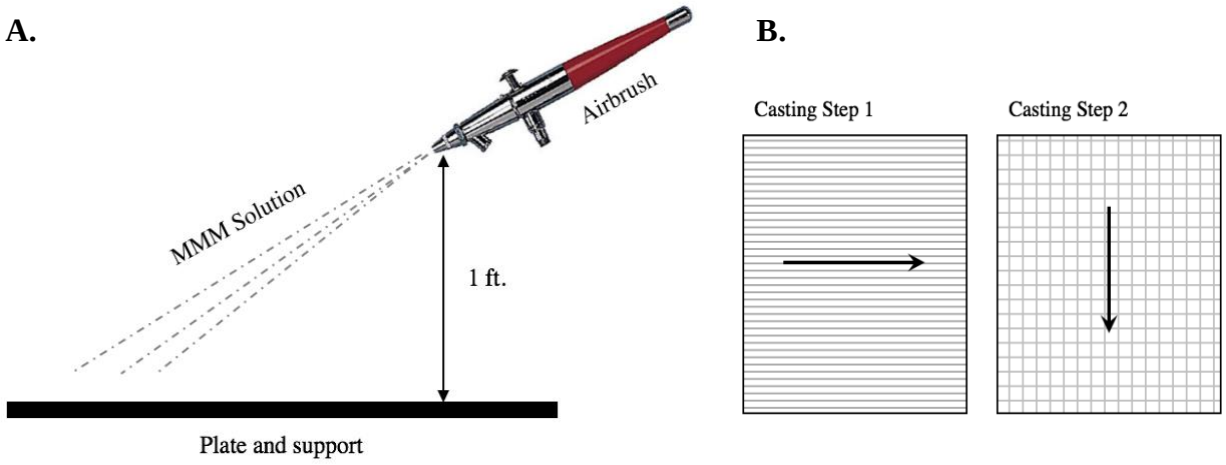

Figure 4-3: A – Membrane casting technique; B – Direction of application to PAN support

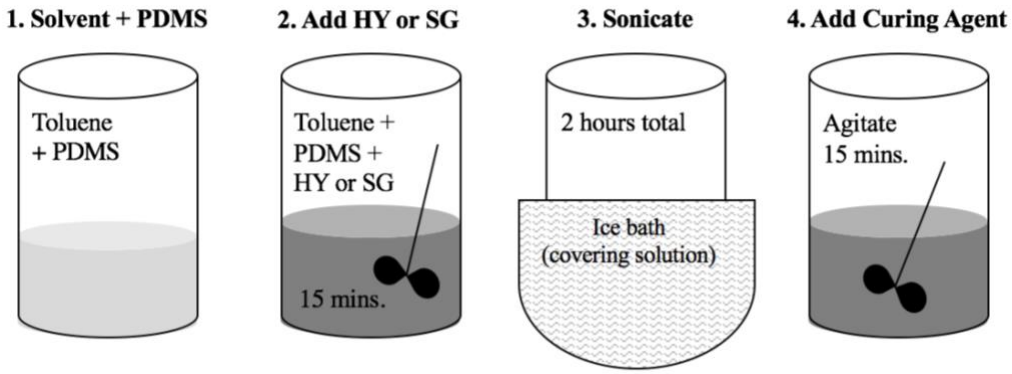

Figure 4-4: HY, SG in PDMS on PAN I/II synthesis steps prior to casting

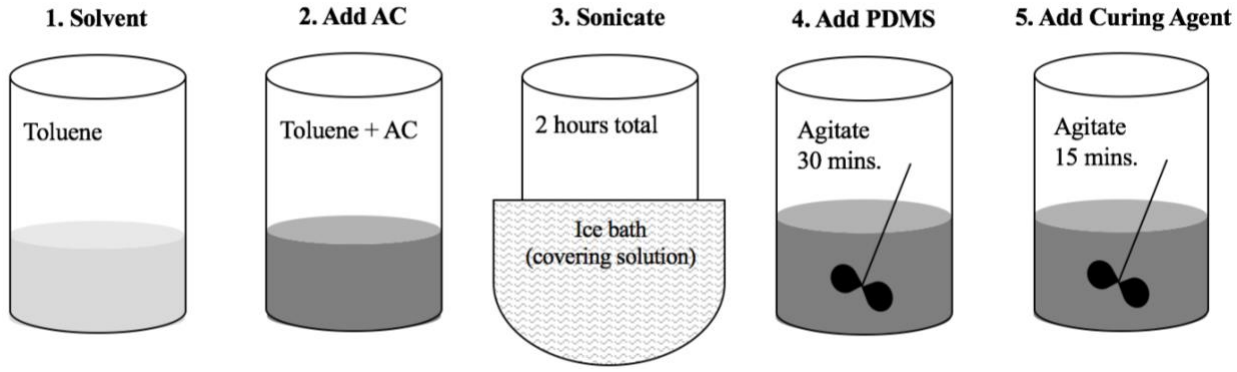

Figure 4-5: AC-PDMS-PAN II synthesis steps prior to casting

4.3.2 Experimental Set-up

A flat-sheet membrane system, seen in Figure 4-6, was used to test each membrane from 3 to 11 atm in total feed pressure. A description of all units shown in this diagram are outlined in Table 4-5. The system was constructed from stainless steel 1/8" OD tubing. A Varian Aerograph 1400 series gas chromatograph was used with an 8-port sampling valve and a ShinCarbon 1/8" OD x 2 m packed column (Chromatographic Specialties Inc.: Brockville, ON, Canada) to analyze gas mixture samples of CO_2, CO and H_2 on a LabView program. Membrane cell images (Figure 6-1 to Figure 6-4), graphed gas peaks from the ShinCarbon adsorbent (Figure 6-5) and a sampling port diagram (Figure 6-6) are outlined in detail in Appendix A.

OMEGA® rotameters (Laval, QC, Canada) were calibrated and used to control gas feed flow rates before entering the mixing chamber. 1 L and 500 µL bubble flow meters were used for the retentate/feed and permeate volumetric flow rate measurements, respectively. Pressure gauges purchased from Swagelok® (Ottawa, ON, Canada) were utilized prior and post membrane cell to ensure accurate pressure readings of the feed and permeate during experiments. A series of valves were implemented to control gas flow and redirect its movement for purging or volumetric flow rate measurements.

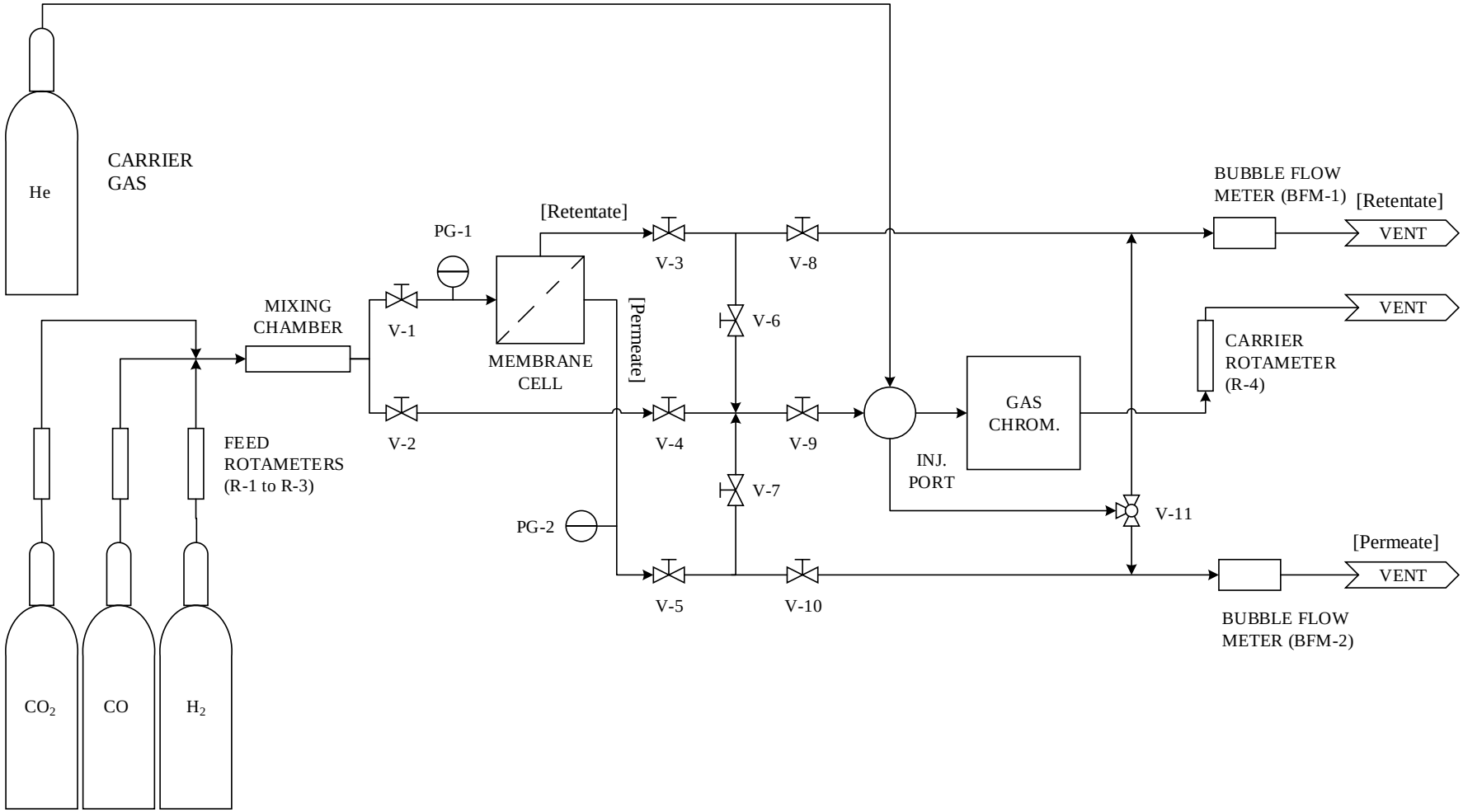

Figure 4-6: Schematic diagram of the experimental set-up used in this study

Table 4-5: Equipment description for entire laboratory experimental schematic

Equipment ID.	Description	Use
CO_2, CO, H_2, He	Gas cylinders	Feed and carrier gases
BFM-1, BFM-2	Bubble flow meters	Measures volumetric flow with timed measurements of quantified bubble travel
Gas Chrom.	Gas chromatograph (Varian Aerograph 1400)	Houses ShinCarbon packed column to analyze sample injection gas concentrations
Inj. Port	Injection sample port for GC (8-port)	Manual injections of samples into GC for analysis
Membrane cell	Solid metal membrane cell	Houses flat-sheet membrane with tight O-ring seal
Mixing Chamber	Enlarged tubing	Provides mixing space for feed gases
PG-1, PG-2	Pressure gauges	Measure feed and permeate gauge pressures up to 160 psig
R-1, R-2, R-3	Feed rotameters	Controlling gas feed flows
R-4	Carrier gas rotameter	Controls volumetric flow of He to the GC
Vents	Tubing to fume hood in laboratory	Bring flammable and poisonous gases to fume hood for proper venting
V-1, V-2, V-11	Two-way valves	Control direction of gas flow
V-3 to V-10	Screw down valves	Control direction and resistance of gas flow

4.3.3 Permeation Measurements

Gases were fed into the system from their respective gas cylinders, entering through the rotameters, feeding the membrane cell at a set pressure and maintaining a total feed flow rate of 4.50 L/min. The effective membrane diameter in this system was approximately 4 cm. Single gas experiments consisted of single gas feeds, while binary experiments (CO_2:H_2 or CO_2:CO) consisted of molar ratios of either 25:75, 50:50 or 75:25. Ternary experiments involved an even molar mixture of all three gases to represent a product stream (without H_2O) from the RWGS reaction, although there exist a multitude of operating parameters that could affect this composition (i.e., reaction temperature, catalyst selection, feed ratio of reactants for the RWGS reactor). Valve V-8 (Figure 4-6) was used to add resistance to the feed to run experiments between 3 and 11 atm of total feed pressure. The system was not temperature controlled, as it was exposed to ambient room temperature conditions (23 – 24 °C).

Pressure gauges PG-1 and PG-2 were used to measure the total pressure drop across the membrane. BFM-1 (1 L bubble flow meter) was used to measure the volumetric flow rates of the

retentate and feed and BFM-2 (500 µL bubble flow meter) was used to measure the volumetric flow rate of the permeate stream. Injections into the GC were carried out periodically to measure the permeate composition along with bubble flow meter data collection to ensure steady state conditions were met (steady permeate flow rate measurements and GC gas peaks, both within a 5 % difference or less). Helium was used as the carrier gas for this GC at a flow rate of approximately 40 mL/min. Retentate flow rates were considered approximately equal to feed flow rates for all experiments. The magnitude of the permeate volumetric flow rates were at most, 0.6 % of the feed volumetric flow rate. Standard error was used in permeability analysis to provide a better understanding of experimental error. The experiments were performed in the following order for each membrane, utilizing only one membrane for the entirety of all experiments (e.g., no fresh membranes were changed out during experimental runs): starting with single gas, followed by binary gas and ending with ternary gas feeds. The detailed order of these experiments is outlined in Table 4-6.

Table 4-6: Order of gas experiments (single, binary and ternary) for all mixed matrix membranes from top to bottom

2) Single Gas Experiments	2) Binary Gas Experiments	3) Ternary Gas Experiments
CO_2	CO_2:H_2 (25:75)	CO_2:H_2:CO (1:1:1)
H_2	CO_2:H_2 (50:50)	
CO	CO_2:H_2 (75:25)	
	CO_2:CO (25:75)	
	CO_2:CO (50:50)	
	CO_2:CO (75:25)	

4.4 RESULTS AND DISCUSSION

4.4.1 SEM Imaging

A scanning electron microscope (SEM) was used to take micrometer scale photos of the cross sections of each membrane to determine the uniformity and thickness of each layer of membrane on the PAN support, shown in Figure 4-7. Images 1 and 4 in this figure were taken at a 50 µm scale, while images 2 and 3 were taken at a 20 µm scale. Due to vibrations during SEM photography, this was the smallest scale attainable to obtain images with optimal picture quality. Unfortunately, at this scale, it is not concretely possible to determine if there exist adsorbent particle agglomerates or void spaces in the membranes. However, upon data analysis, membrane

performance is evaluated to determine if these properties are likely to exist in the synthesized membranes. This includes increasing gas permeabilities with partial pressure due to mass transfer through the void or defective areas of the membrane and a reduction in CO_2 selectivity.

These images were obtained with a JEOL JSM-6610 series SEM using 15 kV electron beams and 30 Pa of vacuum. Samples of each membrane were cut and then mounted perpendicularly on a seven-sample specimen holder; the preparation of these samples have the potential for improvement in terms of quality of the cut edge; freeze-drying the samples would be recommended for future preparation to preserve the cross-sectional structure for visual analysis. In Figure 4-7, the selective, mixed matrix (adsorbent and PDMS) layer is denoted by arrows showing the thickness of this layer. The PAN support is above this layer, which should be clear of particles, although some may be present due to contamination of the sample prior to entering the SEM. The difference between the selective and support layer is more visibly denoted by a change in colour (lighter indicates MMM layer, darker indicates PAN layer).

All membranes show a uniform layer of composite material deposited and cured on the PAN support, with the silica gel-PDMS matrix having the thinnest, measured layer. The average thicknesses of each membrane are displayed in Table 4-4. Although each membrane differs in selective membrane thickness, permeability measurements are normalized to this parameter. Images 1 – 2 in Figure 4-7 display some possible small adsorbent particles, or particle agglomerates. There should be large visible silica gel particles in Image 3 (SG PDMS), however this layer is thinner and SG particles laying on the surface were obvious to the naked eye. Therefore, it is likely that this image only shows PDMS. This is also true for Images 2, as the membrane thickness was not as great as the largest HY particle size measured. The activated carbon and PDMS membrane (image 4) appears like a pure PDMS selective layer. The scale of the activated carbon particles (20 – 40 nm) are not only too small to be detected at this scale but are also black making it more difficult to be seen in SEM imaging. For this reason, the AC-PDMS-PAN II membrane looks to be one continuous phase, like the pure PDMS membranes discussed in Chapter 3.

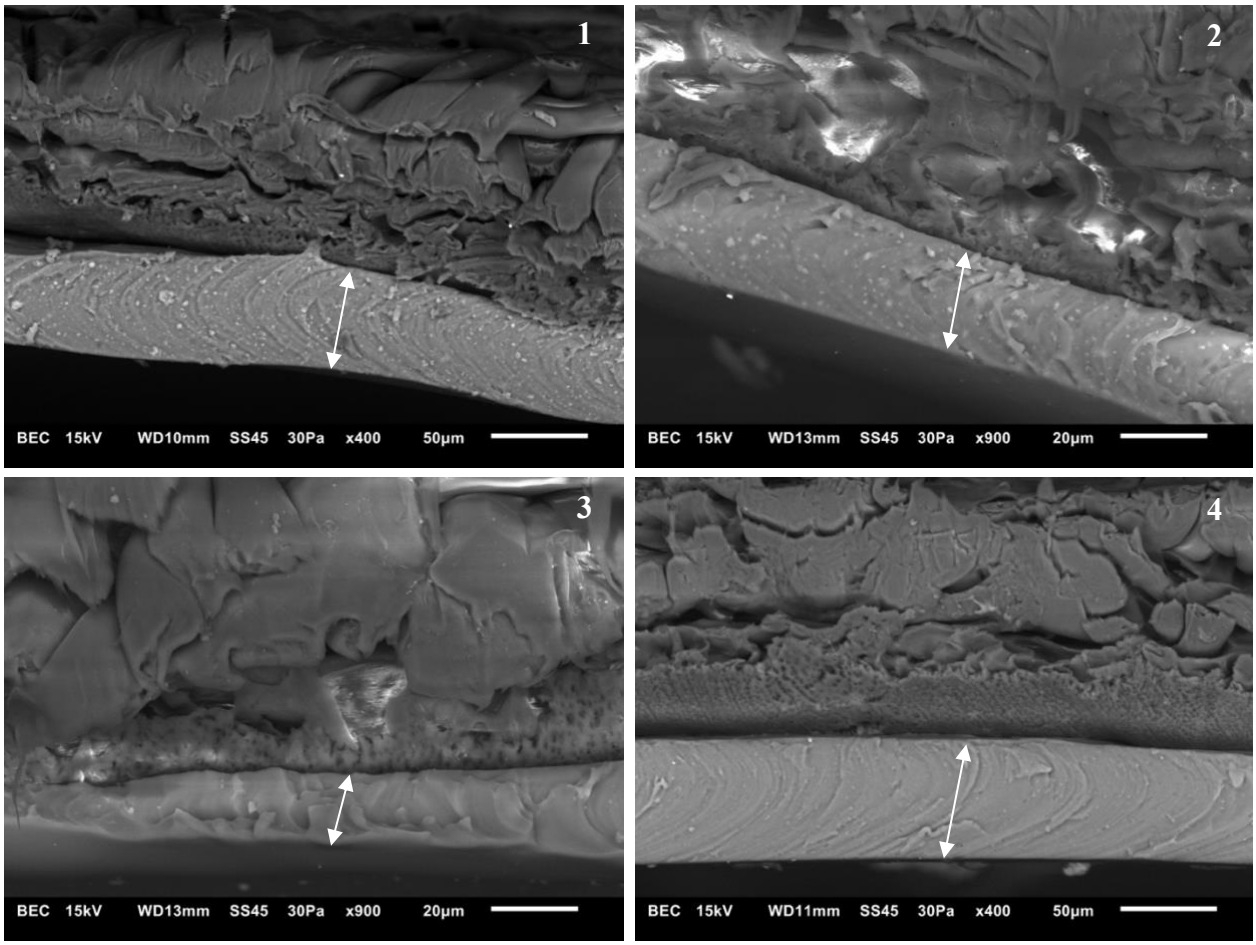

Figure 4-7: Cross-sectional SEM images of MMMs prepared in this study: (1) HY-PDMS-PAN I′, (2) HY-PDMS-PAN I, (3) SG-PDMS-PAN II, (4) AC-PDMS-PAN II

4.4.2 Single Gas Results and Discussion

Each membrane was tested with CO_2, CO and H_2 gas feeds to determine single gas permeabilities and ideal selectivities. The graphs presented in this section include permeabilities and ideal selectivities plotted against the pressure differential measured across the membranes. From previous research on PDMS membranes (Chapter 3), increases and decreases in permeabilities with respect to feed pressure were observed. This was speculated to be caused by two major effects during membrane operations: swelling of PDMS from CO_2 and membrane compaction from higher operating pressures; these are discussed later. All membranes tested exhibited ideal CO_2 selectivity over H_2 and CO. Additionally, adsorbents that observe non-linear adsorption isotherm behaviour would facilitate changes in permeability with respect to pressure.

4.4.2.1 HY-PDMS-PAN I′

Single gas permeabilities of all three gases through the HY-PDMS-PAN I′ membrane, with respect to pressure differential, are displayed in Figure 4-8:A. It was expected for CO_2 to have greater permeability compared to both H_2 and CO, as its combination of solubility and adsorption capacity is greater than syngas components (CO and H_2) in PDMS and HY, respectively. However, this membrane did not approach values close to literature, even for purely polymeric membranes. This was one of the thickest membranes synthesized and tested in this collection of mixed matrix membranes. Permeabilities of each gas appear to be stable within reasonable error and with respect to the pressure differential over the membrane. This would indicate that no major physical membrane defects were present and no swelling occurred during single gas experiments. The fluctuation in selectivities seen in Figure 4-8:B are a direct result of the fluctuation of gas permeabilities along the feed pressure range. The separation of CO_2 from CO was marginally better in this case with slightly higher selectivity values, in comparison to CO_2 from H_2.

From another study, it was reported that the HY zeolite used in this membrane exhibited an average CO_2/CO adsorption capacity ratio of 7 at 30 ºC over a pressure range from 0 to 10 atm [27]. As discussed earlier, H_2 was assumed to not be selectively adsorbed by the adsorbents discussed in this work. Permeability in this work is largely influenced by adsorption capacities, diffusivities and solubilities of gases with respect to adsorbent and polymeric materials. A combination of all effects must be considered, especially with respect to differing feed pressures. Although there is insignificant adsorption of H_2 by the adsorbent materials studied in this work, H_2 observed greater permeability than CO, due to its fast diffusion as a small gas. During the single gas experiments, there is no competition for gas transport. No adsorbing gases (CO_2, CO) are present during H_2 single gas experiments to block it off during transport. For this reason, and because H_2 is the smallest molecule among the gases studied, it is able to diffuse quickly through the matrix and permeate in greater quantities than the largest gas, CO.

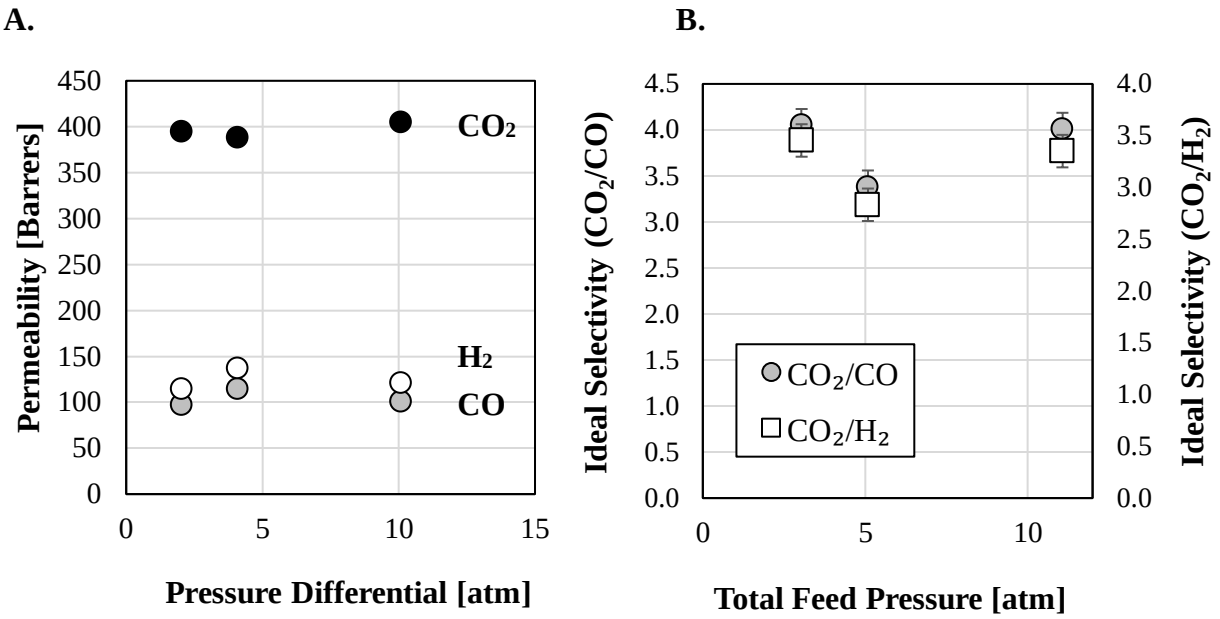

Figure 4-8: A – CO_2, CO, H_2 single gas permeabilities with respect to pressure differential for HY-PDMS-PAN I′ at 24 ºC; B – CO_2/CO and CO_2/H_2 ideal selectivities with respect to feed pressure

4.4.2.2 HY-PDMS-PAN I

Single gas permeability trends with respect to pressure differential are shown in Figure 4-9:A for HY-PDMS-PAN I. There was a significant decrease in overall gas permeability seen with this membrane in comparison to HY-PDMS-PAN I′. It is speculated that the reduction in permeability in HY-PDMS-PAN I may be due to the fact that water was involved in the synthesis process. The exact effects on the membrane component interactions (polymer, support and adsorbent particles) are unknown. However, with the presence of water it is speculated that the mixed matrix solution used to synthesize HY-PDMS-PAN I physically prevented the PDMS-HY matrix from sinking into the pores of the PAN sheet which would effectively decrease the total selective membrane thickness in this cross section, in comparison to HY-PDMS-PAN I′. In addition to this HY-PDMS membrane having minimal selective material in the PAN support, it also measured 20 µm thinner than HY-PDMS-PAN I′ from the support surface, upwards. The addition of HY adsorbent into a PDMS matrix enhances permeate gas flux and permeability as it provides additional sorption sites, meaning additional mass transfer pathways. It is probable that both HY-PDMS membranes had defects or void areas within the membrane matrix, due to the nature of MMM synthesis and the particle size of this adsorbent. A thinner membrane therefore is likely to have less presence of these defects based

on membrane thickness. This causes an overall reduction in gas permeabilities as this avenue for mass transport is less available.

CO_2 had the highest permeability, and CO permeated over H_2 under 5 atm of feed pressure. H_2 permeability increased notably across the tested pressure range, likely outside of the experimental error range. Again, membrane defects are probable in the membranes discussed in this work. At higher feed pressures, small, non-interactive gases experience an increase in mass transport due to higher diffusivity through these defects. It is probable that CO_2 permeabilities are within acceptable error limits. The permeability data in Figure 4-9:A dictates the differences in ideal selectivities seen in part B of Figure 4-9.

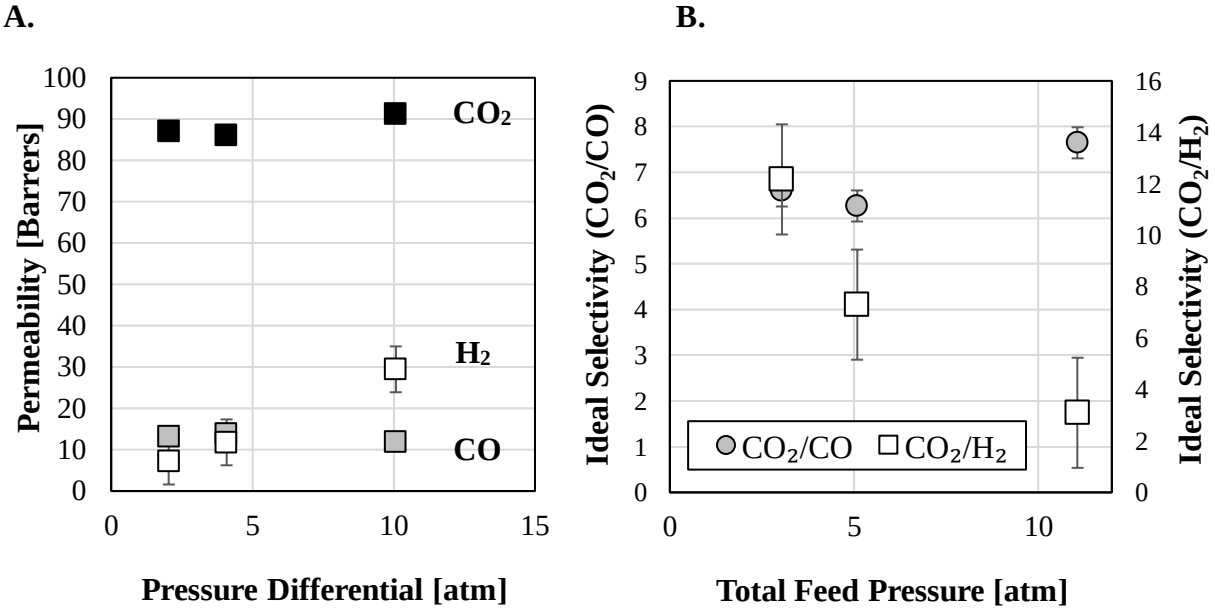

Figure 4-9: A – CO_2, CO, H_2 single gas permeabilities with respect to pressure differential for HY-PDMS-PAN I at 24 ºC; B – CO_2/CO and CO_2/H_2 ideal selectivities with respect to feed pressure

4.4.2.3 SG-PDMS-PAN II

The silica gel (SG) adsorbent used in this work reported an adsorption capacity for CO_2 six times greater than CO at 10 atm and 30 ºC (and 14 under vacuum) [27], making it comparable to HY and a good candidate as a MMM adsorbent additive in this study. Single gas permeability trends are plotted with respect to the studied pressure range in Figure 4-10:A. Among the membranes tested, the SG-PDMS-PAN II membrane was the least permeable for CO_2 in single gas experiments.

SG-PDMS-PAN II was synthesized on the more porous PAN II support, however the silica gel particles used to synthesize this membrane reported a much larger particle size than the membrane thickness measured from SEM imaging. This would lead one to believe that the SG particles were not correctly sized with respect to the applied membrane layer thickness. The specific surface area of SG particles was the smallest in comparison to HY and AC (seen in Table 4-2) which would indicate a less effective adsorbent, given less surface area available for gas interaction. Silica gel is also commonly known as a desiccant, so it has a strong ability to adsorb water [34]. Water is involved in the synthesis process in terms of preparation of the support layer. It can be speculated that the presence of water and the size of the SG particles do impact this membrane in terms of low permeability and selectivity. These factors are hypothesized to change the interfaces between the PAN support, PDMS and adsorbent particles, causing a reduction in separation and permeability capability, as evident from the experimental data.

The adsorption isotherm for CO_2 in this SG adsorbent shows decreasing slope at pressures up to 10 atm [27]. Therefore, a decrease in gas permeability would be expected as the rate of uptake decreases at higher pressure. However, membrane swelling could also be the reason for the increase in CO_2 permeability with greater driving force. After being exposed to CO_2 for a single gas experiment CO_2 exposure and concentration in the membrane increases and has greater opportunity to swell the PDMS; this increases polymer chain mobility, free fractional volume and overall gas permeability with additional volume for mass transport [21,35]. In the case of all gas permeabilities the likelihood of void space in the matrix is high given the size and SSA of the silica gel particles, including the selective membrane thickness. When void space is present within a membrane matrix, gases have the least resistance for mass transport in these areas which increases gas diffusivity. This would be amplified with increasing feed pressure and results in increasing gas permeability. In this case, CO permeability increases at a greater rate than CO_2 and H_2. This is hypothesized to be due not only to void space, but also that CO solubility in PDMS and adsorption in SG is favoured over H_2. Part B of Figure 4-10 dispays ideal selecitivies of CO_2 over both CO and H_2, respectively.

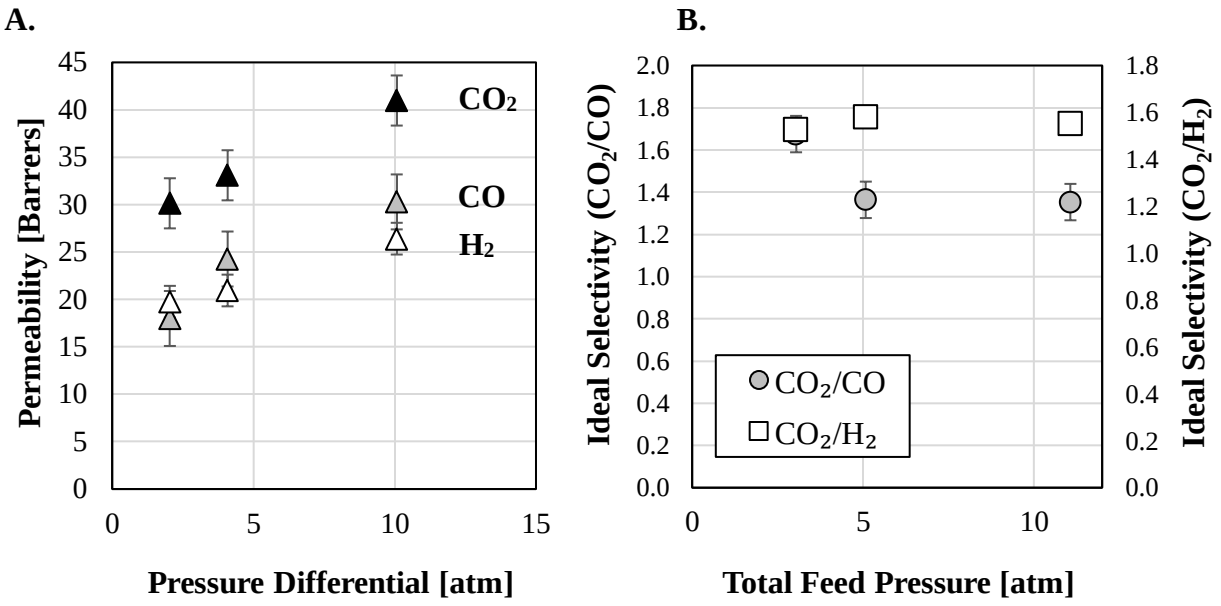

Figure 4-10: A – CO_2, CO, H_2 single gas permeabilities with respect to pressure differential for SG-PDMS-PAN II at 23 ºC; B – CO_2/CO and CO_2/H_2 ideal selectivities with respect to feed pressure

4.4.2.4 AC-PDMS-PAN II

Single gas permeabilities of all gases are graphed in Figure 4-11:A for this membrane, with respect to pressure differential across the membrane. Activated carbon (AC) in PDMS was by far the most permeable mixed matrix membrane tested in this work for single gas experiments, for all gases. This is speculated to be due to using a more porous PAN II support layer, nano-sized adsorbent particles with a higher adsorption capacity and higher specific surface area in comparison to the other adsorbents tested in this work.

Permeabilities across the pressure range showed stability with minor fluctuation. Membrane swelling by CO_2 is a possibility for CO_2 data, as there may be an increasing trend for single gas data. However, these effects are minimal in comparison to the other MMM's examined thus far. This is likely a direct result of the particle size of the activated carbon used in this mixed membrane matrix, allowing optimal contact and dispersion between the polymer and adsorbent phases and minimizing void or empty volumes within the matrix. Additionally, the more linear nature of activated carbon adsorption capacity with respect to pressure dictates stable permeabilities of all gases.

The difference between CO_2 permeability in comparison to CO and H_2 is greater with AC-PDMS-PAN II than the other membranes studied in this work, which is also evident in higher values for selectivities in part B of Figure 4-11. This is a result of successful membrane synthesis and appropriate material selection. With the small scale of the activated carbon particles (20 – 40 nm in size), it can be assumed from the data presented for single gas experiments that there was sufficient contact between the particles and polymer to create a well dispersed matrix in comparison to those prepared with HY and SG. With consistent contact between polymer and particle, this membrane could optimize the transport between polymer and adsorbent phase and achieve high single gas permeability and separation of CO_2 over H_2 and CO. On top of a more successful synthesis, activated carbon also has an adequately high adsorption capacity ratio for CO_2 over CO. Based on studies performed with adsorbents with surface areas similar to the carbon used in this study (1,400 m^2/g), the capacity for CO_2 adsorption was 1.5 – 1.8 mmol/g at 1 atm and upwards of 6 mmole/g at 10 atm [36,37]. This was similar to activated carbon studied with surface areas of 850 m^2/g by Wilson, with reported CO_2/CO adsorption capacity ratios of 5 at pressures 1 atm and greater, and drops to 3 at 10 atm [27]. As can be seen from part B in Figure 11, the selectivity values obtained with this mixed matrix membrane containing activated carbon are much higher than the adsorption capacity ratios for the separation of CO_2 and CO gases.

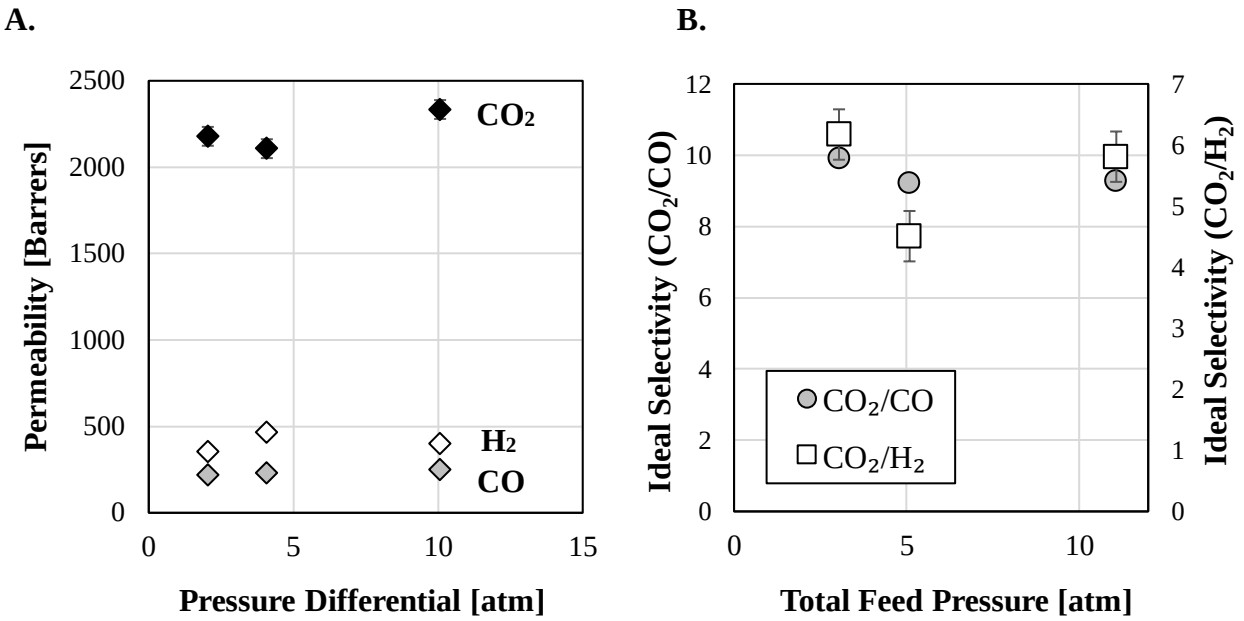

Figure 4-11: A – CO_2, CO, H_2 single gas permeabilities with respect to pressure differential for AC-PDMS-PAN II 23 ºC; B – CO_2/CO and CO_2/H_2 ideal selectivities with respect to feed pressure

4.4.3 Binary Gas Results and Discussion

4.4.3.1 CO_2:H_2

CO_2 and H_2 permeability data obtained for binary experiments with feeds composed of 25:75, 50:50 and 75:25 mole ratios of CO_2:H_2 are shown in Figure 4-12, 4-13 and 4-14Figure 4-14, respectively. Permeability is graphed with respect to partial pressure differences for each respective gas – the driving force used to induce separation. All the membranes tested were selective for CO_2 over H_2 for each feed composition. AC-PDMS-PAN II was again the observed the greatest gas permeabilities for all CO_2:H_2 binary experiments. SG-PDMS-PAN II observed the lowest gas permeabilities for all CO_2:H_2 binary experiments. When the two MMM's prepared from HY zeolite are compared, it can be seen that the MMM prepared on dry PAN I′ (HY-PDMS-PAN I′) had consistently higher permeabilities than the one prepared on wetted PAN I (HY-PDMS-PAN I). This would be due to a probable increase in the number of void spaces present in the HY-PDMS matrix, with an increase in the membrane thickness. Increasing the amount of selective material in the support pores is likely the reason for an increase in gas permeability and overall selectivity.

HY-PDMS-PAN I and SG-PDMS-PAN II showed slight increases in both CO_2 and H_2 permeabilities with increasing transmembrane pressure differential for CO_2:H_2 binary experiments.

HY-PDMS-PAN I′ observed stable CO_2 permeabilities and increases in H_2 permeability, within reasonable error for the amount of data collected over the pressure range. This was true across all CO_2:H_2 binary experiments, with the possible exception in Figure 4-14. In addition to the void spaces discussed earlier, membrane swelling could be responsible for these increases in CO_2 and H_2 permeabilities observed in HY and SG mixed matrix membranes. With higher feed pressures of CO_2 and by increasing the total CO_2 concentration as binary experiments progressed, more CO_2 is sorbed in the membrane which allows for greater degree of swelling. Therefore, the resistance for mass transport is decreased, and increases in gas permeabilities are possible. Alternatively, adsorption capacities for CO_2 in HY increase with increasing pressure, however the rate of adsorption capacity with respect to pressure is observed to be more linear at pressures upwards of 10 atm [38], indicating that permeability should be stable with respect to partial pressure difference. However, the adsorption capacity for CO_2 in the SG adsorbent exhibits a decreasing rate of adsorption isotherm slope with respect to these high feed pressures, indicating that the reasons discussed above overrule any changes to HY or SG performance with respect to pressure.

AC-PDMS-PAN II showed decreases in CO_2 and H_2 permeabilities, but not consistently across all feed compositions. This trending would be indicative of the CO_2 adsorption isotherm for activated carbon with increasing feed pressure, assuming the PDMS phase does not experience compaction. As pressure increases, the slope of the CO_2 isotherm decreases, causing CO_2 permeability in activated carbon to decrease at higher pressure. Adsorbent particles added to a polymer matrix offer some resistance to compaction [18]. However, at low weight loadings (4 wt % of AC adsorbent in PDMS) this resistance may be limited, as observed with these trends.

Figure 4-15 displays CO_2:H_2 binary data CO_2 permeability as a function of CO_2/H_2 selectivity, with respect to literature data from Lin et al. [21]. This plot is used to view where the membranes in this work fall in comparison to polymeric membrane literature data (seen as Literature Ref. in the legend). This plot includes data across the tested pressure range (three data points per feed composition, at 3, 5 and 11 atm feed pressure) from Figures 4-12 to 4-14, and are shown in a different format to better illustrate each membrane's ultimate performance. Permeability and selectivity are two gas membrane performance characteristics that cannot often both be maximized [21]. With the addition of selective adsorbent particles, this separation should be even more optimal by utilizing additional transport mechanisms. Membranes achieving high permeability and selectivity should approach the top right quadrant corner of this log-log graph. It is evident that AC-

PDMS-PAN II falls in this region of the graph for all binary concentrations, and HY-PDMS-PAN I′ approaches this area as well. This suggests that these membranes were synthesized to form well dispersed matrices, to allow the polymeric and adsorbent phases to work harmoniously for this separation. AC-PDMS-PAN II was the best membrane for CO_2/H_2 separation, having the largest selectivity, as well as the largest CO_2 permeability, as can be seen in Figure 4-15.

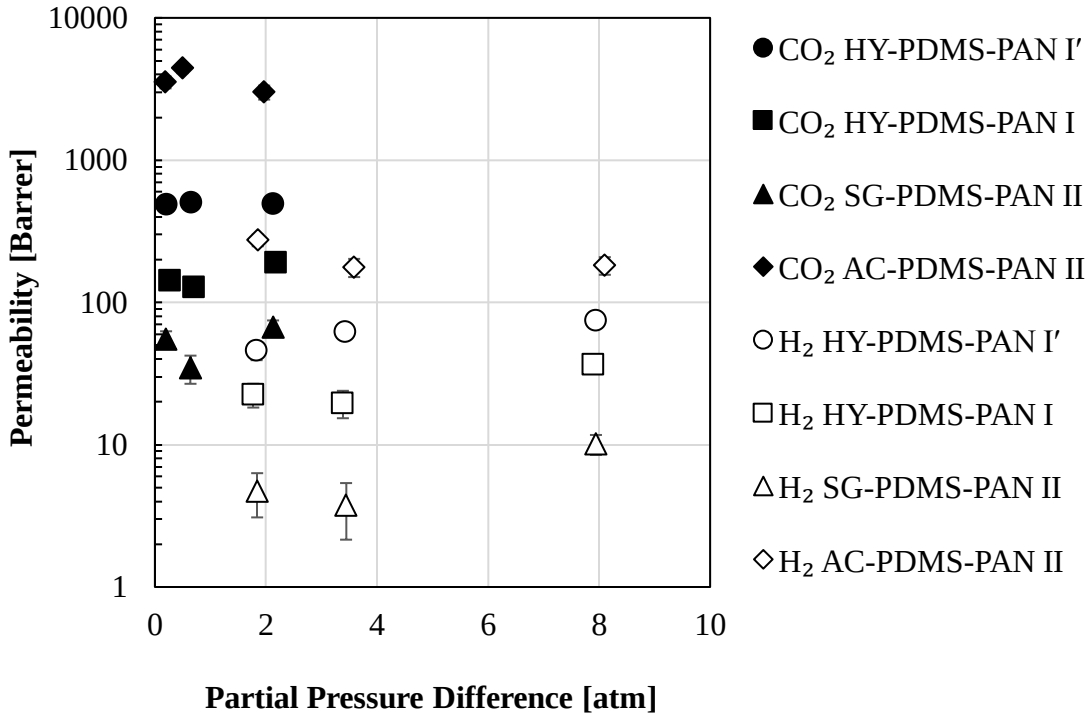

Figure 4-12: CO_2, H_2 permeabilities with respect to individual gas transmembrane partial pressure difference (25:75 CO_2:H_2) at 23 ºC and 3 – 11 atm total feed pressures

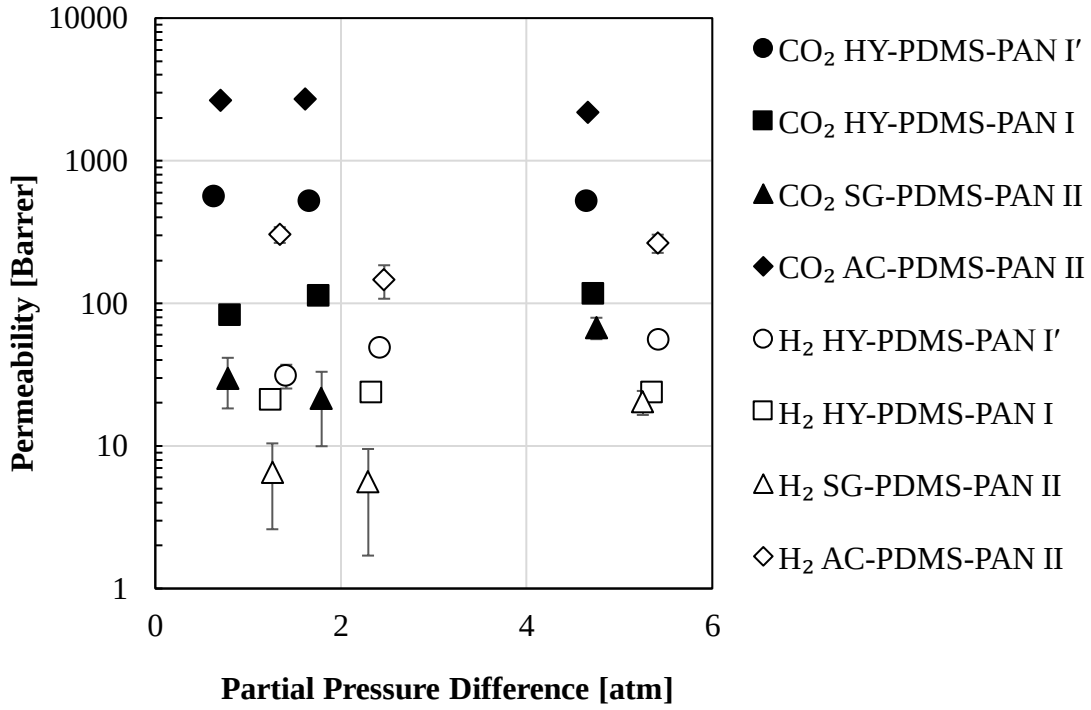

Figure 4-13: CO_2, H_2 permeabilities with respect to individual gas transmembrane partial pressure difference (50:50 CO_2:H_2) at 23 ºC and 3 – 11 atm total feed pressures

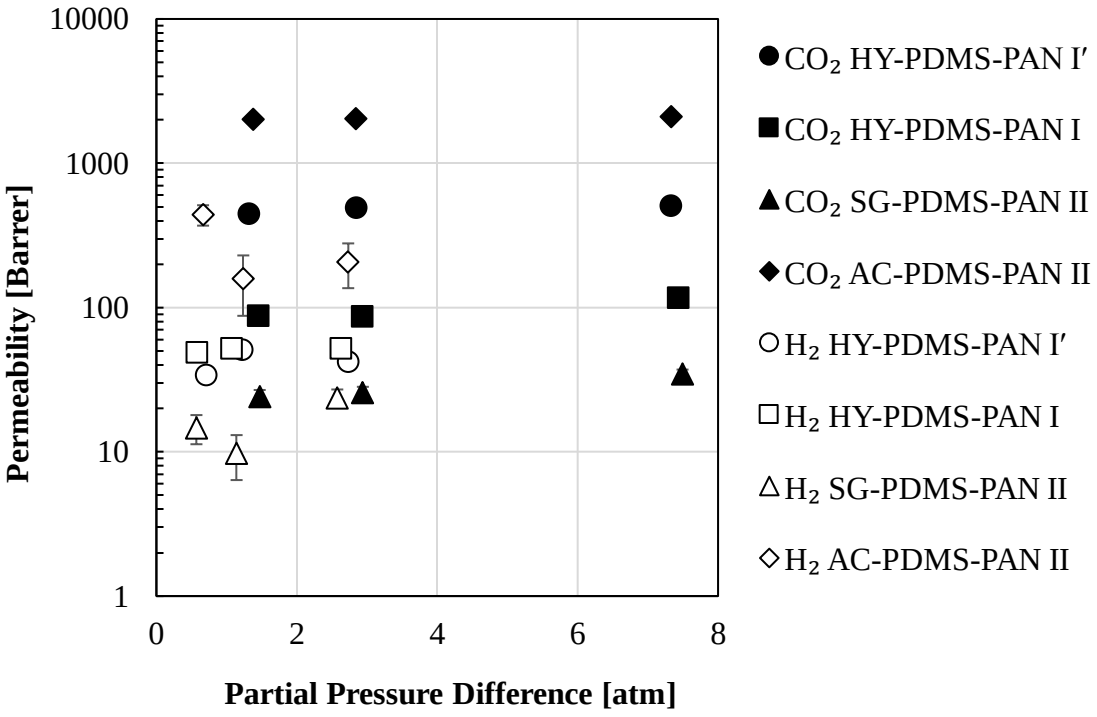

Figure 4-14: CO_2, H_2 permeabilities with respect to individual gas transmembrane partial pressure difference (75:25 CO_2:H_2) at 24 ºC and 3 – 11 atm total feed pressures

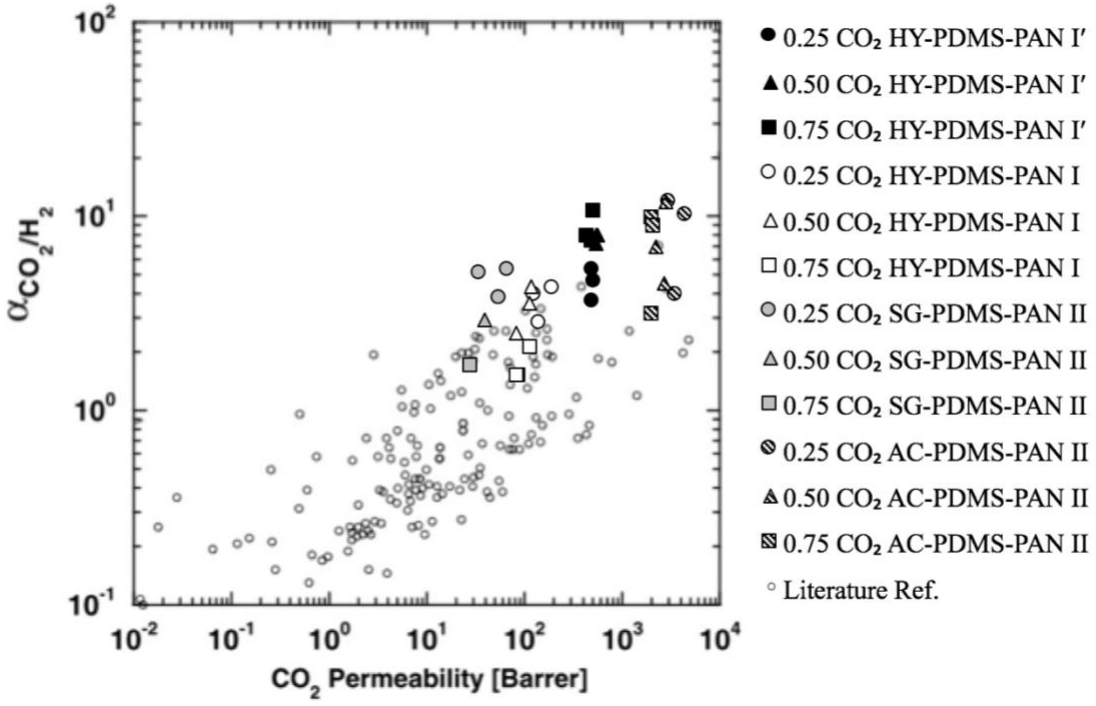

Figure 4-15: CO_2/H_2 selectivity with respect to CO_2 permeability binary data from Figure 4-12 to Figure 4-14, plotted in comparison to literature data (0.25, 0.50, 0.75 refers to CO_2 mole fraction in CO_2:H_2 feed) [21]

4.4.3.2 CO_2:CO

Binary experimental results for feeds composed of 25:75, 50:50 and 75:25 mole fractions of CO_2:CO are shown in Figure 4-16, 4-17 and 4-18, respectively. CO_2 and CO permeabilities are graphed with respect to partial pressure difference for each gas, respectively. All membranes tested were CO_2 selective over CO, with CO_2 permeabilities greater than CO. AC-PDMS-PAN II and SG-PDMS-PAN II continued to be the most and the least permeable, respectively. This was the same as CO_2-H_2 binary experiments. This is likely due to the size of the adsorbent particles for each membrane, as smaller particles create a more uniform matrix and allow for more consistent polymer-adsorbent interfaces. This creates a membrane that permits gas molecules to transport optimally between polymer and adsorbent phases. When the two MMM's prepared from HY zeolite are compared, we can see that HY-PDMS-PAN I′ had consistently higher permeabilities than HY-PDMS-PAN I. This would again be due to the probable void spaces within the HY-PDMS matrix. A thicker selective membrane would have a higher concentration of these void spaces, which would be present due to the size of the HY particles and how they interact with the PDMS phase. In addition

to this, a dry support (PAN I′) allowed the membrane matrix (PDMS-HY) to penetrate into its pores, where a wetted support (PAN I) would minimize this from happening during synthesis. The result of a dry support would be an increase in MMM volume, specifically within the pores of the support layer. Therefore, feed gases would be forced to interact with this extra material, allowing higher permeabilities.

HY-PDMS-PAN I′ exhibited increases in CO permeability in Figure 4-16, with respect to driving force. CO_2 permeability appeared to remain stable in this plot upon analysis of permeabilities across the tested feed pressure range. The CO_2/CO adsorption capacity ratio with respect to pressure for this HY adsorbent decreases going from a pressure of 0 to 10 atm [27]. This would support this trend, where CO_2 permeability does not observe the same increases in permeability with pressure as the CO, in the adsorbent phase. However, this observation was not repeated for permeability values at higher concentration of CO_2 in the feed in Figure 4-17 and Figure 4-18. CO permeability instead showed decreases from low to high partial pressure difference. In this case, CO_2 concentration in the feed is increasing as binary experiments continued, allowing more CO_2 to be sorbed in the membrane. CO_2 can therefore take up a larger volume in the PDMS and HY phases, as it has preferential solubility and adsorption capabilities over CO. In addition to this, consistent exposure to pressures up to 11 atm in total feed pressure (which is significant for a small flat-sheet, paper-like membrane) could begin compressing the membrane structure [39]. This would cause permeabilities to decrease with increasing applied pressure, as resistance to gas transport would increase through the membrane with a compacted structure. Since the adsorption capacity of CO in this HY zeolite is more linear in nature for pressures up to 10 atm [27], compaction is the likely cause for this deviation.

HY-PDMS-PAN I′ and AC-PDMS-PAN II were the two membranes that observed the greatest gas permeabilities thus far in experimentation. This is speculated to be due to the direct result of: higher specific surface areas, smaller particle sizes of HY and AC adsorbents – in comparison to SG – and greater selective membrane thicknesses. AC-PDMS-PAN II did observe some increases in CO permeability in Figure 4-16. This would suggest probable membrane swelling via CO_2 sorption, as the CO isotherm slope for this adsorbent would not indicate an increase in permeability with respect to pressure. However, from 50:50 and 75:25, CO_2:CO binary experiments the data suggests an opposite trend. At higher compositions of CO_2 in the feed gas, CO permeability decreased with increasing partial pressure difference. Again, as CO_2 concentration in the feed

increases, the amount of CO_2 sorbed in the membrane – in both phases – increases. This prevents CO gas molecules from permeating to the same extent. In addition to this, compaction is believed to be another probable cause, as the effect of adsorption isotherms of CO_2 in activated carbon would dictate decreasing gas permeability with respect to pressure, specifically at higher feed pressures.

HY-PDMS-PAN I and SG-PDMS-PAN II continued to observe the effects of membrane swelling and poor PDMS-adsorbent interfaces in CO_2:CO binary experiments. CO and CO_2 permeability through SG-PDMS-PAN II consistently increased across the tested pressure range for all tested CO_2:CO feed compositions. The particle size and smaller SSA contributed to an unsuitable matrix, leading to an increase in mass transport with respect to CO_2 and CO. The presence of void space within this membrane would cause gas permeabilities for both components to increase with higher feed pressure. Membrane swelling is also probable and could be expected to also cause increases in permeability with respect to pressure, especially with increasing CO_2 concentration in the gas feed as binary experiments were carried out. HY-PDMS-PAN I data was analogous to SG-PDMS-PAN II, where the increase in permeability was amplified from Figure 4-16 to Figure 4-18, for both gases.

Figure 4-19 displays selectivity values of CO_2 over CO with respect to CO_2 permeability (graph outline and axis from Lin et al. [21]), however less published data exists for this CO_2:CO separation. A smaller collection of data is available from published literature for comparison to the data in this work (seen as Literature Ref. in the legend) [22,23,40]. The data plotted on this figure is a compilation of the permeability-partial pressure graphs presented in Figure 4-16 to Figure 4-18, but shown in a different fashion to compare performance parameters to literature. Several data points exist for each feed concentration as permeability trends cannot be omitted across the feed pressure range. AC-PDMS-PAN II and HY-PDMS-PAN I′ were again the membranes that achieved higher CO_2 permeability and CO_2/CO separation, as the plotted data proved in Figure 4-19. It can be harder to achieve better and better separation with an increase in feed concentration of the desired permeate component with a single pass membrane system (as seen in Chapter 3 with purely polymeric PDMS membranes), however both AC-PDMS-PAN II and HY-PDMS-PAN I′ saw the best separation with 75 mol % CO_2 in the feed. This is likely a demonstration of how selectively adsorbent material can work in conjunction with a selective polymer to overcome the separation limits of the polymeric material.

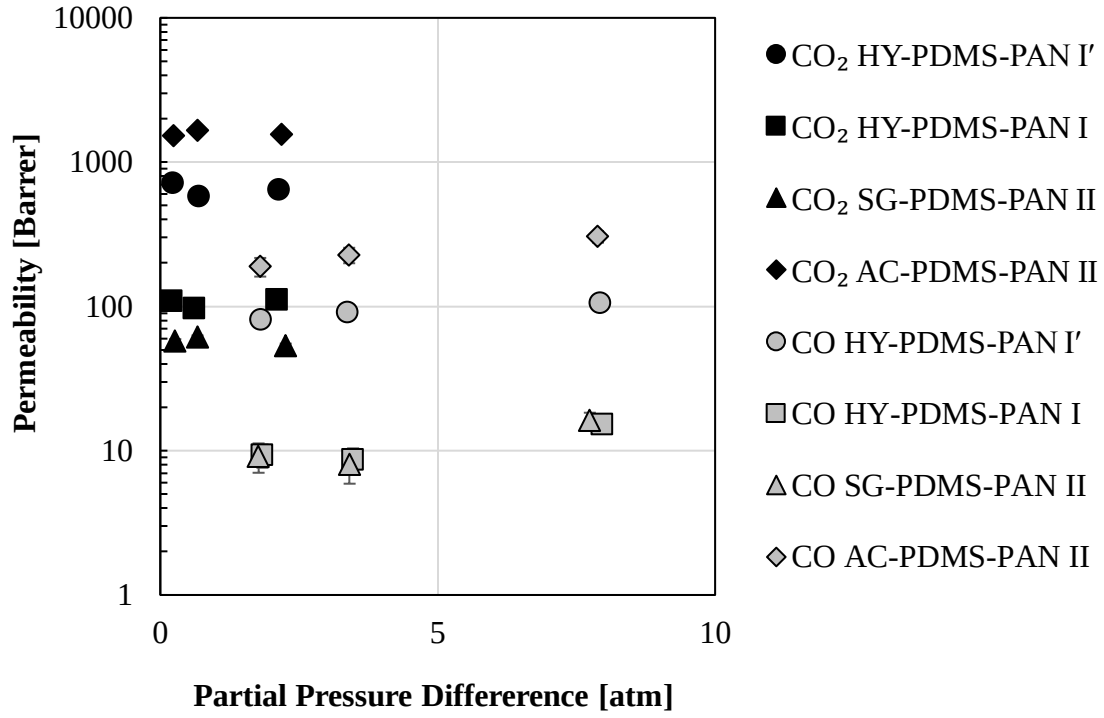

Figure 4-16: CO_2, CO permeabilities with respect to individual gas transmembrane partial pressure difference (25:75 CO_2:CO) at 24 ºC and 3 – 11 atm total feed pressures

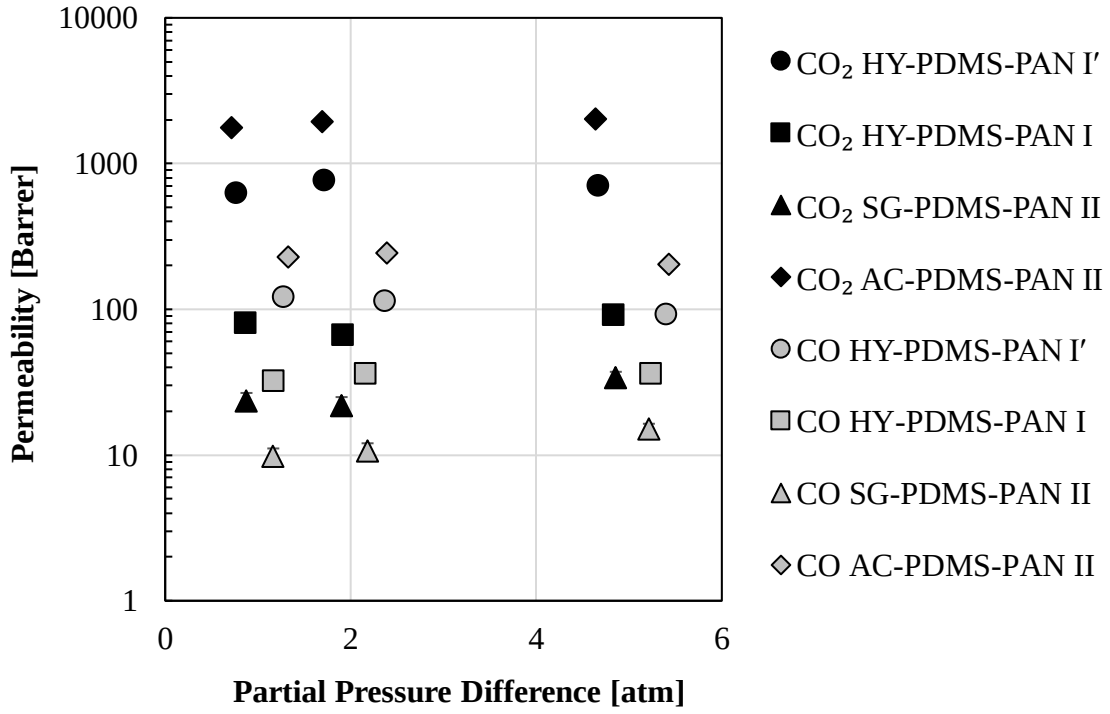

Figure 4-17: CO_2, CO permeabilities with respect to individual gas transmembrane partial pressure difference (50:50 CO_2:CO) at 24 ºC and 3 – 11 atm total feed pressures

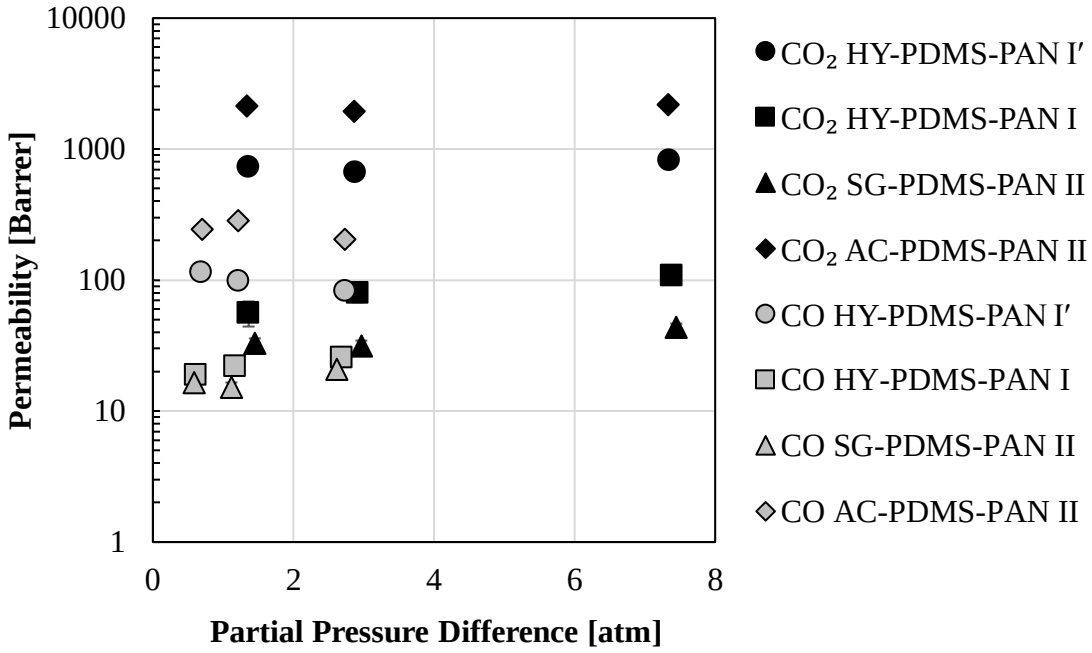

Figure 4-18: CO_2, CO permeabilities with respect to individual gas transmembrane partial pressure difference (75:25 CO_2:CO) at 24 ºC and 3 – 11 atm total feed pressures

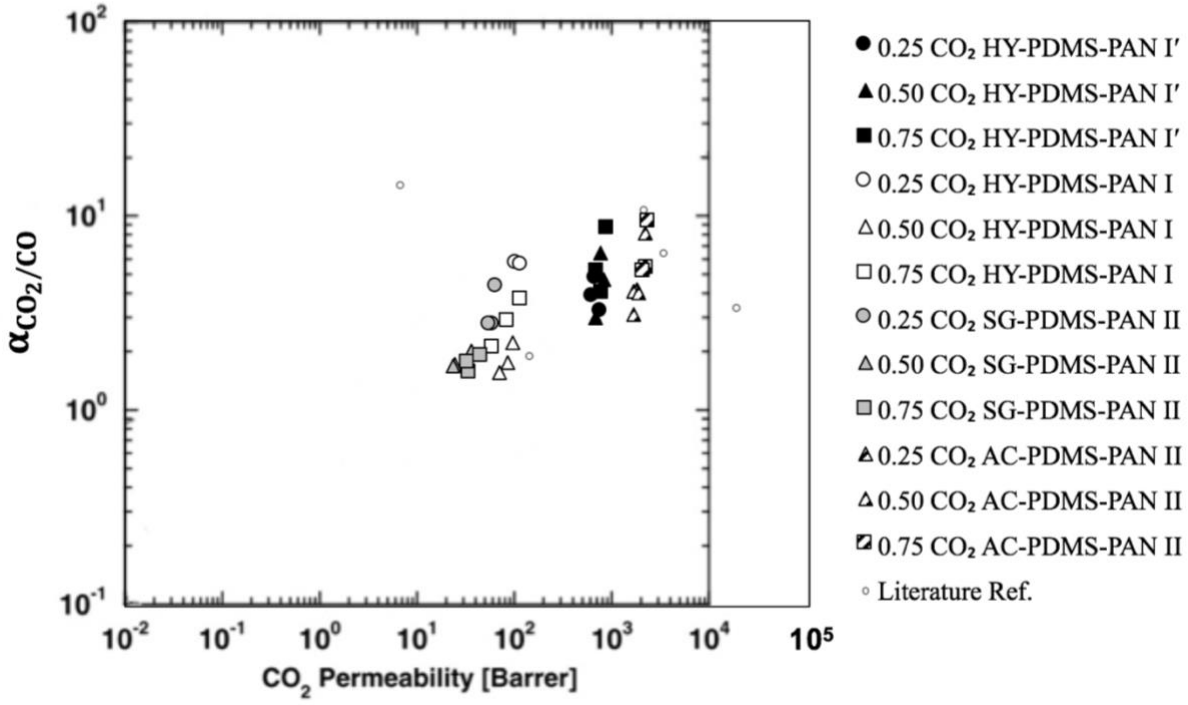

Figure 4-19: CO_2/CO selectivity with respect to CO_2 permeability binary data from Figure 4-16 to Figure 4-18, plotted in comparison to literature data (0.25, 0.50, 0.75 refers to CO_2 mole fraction in CO_2:CO feed) [21–23,40]

4.4.4 Ternary Gas Results and Discussion

In this study, a ternary gas feed was introduced to each mixed matrix membrane in an even mixture of all three gases in the molar ratio 1:1:1 of CO_2:CO:H_2. Corresponding permeability data trends with respect to partial pressure difference can be viewed in Figure 4-20. Overall, AC-PDMS-PAN II was the best membrane tested for ternary gas feeds, with the highest CO_2 permeability (2,447 Barrers, at feed pressure of 5 atm) and CO_2 selectivities (14 for CO_2/H_2 and 9 for CO_2/CO, at feed pressure of 11 atm). Again, the difference in dry and wetted PAN supported membranes – between HY-PDMS-PAN I′ and HY-PDMS-PAN I – was evident in ternary experiments. In this case, a thicker selective membrane on a dry PAN support allowed for a more permeable membrane. Unlike polymeric membranes, a thicker selective membrane can facilitate greater permeabilities than selective membranes with smaller thicknesses. This is thanks to the addition of adsorbent particles that are selective and the possibility of a greater presence of void or defect areas within the membrane, aiding favourable mass transport. The presence of HY in PDMS, including an additional 20 µm of MMM, made a significant difference in overall membrane permeability.

The permeability trends from binary gas experiments for each membrane continued into ternary gas experiments. HY-PDMS-PAN I′ and AC-PDMS-PAN II showed minor decreases in gas permeability with respect to feed pressure for CO and H_2, indicating the effects increase CO_2 concentration with higher partial pressures at higher feed pressure. HY-PDMS-PAN I and SG-PDMS-PAN II continued to show increasing permeability of CO and H_2 with higher partial pressure differentials, as with previously mentioned for binary experiments. This increase was more pronounced for SG-PDMS-PAN II. Again, this can be attributed to physical intricacies within the matrix, where the polymer-adsorbent interfaces are sub-optimal. These interfaces are critical in a successful separation for mixed gases. Any space between the adsorbent and polymer phases will be taken advantage of by any gas, specifically at higher pressures when the path of least resistance becomes more and more opportune. This coupled with membrane swelling are probable causes to increases in gas permeabilities with pressure.

Although H_2 permeability was greater than CO for single gas experiments, it was expected for CO permeability to be greater than H_2 for ternary gas experiments. Competitive sorption in the membrane would introduce an advantage for the more soluble, larger gas molecule, CO. Penetrants with higher solubility and adsorption affinity to the materials present in the mixed matrix membranes would essentially occupy more space within the membrane and prevent the less

attractive gas molecules from penetrating. However, HY-PDMS-PAN I did not consistently observe this CO-H_2 permeability order, where CO permeated more than H_2. Again, this could be due to inconsistent contact between the particle and polymer phases, a result from the larger size of these adsorbent particles. The void volume between the polymer and adsorbent phases (for any MMM) is not selective for any gas so with enough void space in the membrane, H_2 diffusivity could increase more significantly and result in an increased gas permeability in comparison to CO. However, the permeabilities of CO and H_2 are relatively close in comparison to the difference of CO_2.

The MMM ternary data presented in this work was compared against three PDMS membranes studied previously in Chapter 3, to identify the differences of adding adsorbents into a PDMS matrix. These purely polymeric membranes included a commercial PDMS membrane and two synthesized PDMS membranes, varying in selective thicknesses. The commercial PDMS membrane was purchased from Sulzer Chemtech (Tulsa, OK, USA). PDMS-PAN I was synthesized in the laboratory on the same wetted PAN I support discussed in this work with a PDMS thickness of 75 µm. PDMS-PAN II was also synthesized in the laboratory on the same wetted PAN II support discussed in this work with a PDMS thickness of 55 µm.

A CO_2/H_2 selectivity versus CO_2 permeability plot from Lin et al. [21], seen in Figure 4-21, was used again to demonstrate which membrane maximized permeability and selectivity simultaneously. From this graph, every membrane includes three data points to summarize the differences in permeability and selectivity at the feed pressure intervals during the experiment from Figure 4-20 (3, 5 and 11 atm). Every MMM exposed to a ternary gas mixture (of all three gas components) could successfully separate CO_2 from both CO and H_2, however AC-PDMS-PAN II was not defeated. In Figure 4-21, it is easy to see AC-PDMS-PAN II is the membrane that achieves the highest CO_2 permeability and CO_2/H_2 selectivity across all tested MMMs, as well as the literature. In comparing this performance to the PDMS membranes in Chapter 3, PDMS-PAN I achieved the highest selectivity for CO_2 over H_2. Commercial PDMS achieved the highest CO_2 permeability. In terms of separation capabilities, AC-PDMS-PAN II was approximately 20 µm thinner than PDMS-PAN I, but was able to achieve similar selectivities for CO_2 over H_2. This is due to the additional sorption sites provided by activated carbon where CO_2 has preferential adsorption capacities.

A CO_2/CO selectivity versus CO_2 permeability plot from Lin et al. [21], seen in Figure 4-22, was used finally to observe optimal permeabilities and selectivities of the MMM studied in this

work, in comparison to the PDMS membranes from Chapter 3. Again, this is the same data presented in Figure 4-20, plotted to observe permeability and selectivity differences across the tested pressure range. There was less of a difference in CO_2/CO separation between all membranes examined. AC-PDMS-PAN II and PDMS-PAN II observed the best CO_2/CO separation at the highest tested feed pressure. However, AC-PDMS-PAN II exhibited the highest selectivity for CO_2 over CO – excluding, but close to, literature data. From these experiments and data analysis, the addition of activated carbon nano-particles to a PDMS polymer matrix do offer some performance advantages over purely polymeric membranes due to the addition of multi-transport mechanisms for mass transport.

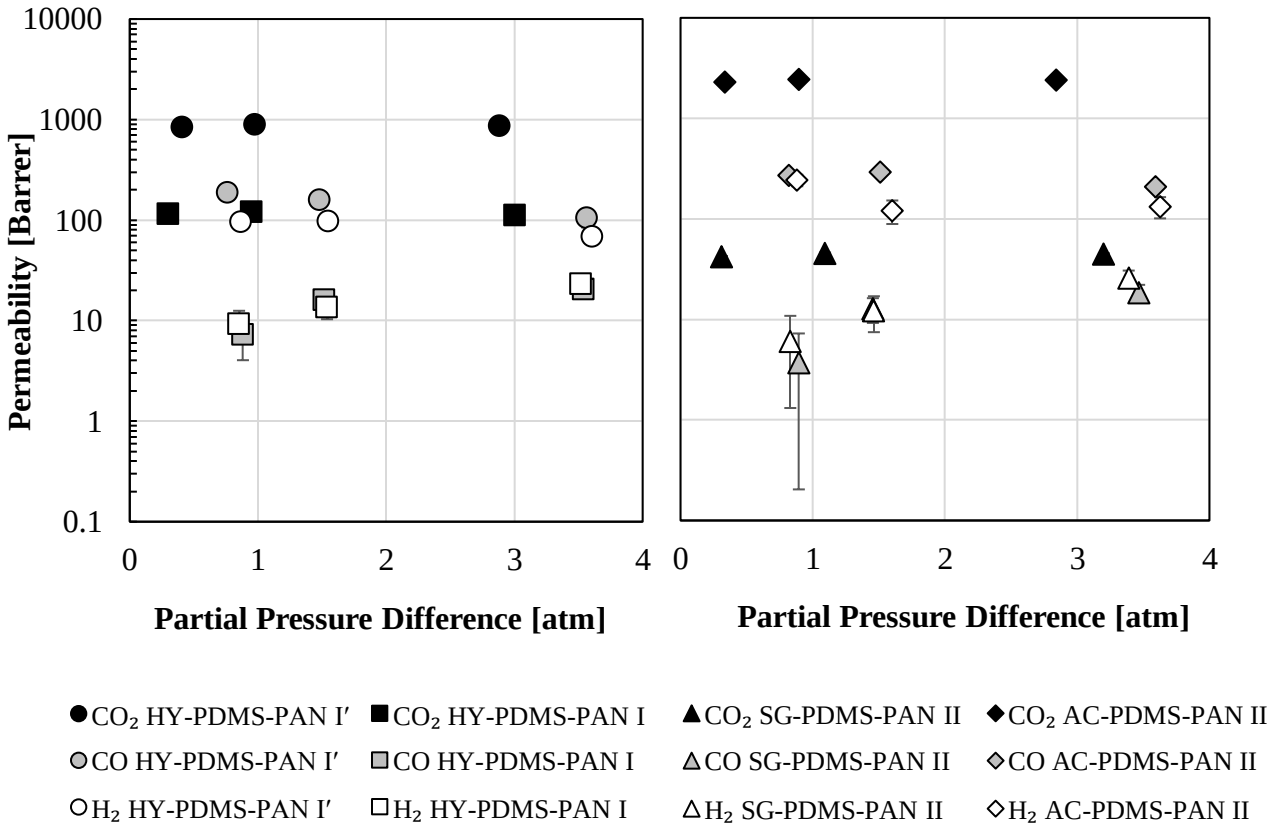

Figure 4-20: CO_2, CO, H_2 permeabilities with respect to individual gas transmembrane partial pressure difference for ternary gas system (33:33:33 CO_2:CO:H_2) at 23 ºC and 3 – 11 atm total feed pressure

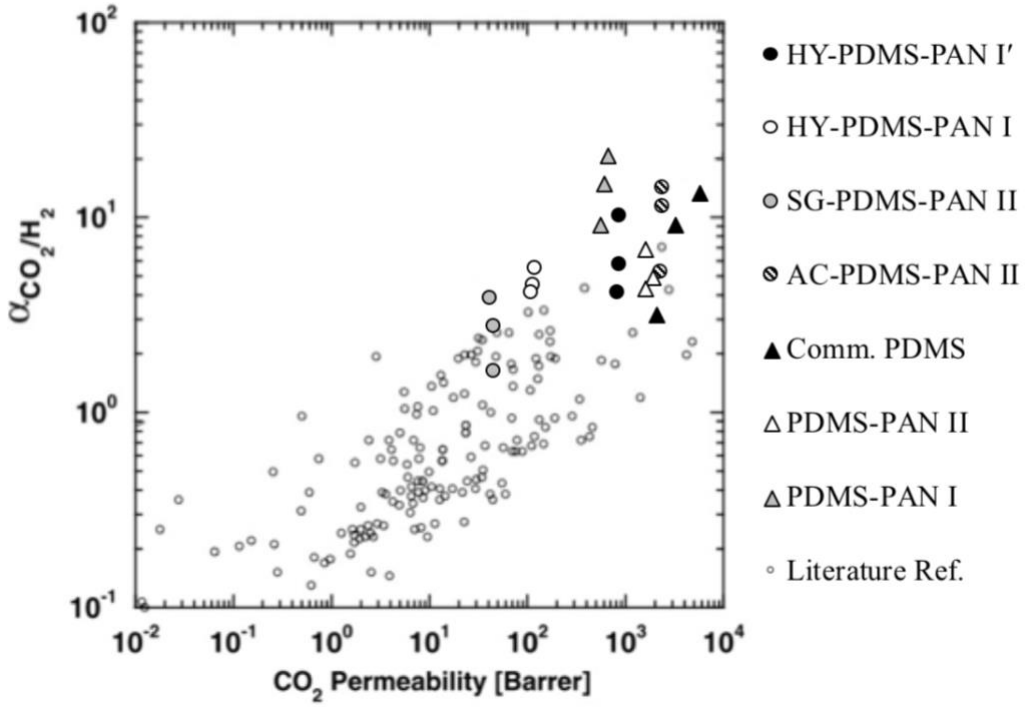

Figure 4-21: CO_2/H_2 selectivity with respect to CO_2 permeability ternary data from Figure 4-20, plotted in comparison to literature data [21]

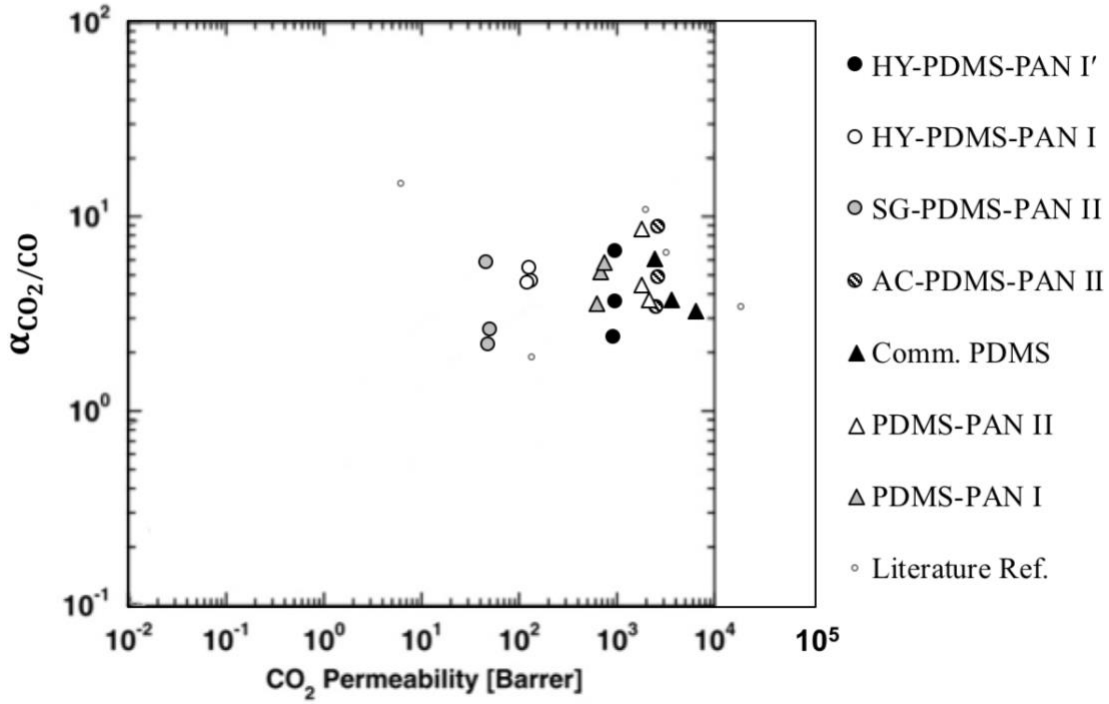

Figure 4-22: CO_2/CO selectivity with respect to CO_2 permeability ternary data from Figure 4-20, plotted in comparison to literature data [21–23,40]

4.5 CONCLUSIONS AND FUTURE WORK

Mixed matrix membranes, synthesized with a PDMS polymer, were prepared using HY zeolite, silica gel and activated carbon particles with a 4 wt % loading in PDMS on PAN flat-sheet supports. A single cell membrane system was used to perform single, binary and ternary gas feed experiments up to 11 atm of total pressure, at room temperature between 23 and 24 ºC for CO_2, CO and H_2 gases.

Single, binary and ternary experiments all confirmed that activated carbon in PDMS, proved to be the best performing material when considering CO_2 permeability and CO_2 selectivity over CO and H_2. Ternary experiments proved this with the highest CO_2 permeability of 2,447 Barrers and the highest separation factors for CO_2 of 14 over H_2 and 9 over CO. Silica gel in PDMS proved to be the most unsuccessful material tested for these separations, due to large particle size and low available adsorbent surface area, in addition to low selective membrane thicknesses on wetted supports. In comparison to three previously studied pure PDMS membranes (from Chapter 3), activated carbon filled PDMS was still competitively selective. Therefore, at this weight loading the nano-sized activated carbon in PDMS did not significantly increase the ability for PDMS to selectively separate CO_2 from either syngas component. Different weight loadings of the adsorbent in PDMS could be investigated to observe differences in permeability and selectivity.

HY-PDMS-PAN I and SG-PDMS-PAN II mixed matrix membranes were observed the behaviour of unsuitable polymer-adsorbent and probably membrane swelling, denoted by increasing gas permeabilities with increasing pressure, consistently throughout all experiments. Higher gas permeabilities and selectivities of the HY-PDMS membrane fabricated on a dry PAN support, compared to a wet PAN support, in addition to a larger selective thickness were speculated to be due to a greater MMM selective volume occupying the pores of the support.

It would be of interest to prepare and test more MMMs with nano-scale HY and silica gel particles to observe any differences in performance. This may increase the permeabilities and selectivities of these membranes by optimizing the contact between the adsorbent and polymer, maximizing available surface area and creating a more uniform matrix. Lastly, alternate weight loadings of the adsorbent materials used in this work should be investigated for permeability and selectivity differences, including resilience to compaction and swelling.

4.6 ACKNOWLEDGEMENTS

The authors would like to thank and acknowledge the financial support received from MITACS (Mathematics of Information Technology and Complex Systems), Phoenix Canada Oil Company Limited, NSERC (Natural Science and Engineering Research Council of Canada) and Natural Resources Canada. The authors would like to thank Glenn Poirier on behalf of the University of Ottawa for the SEM imaging, training and assistance in the Advanced Research Centre (ARC). The authors would like to thank Hoda Azimi for providing the activated carbon-PDMS mixed matrix membrane tested in this work and providing guidance and information for the synthesis method. The authors would also like to thank Maja Mujcin for performing a sieve analysis on the HY zeolite discussed in this chapter. Finally, the authors thank Mohammadali Baghbanzadeh, Dr. C. Lan and Dr. T. Matsuura for use of their laboratory space and sonicator for the mixed matrix membrane synthesis.

4.7 NOMENCLATURE

Term	Definition	Units
C	Concentration in the membrane	mol/cm^3
D	Diffusivity coefficient	cm^2/s
J	Permeate flux	$cm^3\ (STP)/s \cdot cm^2$
MWCO	Molecular weight cut-off	kDa
P	Permeability	$10^{-10}\ \frac{cm^3\ (STP) \cdot cm}{s \cdot cm^2 \cdot cmHg}$ = 1 Barrer
ΔP	Partial pressure difference across membrane	cmHg
S	Solubility coefficient	$\frac{cm^3\ (STP)}{cm^3 \cdot atm}$
x	Mole fraction in membrane feed	Dimensionless
y	Mole fraction in membrane permeate	Dimensionless
z	Selective membrane thickness	cm
$\alpha^*_{A/B}$	Ideal selectivity of A over B	Dimensionless
$\alpha_{A/B}$	Selectivity of A over B	Dimensionless

4.8 ABBREVIATIONS AND SYMBOLS

Symbol	Description
AC	Activated carbon
CO_2	Carbon dioxide
CO	Carbon monoxide
H_2	Hydrogen
He	Helium
HY	Y-type zeolite with H^+ ions
MMM	Mixed matrix membrane
OD	Outer diameter
PAN	Polyacrylonitrile
PDMS	Polydimethylsiloxane
RWGS	Reverse Water Gas Shift
SG	Silica gel
SEM	Scanning electron microscope
STP	Standard temperature and pressure (0 °C, 1 bar)

4.9 REFERENCES

[1] F. Abdollahi, F.H. Tezel, S. Aplin, Increasing Conversion of CO_2 To CO Via RWGS Reaction: Simulation and Process Design, Altern. Energy. 2 (2013) 1–6.

[2] U.R. Bajirao, Kinetics and Reaction Engineering Aspects of Syngas Production by the Heterogeneously Catalysed Reverse Water Gas Shift Reaction, Ph.D. Thesis, University of Bayreuth, 2012.

[3] D. Bell, B. Towler, M. Fan, Coal Gasification and It's Applications, in: 1st ed., William Andrew (Elsevier), Great Britain, 2011: pp. ix–xi.

[4] A. Steynberg, M. Dry, Studies in Surface Science and Catalysis, in: M. Dry (Ed.), Stud. Surf. Sci. Catal., Science Direct (Elsevier), 2004: pp. 1–63.

[5] C.A. Scholes, G.W. Stevens, S.E. Kentish, The effect of hydrogen sulfide, carbon monoxide and water on the performance of a PDMS membrane in carbon dioxide/nitrogen separation, J. Memb. Sci. 350 (2010) 189–199.

[6] J. Estephane, S. Aouad, S. Hany, B. El Khoury, C. Gennequin, H. El Zakhem, et al., CO_2 reforming of methane over Ni-Co / ZSM5 catalysts: Aging and carbon deposition study, Int. J. Hydrogen Energy. 40 (2015) 69–80.

[7] J.D. Seader, E.J. Henley, K.D. Roper, Separation Process Principles: Chemical and Biochemical Operations, in: 3rd ed., Wiley, 2010: p. 848.

[8] T. Matsuura, Synthetic Membranes for Membrane Processes, in: Synth. Polym. Membr., Springer Berlin Heidelberg, Berlin, Heidelberg, 2008: pp. 5–18.

[9] M. Hussain, A. König, Mixed-Matrix Membrane for Gas Separation: Polydimethylsiloxane Filled with Zeolite, Chem. Eng. Technol. 35 (2012) 561–569.

[10] C.M. Zimmerman, A. Singh, W.J. Koros, Tailoring mixed matrix composite membranes for gas separations, J. Memb. Sci. 137 (1997) 145–154.

[11] D. Bastani, N. Esmaeili, M. Asadollahi, Polymeric mixed matrix membranes containing zeolites as a filler for gas separation applications: A review, J. Ind. Eng. Chem. 19 (2013) 375–393.

[12] V. Kramer, M. Kraume, Development of a Mechnistic Model for Sorption Selective Mixed-Matrix Membranes for Gas Separation, Tech. Trans. 109 (2012) 126–135.

[13] P. Bernardo, E. Drioli, G. Golemme, Membrane Gas Separation: A Review / State of the Art, Ind. Eng. Chem. Eng. Res. 48 (2009) 4638–4663.

[14] S. Shelley, Capturing CO_2: Membrane Systems Move Forward, Chem. Eng. Prog. 105 (2009) 42–47.

[15] W.J. Koros, Evolving Beyond the Thermal Age of Separation Processes: Membranes Can Lead the Way, AIChE J. 50 (2004) 2326–2334.

[16] T.C. Merkel, V.I. Bondar, K. Nagai, B.D. Freeman, I. Pinnau, Gas sorption, diffusion, and permeation in poly(dimethylsiloxane), J. Polym. Sci. Part B Polym. Phys. 38 (2000) 415–434.

[17] J. Maxwell, A Treatise on Electricity and Magnetism : Volume II, Dover Publications, 1873.

[18] Y. Zhao, B.T. Jung, L. Ansaloni, W.S.W. Ho, Multiwalled carbon nanotube mixed matrix membranes containing amines for high pressure CO_2/H_2 separation, J. Memb. Sci. 459 (2014) 233–243.

[19] L.M. Robeson, The upper bound revisited, J. Memb. Sci. 320 (2008) 390–400.

[20] L.M. Robeson, Correlation of separation factor versus permeability for polymeric membranes, J. Memb. Sci. 62 (1991) 165–185.

[21] H. Lin, E. Van Wagner, B.D. Freeman, L.G. Toy, R.P. Gupta, Plasticization-Enhanced Hydrogen Purification Using Polymeric Membranes, Science. 311 (2006) 639–642.

[22] C.A. Scholes, J. Bacus, G.Q. Chen, W.X. Tao, G. Li, A. Qader, et al., Pilot plant performance of rubbery polymeric membranes for carbon dioxide separation from syngas, J. Memb. Sci. 389 (2012) 470–477.

[23] T.C. Merkel, R.P. Gupta, B.S. Turk, B.D. Freeman, Mixed-gas permeation of syngas components in poly(dimethylsiloxane) and poly(1-trimethylsilyl-1-propyne) at elevated temperatures, J. Memb. Sci. 191 (2001) 85–94.

[24] A. Lamberti, A. Virga, P. Rivolo, A. Angelini, F. Giorgis, Easy Tuning of Surface and Optical Properties of PDMS Decorated by Ag Nanoparticles, J. Phys. Chem. 119 (2015) 8194–8200.

[25] A. Lamberti, S.L. Marasso, M. Cocuzza, PDMS membranes with tunable gas permeability for microfluidic applications, R. Soc. Chem. 4 (2014) 61415–61419.

[26] D. Sun, M.Q. Liu, J.H. Guo, J.Y. Zhang, B.B. Li, D.Y. Li, Preparation and characterization of PDMS-PVDF hydrophobic microporous membrane for membrane distillation, Desalination. 370 (2015) 63–71.

[27] S.M. Wilson, Adsorption Separation of CO_2 from CO in Syngas: Improving the Conversion of the Reverse Water Gas Shift Reaction, M.A.Sc. Thesis, University of Ottawa, 2015.

[28] P. Li, H.Z. Chen, T.S. Chung, The effects of substrate characteristics and pre-wetting agents on PAN-PDMS composite hollow fiber membranes for CO_2/N_2 and O_2/N_2 separation, J. Memb. Sci. 434 (2013) 18–25.

[29] J. Peter, K.-V. Peinemann, Multilayer composite membranes for gas separation based on crosslinked PTMSP gutter layer and partially crosslinked Matrimid® 5218 selective layer, J. Memb. Sci. 340 (2009) 62–72.

[30] Q.A. Acton, ed., Patent Issued for Extra Mesoporous Y Zeolite, 2013.

[31] R.T. Yang, Silica Gel, MCM, and Activated Alumina, in: Adsorbents Fundam. Appl., John Wiley & Sons Inc., 2003: pp. 131–156.

[32] US Research Nanomaterials, Inc: The Advanced Nanomaterials Provider, (2016). www.us-nano.com (accessed November 1, 2016).

[33] Ultrafiltration (UF) Flat Sheet Membranes, (n.d.). http://www.sterlitech.com/membrane-process-development/flat-sheet-membranes/ultrafiltration-uf-membrane.html (accessed July 31, 2016).

[34] D.G.R. Bonnell, Studies in Gels IV. - The Swelling of Silica Gel., Trans. Faraday Soc. 29 (1933) 1217–1220.

[35] E.H. Immergut, H.F. Mark, Principles of Plasticization, Plast. Plasticizer Processes. 48 (1965) 1–26.

[36] Y. Park, D.K. Moon, Y.H. Kim, H. Ahn, C.H. Lee, Adsorption isotherms of CO_2, CO, N_2, CH_4, Ar and H_2 on activated carbon and zeolite LiX up to 1.0 MPa, Adsorption. 20 (2014) 631–647.

[37] A.-H. Lu, G.-P. Hao, X.-Q. Zhang, Porous Materials for Carbon Dioxide Capture, in: A.-H. Lu, S. Dai (Eds.), Springer, 2014: p. 106.

[38] P.J.E. Harlick, F.H. Tezel, An experimental adsorbent screening study for CO_2 removal from N_2, Microporous Mesoporous Mater. 76 (2004) 71–79.

[39] K.W. Lawson, M.S. Hall, D.R. Lloyd, Compaction of microporous membranes used in membrane distillation. I. Effect on gas permeability, J. Memb. Sci. 101 (1995) 99–108.

[40] O.C. David, Membrane technologies for hydrogen and carbon monoxide recovery from residual gas streams, Ph.D. Thesis, Universidad de Cantabria, 2012.

Chapter 5: Conclusion and Recommendations

The CO_2 gas from large emission sources can not only be successfully captured but it also has the potential to be consumed in the RWGS reaction to more useful value-added products. Introducing a recycle stream to this reaction could make the scale-up process more economically sustainable and environmentally attractive. Using membranes as a means for separation allows CO_2 to be isolated from syngas components: CO and H_2. The Fischer-Tropsch process is a desirable strategy to pursue where the syngas is used as a feedstock to produce synthetic liquid fuels. Not only can CO_2 be controlled from further release into the atmosphere, it can be converted into fuels.

A literature review was completed to identify the most suitable polymeric, inorganic and mixed matrix membranes for separation of CO_2 from CO and H_2 to increase the overall conversion of the RWGS reaction. Permeability and selectivity were analyzed for several membranes. While there were several contenders, PDMS was selected to be studied further based on factors such as performance, cost, versatility and availability.

The separation of CO_2 from CO and H_2 via single, binary and ternary gas experiments was investigated with the use of pure PDMS membranes. This separation was easily accomplished at room temperature conditions (23 – 25 ºC) with absolute feed pressures of 3 to 11 atm. A commercial PDMS membrane along with membranes which were synthesized in the lab were used for this study. It was determined that PDMS alone could successfully separate CO_2 from these two syngas components (CO, H_2) with higher CO_2 permeabilities and selectivities compared to those studied in the literature. Ternary gas experiments involving CO_2, H_2 and CO observed CO_2 permeabilities as high as 5,883 Barrers, with CO_2 selectivities over H_2 and CO of 21 and 9, respectively. Of the three pure PDMS membranes tested in this study, the PDMS with the thickness of 55 µm performed the best with respect to maximizing CO_2 permeability and selectivity. These membranes also experienced changes in permeability with respect to driving force (membrane partial pressure differential), suggesting PDMS was susceptible to both swelling from CO_2 and to compaction at higher operating pressures.

Mixed matrix membranes were also investigated in this study, using PDMS as the continuous phase to disperse selectively adsorbent particles. HY zeolite, silica gel and activated carbon adsorbents were individually incorporated into these membrane matrices for experimental use at 4 wt % loadings. CO_2 separation from H_2 and CO was also successful with all mixed membranes tested in single, binary and ternary gas experiments at room temperature conditions (23 – 24 ºC) and at absolute feed pressures from 3 to 11 atm. The activated carbon-PDMS matrix was

determined to be the most successful membrane material combination, with CO_2 permeability values as high as 2,447 Barrers for ternary gas feeds. Of the MMMs examined, CO_2 selectivities over H_2 and CO were the highest for the activated carbon-PDMS matrix: 14 and 9, respectively. The activated carbon used to form this matrix was assumed to be the most uniformly dispersed due to its small particle size in comparison to the HY and silica gel adsorbents. Additionally, it was determined that a thicker selective MMM observed greater gas permeability and selectivity for CO_2. Overall, the separation of CO_2 from H_2 and CO was successfully performed by all mixed matrix membranes examined in this work.

While the addition of adsorbent particles into a polymer matrix provided some mechanical support, the MMMs tested also observed the effects of swelling and compaction. Since the weight loadings of adsorbent particles were relatively low at 4 %, it would be useful to investigate increased weight loadings to determine any differences in mechanical and chemical strength with respect to compaction and membrane swelling. It could also be of interest to synthesize mixed matrix membranes with smaller particle sizes of activated carbon, HY and silica gel, to determine how this effects the polymer-particle interface and in turn, membrane performance.

Furthermore, it would be useful to conduct experiments where a new membrane is used for each gas or gas combination in the experiments. Since only one of each membrane was used for all gas experiments (single, binary and ternary gas feeds), swelling and/or compaction effects carried into the subsequent set of experiments, where this could be standardized in additional testing.

Chapter 6: Appendix A

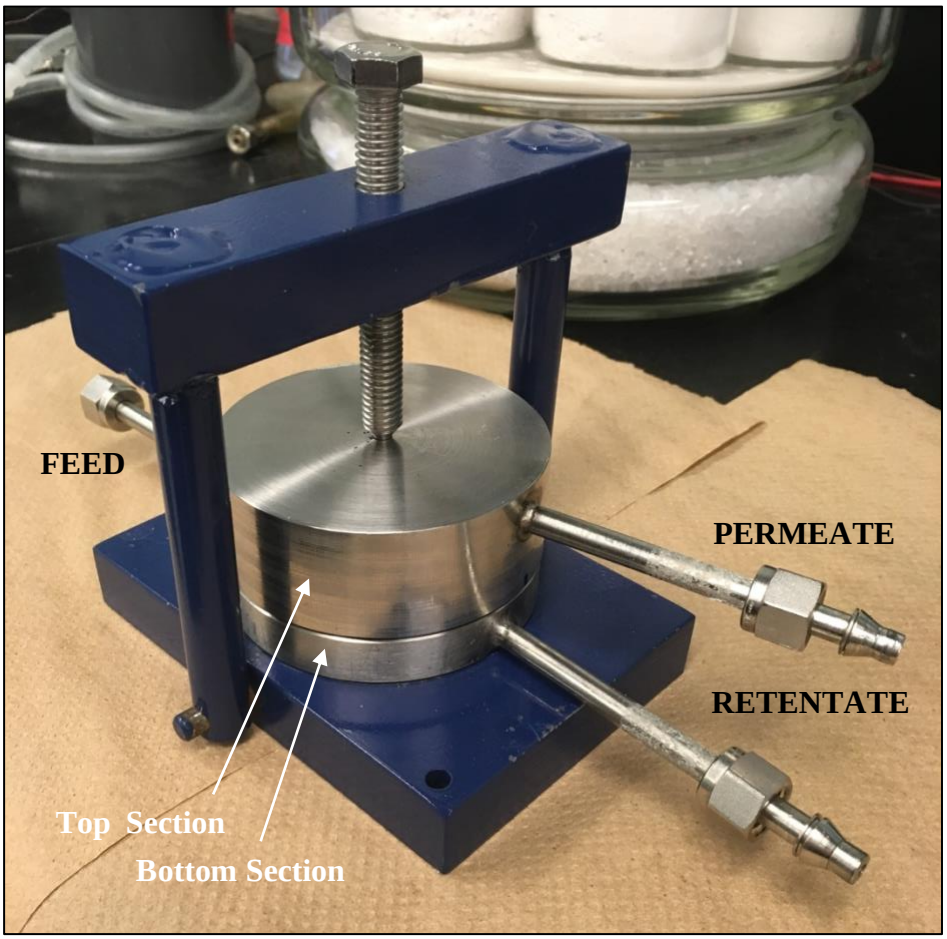

Figure 6-1: Image of flat-sheet membrane cell (top and bottom sections) secured with bolt

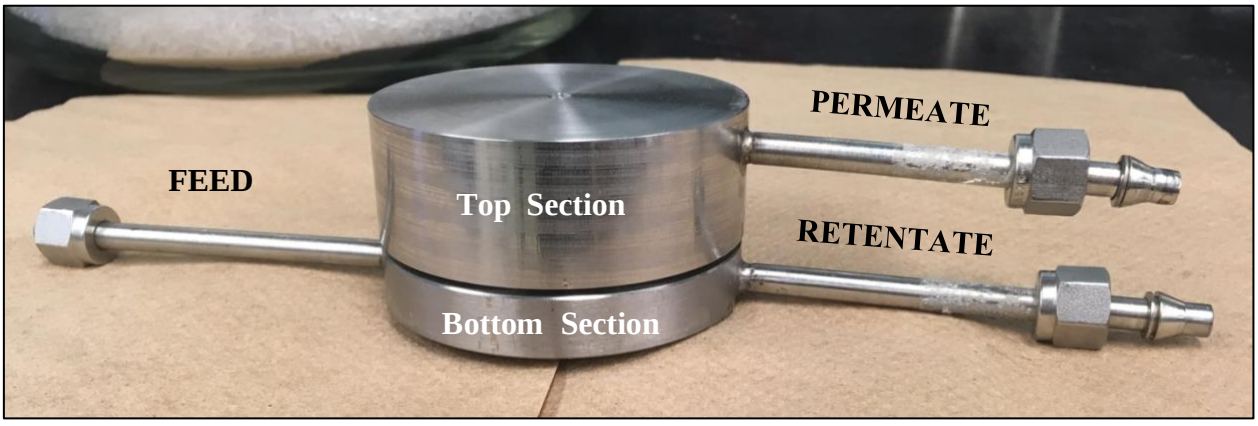

Figure 6-2: Side image flat-sheet membrane cell (top and bottom sections)

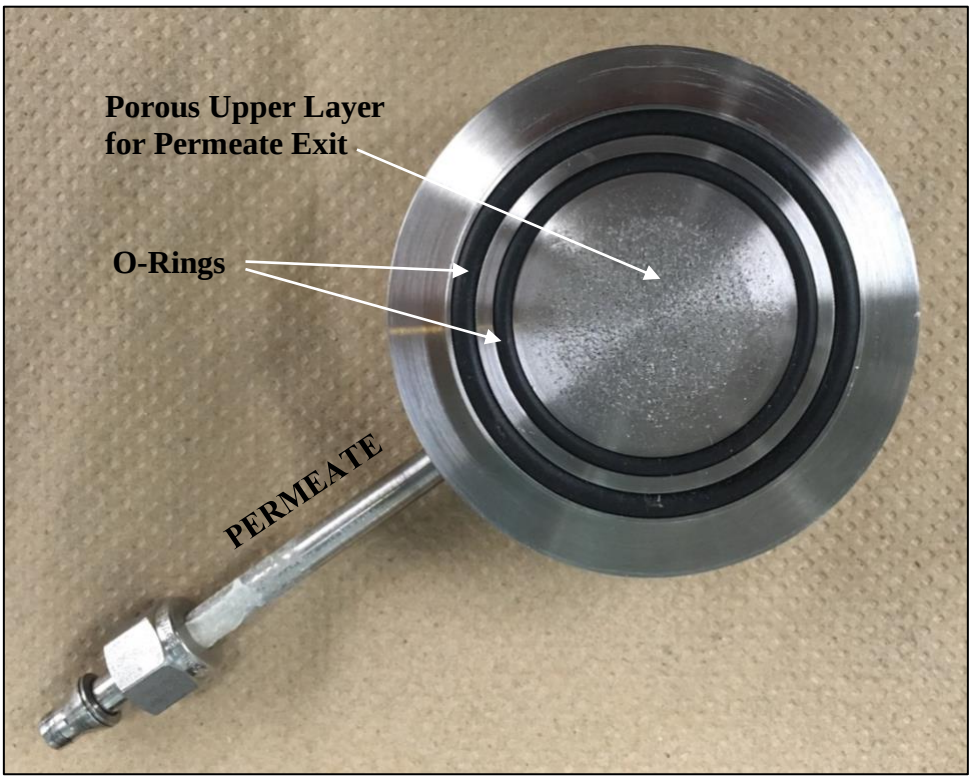

Figure 6-3: Underside view of top section of flat-sheet membrane cell including O-rings and exit point for permeate

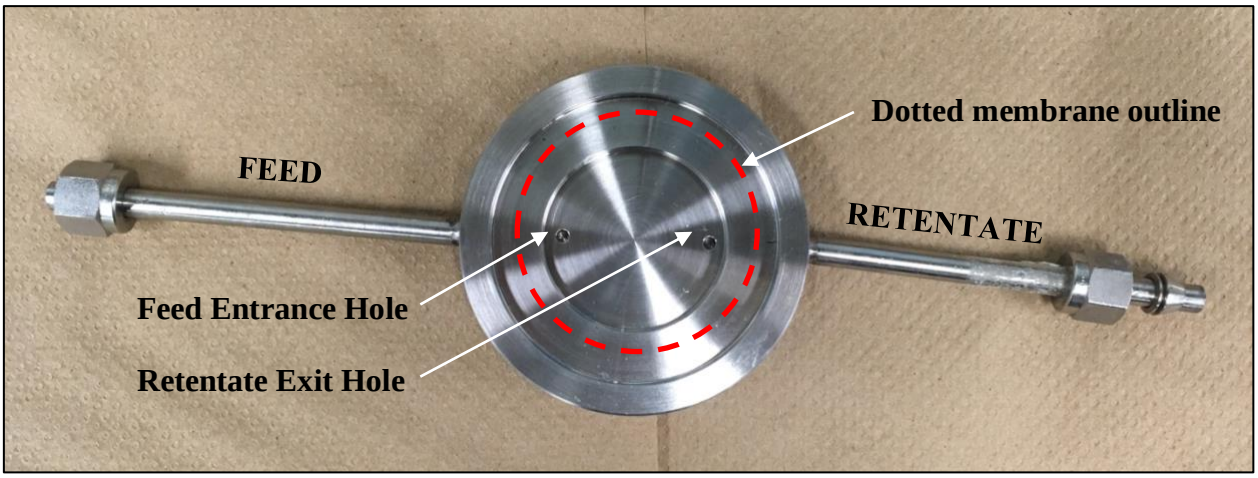

Figure 6-4: Inside view of bottom section of flat-sheet membrane cell including entrance and exit points for feed and retentate, red membrane outline (situated selective side down)

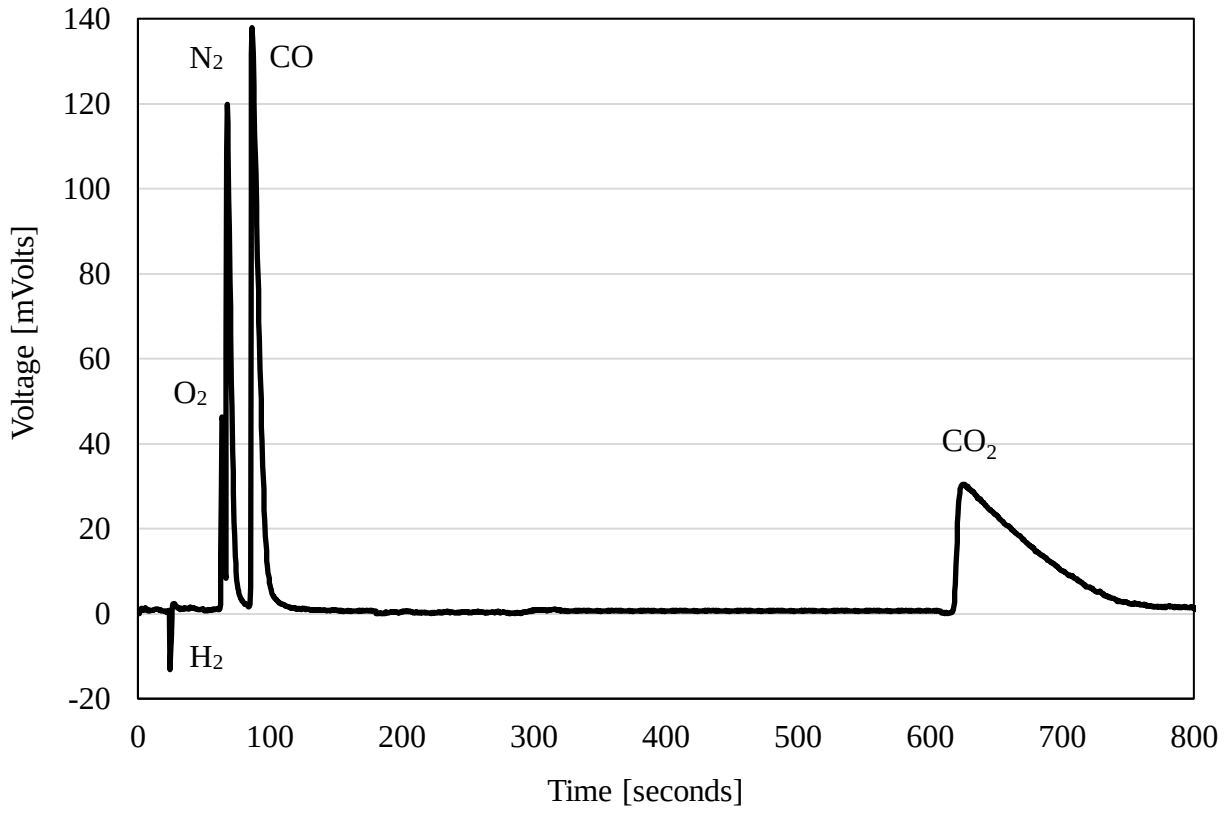

Figure 6-5: Retention times for gas peaks from LabView for H_2, O_2, N_2, CO, CO_2 with column temperature of 40 °C, carrier gas flow (He) 70 mL/min

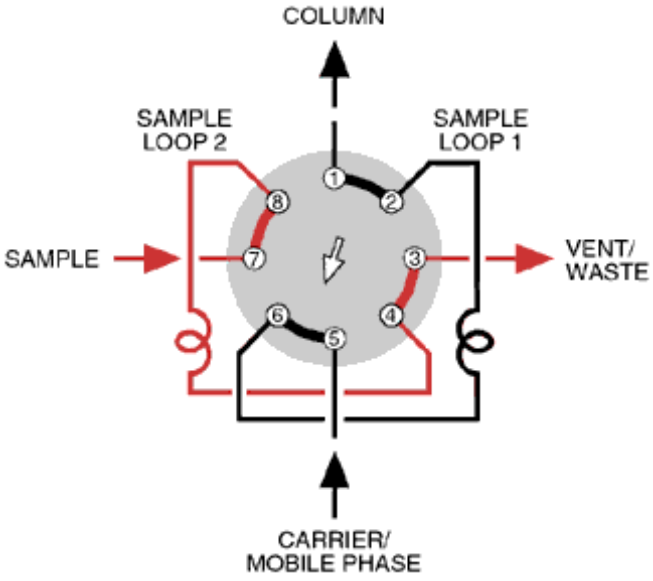

Figure 6-6: 8 Port sampling GC valve diagram from: Valco Instruments Co. Inc. - VICI AG International, (2016). http://www.vici.com/support/app/app9j.php (accessed July 20, 2016).